SUBSURFACE COLLOIDS: STABILITY, SAMPLING, AND TRANSPORT UNDER GRAVITATIONAL AND CENTRIFUGAL ACCELERATIONS

By

SZABOLCS CZIGÁNY

A dissertation submitted in partial fulfillment of
the requirements for the degree of

DOCTOR OF PHILOSOPHY

WASHINGTON STATE UNIVERSITY
Department of Crop and Soil Sciences

August, 2004

To the Faculty of Washington State University:

The members of the Committee appointed to examine the dissertation of SZABOLCS CZIGÁNY find it satisfactory and recommend that it be accepted.

_____

Chair

_____

_____

Acknowledgements

I express my sincere appreciation to those who have assisted and helped me during the course of my studies at WSU. My acknowledgement is primarily directed to my major advisor, Dr. Markus Flury for his supervision, advice, encouragement, guidance, and his genuine support. It has been an exceptional experience working closely with him. I was amazed that he always had the time and made the effort to be available to answer my questions. He never said no when I went to his office without a previously scheduled meeting and bothered him with various questions. I was always impressed with his endless energy and limitless genuine ideas when he was helping me with the experiments, was reviewing my writing, or was discussing research problems. Last but not least, I was really astonished at his athleticism during our regular weekly workouts in the gym and his company, encouragement, and help during these workouts are extremely appreciated.

I was very lucky to have Dr. James B. Harsh and Dr. Glendon W. Gee on my committee. I am indebted to them for their consistent support, ideas, and discussions during these years. Dr. Gee was a great and very fast source obtaining technical reports and documents related to the Hanford site. I am also indebted to Jon Mathison, who acted as my "co-supervisor", and Jeffrey Boyle for their technical support and their constructive suggestions during my experiments. I am extremely grateful to Youjun Deng (for whom time was never important and he devoted a lot of his time to help me), Jorge Jerez, and Geng Chen for their help with the experiments. I wish to

express my gratitude to Dr. Richard Conrey, Dr. Alan Busacca, Dr. John Reganold and Dr. William Pan for their encouragement during my studies. I am also indebted to Chris Davitt and Valerie Lynch-Holm from the Electron Microscopy Center for their patience to teach me the tricks of the scanning and transmission electron microscopes.

I would not have been able to accomplish my studies without the support of my friends and graduate student fellows. Thanks are given, among many others, to Leah Baugher, Jorge Jerez, Limin Yang, Nu Nu Wai, Tabitha Brown, Jennifer Reeve, Thomas Ian Wildey, Tom Drader, Robert Brueggeman and Deric Schmierer for their invaluable and warm friendship.

I also wish to extend my appreciation to the EMSP (Environmental Management Science Program, U.S. DOE), WSU/NSF IGERT Center for Multiphase Environmental Research, and INRA (Inland Northwest Research Alliance) programs for providing funding for this research project.

SUBSURFACE COLLOIDS: STABILITY, SAMPLING, AND TRANSPORT UNDER GRAVITATIONAL AND CENTRIFUGAL ACCELERATION

Abstract

by Szabolcs Czigány, Ph.D.
Washington State University
August, 2004

Chair: Markus Flury

As a legacy of 40-year of Pu production, millions of liters of hazardous waste have been leaking to the vadose zone for the past four decades at the US DOE's Hanford reservation in south-central Washington State. Radionuclides, previously believed relatively immobile, are found deep in the subsurface. Submicron size underground particles, so-called colloids may be responsible for the enhanced mobility of the contaminants. The main objectives of this dissertation were:

1. To assess the stability of reference clay minerals and colloids extracted from Hanford sediments and to compare three experimental methods to determine critical coagulation concentration (CCC).

2. To determine the suitability of fiberglass wicks for *in situ* colloid sampling, and evaluate the effect of colloid type, flow rate, and pH on colloid recovery.

3. To examine the potential for geocentrifuges to study colloid transport.

Critical coagulation concentrations were sensitive to settling time, electrolyte type, and initial colloid concentration. Colloids at low ionic strength (7 mM) can be stable for the time frame of weeks. The lower the initial colloid concentration and shorter the settling times were, the larger the CCC was. Our stability results suggest, that colloids can form a stable suspension in the Hanford pore water for several weeks. However their potential for facilitating the transport of colloids is limited as travel time for the recharged water in the vadose zone is 40 to 100 years. Critical coagulation concentration values obtained by dynamic light scattering were usually higher than those obtained by batch turbidity experiments.

Fiberglass wicks are suitable for colloid sampling under certain conditions. We observed decreasing colloid recovery with decreasing flow rate. Lower recovery rate was observed at pH 7 than at pH 10, as the average surface charge shifted to less negative values at the lower pH. Native colloids at both pH values and ferrihydrite at pH 10 showed almost complete breakthrough. In two cases (kaolinite and ferrihydrite at pH 7) no colloids moved through the wicks.

For natural subsurface colloids, filtration will be different in centrifuge experiments as compared to normal gravity conditions. At typical subsurface flow rates, accelerations as low as 4 g can change the filtration behavior.

Table of Contents

Acknowledgements **iii**

Abstract **v**

List of Tables **xii**

List of Figures **xx**

1 Introduction **1**

1.1 Background 1

1.2 Scope and Objectives 5

1.3 Thesis Outline 6

2 Colloid Stability in Vadose Zone Hanford Sediments **8**

2.1 Abstract 8

2.2 Introduction 9

2.3 Materials and Methods 13

2.3.1 Colloid Material and Fractionation 13

2.3.2 Colloid Stability Experiments 15
2.4 Results and Discussion 22
2.4.1 Colloid Characterization and Hanford Pore Water Composition 22
2.4.2 Colloid Stability 24
2.4.3 Comparison of Methods to Determine Critical Coagulation Concentrations 32
2.5 Implications 33
2.6 Tables and Figures 37
2.7 Appendix A 52

3 Suitability of Fiberglass Wicks to Sample Colloids from Vadose Zone Pore Water 67

3.1 Abstract 67
3.2 Introduction 68
3.3 Materials and Methods 71
3.3.1 Colloidal Material and Fractionation 71
3.3.2 Wick Treatment and Characterization 73
3.3.3 Experimental Setup for Breakthrough Curves 74
3.3.4 Nitrate and Colloid Breakthrough Curves 74
3.4 Results and Discussion 76
3.4.1 Colloid Properties 76
3.4.2 Wick Treatment and Characterization 77

3.4.3 Nitrate Breakthrough Curves 77
3.4.4 Colloid Breakthrough Curves 78
3.4.5 Alternative Wick Materials 82
3.5 Conclusions 83
3.6 Tables and Figures 85
3.7 Appendix B 96

4 Colloid Transport in Saturated Porous Media under Centrifugal Acceleration 98

4.1 Abstract 98
4.2 Introduction 99
4.3 Theory 103
4.3.1 Water Flow 103
4.3.2 Diffusion and Sedimentation 105
4.3.3 Filtration Theory 108
4.4 Experimental Case Study 111
4.4.1 Experimental Methods 111
4.4.2 Experimental Results 114
4.4.3 Comparison of Experiments and Theory 116
4.5 Conclusions 117
4.6 Tables and Figures 119

5 Summary and Conclusions **140**

Bibliography **144**

List of Tables

2.1 Properties of colloids used in this study. 38

2.2 Electrolyte type and concentrations and initial colloid concentrations of the batch experiments. All solutions were adjusted to pH 10. 39

2.3 Electrolyte composition of porewater of vadose zone Hanford sediments at 20°C. 40

2.4 Critical coagulation concentrations (CCC) for the different colloids using the batch turbidity method. 41

2.5 Rate coefficients (k) and collision efficiencies (α) of 2nd-order aggregation model (equations 2.4 and 2.5), and critical coagulation concentrations (CCC) and slope (β) of the stability curves for the different colloids using the light scattering method (equation 2.3). 42

2.6 Annual radioactivity exposure doses for adults due to water consumption and conditions assumed to calculate the dose. Cases 1 and 2 are based on different radioactivity-to-dose conversion factors. 43

3.1 Z-averaged hydrodynamic diameters of the colloids used in this study. 86

3.2 Experimental mass recovery of colloid breakthrough curves at different flow rates. 87

4.1 Single collector efficiencies for colloids with 160-nm diameter and different densities at 3.9×10^{-5} m/s pore water velocity, $1\times g$ acceleration, and collector diameter of $d_m = 462.5$ μm. 120

4.2 Threshold accelerations, where collector efficiency due to sedimentation is equal to that due to diffusion, as function of colloid density and pore water velocity. (Colloid diameter 160 nm diameter, reference pore water velocity $v = 5.09$ cm/h $= 1.4\times10^{-5}$ m/s). 121

4.3 Selected properties of the colloids used in this study and single collector efficiencies (reference pore water velocity $v = 14.1$ cm/h $= 3.9\times10^{-5}$ m/s, $1\times g$ acceleration, and collector diameter of $d_m = 462.5$ μm). . . 122

4.4 Parameters of linear equilibrium transport models for the bench top column experiments. 123

4.5 Threshold accelerations, where collector efficiency due to sedimentation is equal to that due to diffusion, for polystyrene, silica, and ferrihydrite. (reference pore water velocity $v = 14.1$ cm/h $= 3.9\times10^{-5}$ m/s), and pore water velocity, where $\eta_d = \eta_g$ at $1\,g$. 124

List of Figures

1.1 Geological cross section of the S-SX tankfarm. Figure redrawn after McKinley et al. [2001] 2

2.1 Electrophoretic mobility between pH 7 and 10 of the colloids used in this study. Error bars denote ± one standard deviation. Electrophoretic mobilities were determined in 0.01 M NaCl with dynamic light scattering using a Zetasizer 3000HSA with a helium-neon laser of 633 nm wavelength (Malvern Instruments Ltd., Malvern, UK) with particle concentrations adjusted to be between 0.1 and 20 mg/L. 44

2.2 Colloid stability at pH 10 as function of (a) Na concentrations (SAR = ∞) and (b) Ca concentrations (SAR = 0). Error bars denote ± one standard deviation. 45

2.3 Effect of sodium adsorption ratio (SAR) on colloid stability of Hanford colloids at pH 10. (a) Coarse Hanford colloids, (b) fine Hanford colloids, and (c) critical coagulation concentrations (CCC) as function of SAR. Error bars denote ± one standard deviation. 46

2.4 Effect of initial colloid concentration on colloid stability in Na electrolyte solutions (SAR = ∞) at pH 10 for (a) coarse and (b) fine Hanford colloids. Colloid concentrations are normalized with the initial colloid concentration in each experiment. Error bars denote ± one standard deviation. 47

2.5 Colloid suspension concentration as a function of time in the long-term batch experiments in a pH 10 buffered 1.67 mM Na_2CO_3/$NaHCO_3$ solution. Symbols are experimental data and lines are fitted 2nd-order kinetic model. Error bars denote ± one standard deviation. 48

2.6 Colloid stability in mimicked Hanford pore waters for different Ca concentrations at three constant Na concentrations (a) 5.1 $mmol_c$/L, (b) 1 $mmol_c$/L, and (c) 0.5 $mmol_c$/L. Concentrations of K and Mg were kept constant at 0.2 $mmol_c$/L K and 0.6 $mmol_c$/L Mg. Dashed lines indicate Ca and Mg concentrations in vadose zone Hanford sediments measured by Serne et al. (2002b), and represent *in situ* pore water chemistry from several boreholes (Table 2.3). 49

2.7 Colloid effluent concentrations for different eluent Na concentrations (SAR = ∞) for (a) coarse and (b) fine Hanford sediments, and (c) total mass (zeroth moment) of colloids eluted as function of electrolyte concentration. Inflow solutions were buffered at pH 10, 1 pore volume ≈ 21 mL cumulative effluent. 50

2.8 Inverse stability ratio W^{-1} at pH 10 as a function of (a) Na and (b) Ca concentration. The symbols indicate the experimentally determined values (equation 2.2), and the lines are best fits of equation (2.3). . . . 51

2.9 Effect of low and high ionic strengths on colloidal mobility and on the transport of radionuclides. At low ionic strength (right) colloids are stable and mobile in the pore water and might facilitate cesium transport. 53

2.10 Schematic of the experimental setup of the column mobilization experiments. 54

2.11 Average monthly temperatures and precipitation at Hanford (data collected from 1912 to 1980). Figure drawn based on data from Stone et al. [1983] and Hoitink et al. [2002]. 55

2.12 Particle size distribution of the fine and coarse Hanford sediment. The inset magnifies the colloid fraction. 56

2.13 XRD diagram of the (a) fine and (b) coarse Hanford sand effluent colloids (7 $mmol_c/L$). 57

2.14 Thin section images of mobilized minerals from the bulk coarse Hanford sediment. 58

2.15 Thin section images of mobilized minerals from the bulk fine Hanford sediment 59

2.16 SEM micrographs of four of the colloids used in the colloid stability study. 60

2.17 SEM-EDAX spectrum of colloidal aggregates mobilized from the coarse Hanford sands. EDAX spectrum (a) depicts a calcite and spectrum (b) illustrates an Fe-oxide particle. 61

2.18 TEM micrographs of colloids mobilized from the coarse Hanford sand column. 62

2.19 TEM micrographs of colloids mobilized from the fine Hanford sand column. 63

2.20 Effect of settling time on stability of coarse Hanford colloids in Na electrolyte solutions (SAR = ∞) at pH 10 for different initial colloid concentrations: (a) 10 mg/L, (b) 50 mg/L, and (c) 100 mg/L. Error bars denote ± one standard deviation. 64

2.21 Hydrodynamic colloid diameter (Z-averaged) as function of time for selected electrolyte concentrations at pH 10. 65

2.22 Changes in polydispersity as a function of (a) sodium, and (b) calcium concentration for selected colloids. 66

3.1 Experimental setup for the wick experiments. 88

3.2 Electrophoretic mobility of the colloids as a function of pH. Error bars denote ± one standard deviation. 89

3.3 SEM micrographs of (a) nontreated wick fiber (as received from supplier), (b) treated wick fiber (combusted and washed), and (c) treated wick fiber covered with kaolinite particles (after kaolinite breakthrough curve). 90

3.4 Distribution of water content as a function of height above the bottom of the wick for different water flow rates. Error bars denote ± one standard deviation ($n = 3$). 91

3.5 Nitrate breakthrough curves at pH ≈ 7 (a) for different flow rates in the same wick, (b) for 10 mL/h flow rate in three different wicks, and (c) for 55 mL/h flow rate in three different wicks. 92

3.6 Breakthrough curves of native and modified Hanford colloids at different flow rates and pH. Breakthrough curves at the same flow rate within one plot are repetitions with different wicks. 93

3.7 Breakthrough curves of pure mineral colloids at different flow rates and pH. Breakthrough curves at the same flow rate within one plot are repetitions with different wicks. 94

3.8 In-wick and among-wick variability for three repeated breakthrough curves using native colloids at pH ≈ 10. 95

3.9 Setup of the wick experiments (a), and the unfolded wick in the top of the Plexiglas tube held in place by three binder clips and a Plexiglas ring (b). Note the dark band in the wick on picture (a), indicated by an arrow. The discoloration of the wick was caused by the retention of ferrihydrite colloids at pH 7 and at flow rate of 5 mL/h. 97

4.1 Single collector efficiencies as a function of colloid diameter for a colloid density of 2.65 g/cm^3, collector diameter d_c = 462.5 μm, and a pore water velocity $v_0 = 10^{-5}$ m/s. 125

4.2 Effect of centrifugal acceleration on single collector efficiency due to sedimentation and diffusion for colloids of (a) 1.05 g/cm^3 (b) 1.5 g/cm^3, (c) 2 g/cm^3, (d) 3 g/cm^3, and (e) 4 g/cm^3 and 160 nm in diameter. The reference pore water velocity v is equal to 5.09 cm/h = 1.4×10^{-5} m/s. Symbols indicate single collector efficiency due to sedimentation and lines indicate single collector efficiency due to diffusion. 126

4.3 Relationship between acceleration and pore water velocity as affected by particle density for colloids of 160-nm diameter (equation 4.22). Figures (a), (b), and (c) show the same data, but with different axis scales. . . 127

4.4 Relationship between acceleration and density difference $\Delta\rho$ as affected by pore water velocity (equation 4.22). The reference pore water velocity v is equal to 5.09 cm/h = 1.4×10^{-5} m/s. 128

4.5 Effect of particle density on single collector efficiency due to sedimentation at 0.1 ×, 1 × and 10 × pore water velocity. The reference pore water velocity v is equal to 5.09 cm/h = 1.4×10^{-5} m/s. 129

4.6 Picture of the bench top column filtration setup. The particular setup shown is for upward flow. 130

4.7 Schematic of the CO_2 trap and the column inflow system. 131

4.8 Excitation and emission spectra of the fluorescent silica particles. . . . 132

4.9 Scanning electron micrographs of the fluorescent silica (a, b) and polystyrene colloids (c, d). 133

4.10 Transmission electron micrographs of the 2-line ferrihydrite colloids. Note, that the individual particles are only 2–3 nm in diameter, but they have a high tendency to form aggregates. 134

4.11 Electrophoretic mobility of the colloids as a function of pH. Error bars denote ± one standard deviation. 135

4.12 Breakthrough curves from bench top experiments using (a) polystyrene latex colloids (1.05 g/cm^3), (b) fluorescent silica beads (2 g/cm^3), and (c) ferrihydrite colloids (4 g/cm^3) in upward (+1 g), horizontal (0 g) and downward (-1 g) flow directions. Symbols are the measured data and lines are fitted ADE model. 136

4.13 Effect of centrifugal acceleration on single collector efficiency due to sedimentation and diffusion for colloids of (a) polystyrene, (b) silica, and (c) ferrihydrite. The reference pore water velocity is $v = 14.1$ cm/h $= 3.9 \times 10^{-5}$ m/s. Symbols indicate single collector efficiency due to sedimentation and lines indicate single collector efficiency due to diffusion. 137

4.14 Relationship between acceleration and pore water velocity for polystyrene, silica, and ferrihydrite. Figures (a), (b), and (c) show the same data, but with different axis scales. 138

4.15 The 50 g-ton, 2-m radius geocentrifuge at the Idaho National Engineering and Environmental Laboratory (INEEL), in Idaho Falls, ID. 139

Chapter 1

Introduction

1.1 Background

The Department of Energy's (DOE) Hanford reservation played an important role in plutonium-based nuclear weapon production during World War II and in the subsequent Cold War era. Because of its arid climate and the proximity of an abundant water source, the site was considered ideal for nuclear weapon and power production. As a result of chemical extraction processes designed to extract ^{239}Pu from irradiated uranium fuel, plutonium production generated an enormous amount of highly hazardous waste. Most of this waste was stored in short-lifespan single- or double-shell underground tanks (Figure 1.1). The composition of the waste is only vaguely known, and differs among the tanks, but generally the waste has high ionic strength, temperatures above 50 °C and extremely high alkalinity [*Serne et al.*, 1998*; Pruess et al.*, 2002].

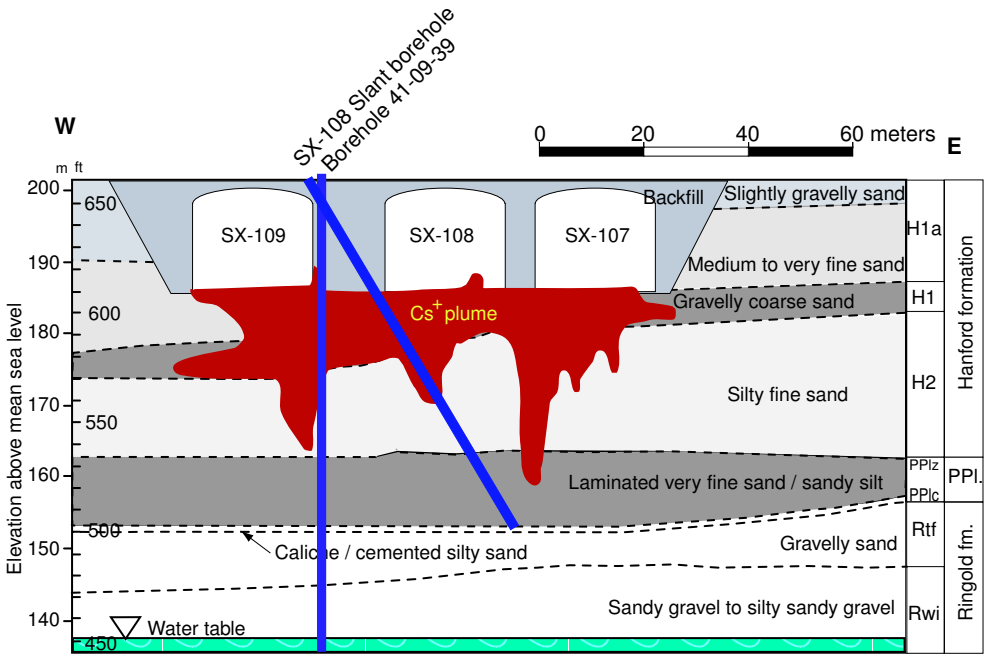

Figure 1.1: Geological cross section of the S-SX tankfarm. Figure redrawn after McKinley et al. [2001]

Millions of liters of hazardous waste have leaked from 177 underground tanks during the past four decades [*Gephart and Lundgren*, 1998]. Some of the waste was also spilled either intentionally or accidentally into the subsurface during waste transfer and moving processes [*Marshall*, 1987*; Gephart and Lundgren*, 1997].

After the cessation of the plutonium production and the shutdown of the N-reactor in 1987 the mission of the Hanford site shifted to environmental remediation. Most of the positively charged radionuclides are relatively immobile in the subsurface as they electrostatically interact with the sediments, are bound to clay minerals (*e.g.*

a classical example is the preferential sorption of Cs^+ to micaceous minerals) and do not move far in the vadose zone [*McKinley et al.,* 2001]. However, some of the contaminants, such as Cs^+ have been found in the vadose zone 20.1 and 25.6 m below leaking waste tanks at Hanford (Serne et al., 2002b; Serne et al., 2002c).

Annually, 6,000 curies of radioactive tritium are added to the Columbia river when it flows through the Hanford reservation [*Gephart and Lundgren,* 1997]. The occurrence of contaminants, such as Pu and Cs, deep in the subsurface indicate unexpectedly high contaminant mobility. There are several possibilities for the observed enhanced mobility of the radionuclides, such as: (i) high ionic strength and competition of cations for exchange sites (e.g. Na^+ and Cs^+ competition) (ii) preferential flow, or (iii) colloid-facilitated transport [*Apps et al.,* 1982*; Pruess et al.,* 2002*; Zachara et al.,* 2002*; Flury et al.,* 2004].

This dissertation focuses on colloids and colloid-facilitated transport. Colloid-facilitated radionuclide transport is a major concern at nuclear facilities, such as the Hanford Reservation [*National Research Council,* 2001], the Yucca Mountain high-level waste repository [*Triay et al.,* 1995], and the Nevada Test Site [*Kersting et al.,* 1999]. Under the conditions in the Hanford vadose zone, soil and sediment colloids are predominantly negatively charged. Thus, the positively charged radionuclides, such as plutonium, americium, europium and cesium can be electrostatically attracted to the surface of the colloids. Colloids can be flushed downward with the infiltrating pore water, simultaneously mobilizing and enhancing the transport of the radionuclides.

However, for colloid-facilitated transport of low-solubility contaminants to occur, the colloids must both exist and be stable [*McCarthy and Zachara,* 1989].

The lifespan of the mobile colloids will determine their ability to enhance the transport of certain contaminants. According to the classical Derjaguin-Landau-Verwey-Overbeek (DLVO) theory the stability of colloidal systems is determined by the balance between the attractive van der Waals forces, which promote aggregation, and the repulsive electrostatic forces which keep the particle apart. Depending on surface charge properties, colloid-surface contact, grain size, flow rate, solution chemical properties and the thickness of the electric double layer, colloid mobility and stability in the dispersing solution can vary considerably [*McCarthy and Zachara,* 1989]. Colloids remain dispersed in suspension when their net surface charge is considerably less or more than zero and their double layers are sufficiently expanded, i.e., the sum of the repulsive forces is considerably larger than the sum of the attractive forces.

Despite their temporary stability, ultimately all colloidal systems are unstable and will settle out form the dispersing phase. In some cases, however, colloid suspensions can be stable for years, decades, or even centuries. For instance, the English chemist Michael Faraday (1791–1867) prepared a colloidal gold suspension in 1857, which is still stable today and his experiment is still shown in the Royal Institution in London. The example of the stability of the gold sol is quite unique and in most cases colloids remain suspended for much shorter times. To determine whether colloids can function as "vehicles" for the subsurface contaminants over larger scales, we need to quantify

under what conditions, if any, colloids are able to remain suspended in the vadose zone pore water.

Further knowledge on colloid behavior can have site specific impact i.e., on the remediation of the Hanford reservation) but can also have broader influence on colloid science and various industrial applications.

1.2 Scope and Objectives

The overall goal of this dissertation is to provide further evidence about the existence of colloid-enhanced transport in general and site-specifically in the Hanford vadose zone. To determine whether colloid facilitated radionuclide transport exists, we need to demonstrate colloidal subsurface mobility and we need to know whether colloids remain suspended in the infiltrating pore water for a time frame relevant to colloid transport through several hundreds of feet of unsaturated porous media. If colloids are stable in the suspension, how long can they function as "vehicles" for the contaminants? To answer these questions, adequate sampling techniques are required, colloid lifespan in suspension needs to be determined, and a better understanding of colloid transport behavior in the vadose zone is needed. This study focuses on three topics associated with colloids, and each aspect is organized in a chapter of this dissertation. The objectives of each study can be summarized as follows:

1. To quantify how long and under what conditions colloids can remain stable in aqueous suspensions, and to determine whether colloids are capable to fa-

cilitate the transport of the radionuclides leaking from the underground tanks at Hanford. We compared three different analytical methods (batch turbidity experiments, column experiments, and dynamic light scattering) to determine critical coagulation concentrations (CCC) of colloidal suspensions.

2. To evaluate the performance of fiberglass wicks, as passive capillary samples, for *in* situ colloid sampling. We studied the effect of colloid type, flow rate, and solution pH on the recovery of the colloids passed through the wick material.

3. To evaluate the applicability of geocentrifuges to investigate colloid transport under saturated and unsaturated conditions. Under low water contents and water potentials transport experiments take prohibitively long times. Centrifuges can be potentially applied to overcome this limitation and shorten transport times. To asses the applicability of centrifuges for colloid transport studies, we carried out theoretical calculations to study how altered force fields, particle density, and flow velocity affect colloid transport and retention. We also performed column transport experiments with polystyrene, silica, and ferrihydrite colloids to study the effect of specific density and flow direction on colloid transport.

1.3 Thesis Outline

This dissertation is organized in three main chapters. The core of each chapter is a paper that has been prepared for submission to a peer reviewed journal. In Chapter 2

we quantify solution chemical properties under which Hanford vadose zone colloid can be stable and can facilitate transport of contaminants, and compare different methods to determine colloidal stability in suspensions under various chemical conditions. In Chapter 3 we test the suitability of fiberglass wicks for colloid sampling in the vadose zone. In Chapter 4 we test the applicability of geocentrifuges for colloid transport experiments, based on theoretical calculations. We present the theoretical calculations and the results of bench top experiments, which were carried out under normal gravitational acceleration. A summary and an overall conclusion are presented in Chapter 5. Tables and figures are presented at the end of each chapter following the format of manuscripts submitted to a journal. Additional figures, which are not included in the technical papers, are found in the Appendices A and B after Chapters 2 and 3. The discussion of these figures are included in the main text as comments, separated from the main text by solid horizontal lines.

Chapter 2

Colloid Stability in Vadose Zone Hanford Sediments

2.1 Abstract

We experimentally determined colloid stability of natural colloids extracted from vadose zone sediments from the US Department of Energy's (DOE) Hanford Reservation. We also used reference minerals, kaolinite, montmorillonite, and silica for comparative purposes. Colloid stability was assessed with three different methods: the batch turbidity method, column mobilization experiments, and dynamic light scattering. Critical coagulation concentrations (CCC) were determined for pure Na and pure Ca electrolyte solutions, as well for mimicked Hanford vadose zone pore waters with varying sodium adsorption ratio (SAR). Critical coagulation concentrations obtained

A modified version of this chapter has been submitted for publication: Czigány, S., M. Flury, J. B. Harsh, Colloid Stability in Vadose Zone Hanford Sediments, Environ. Sci. Technol. (in review).

from the batch turbidity method were sensitive to initial colloid mass concentrations, settling time, and CCC criteria. The lower the initial colloid concentration and the shorter the settling times were, the larger was the CCC. The CCC determined from the dynamic light scattering, where diluted colloidal suspensions are used, were not dependent on settling time and arbitrary CCC criteria and dynamic light scattering is therefore the preferred method to determine colloid stability. The CCC values determined from dynamic light scattering ranged from 90 to 200 mmol/L for Na systems and 1.7 to 3.8 mmol/L for Ca systems. The stability of natural colloids was between that of pure kaolinite and montmorillonite. The results indicate that colloids in the Hanford vadose zone form stable suspensions, *i.e.* are in the slow aggregation regime. Nonetheless, due to the long travel times in the vadose zone, colloids are unlikely to remain in suspension in significant amounts.

2.2 Introduction

Colloid-facilitated radionuclide transport is a major concern at nuclear facilities, such as the Hanford Reservation [*National Research Council,* 2001], the Yucca Mountain high-level waste repository [*Triay et al.,* 1995], and the Nevada Test Site [*Kersting et al.,* 1999]. A prerequisite for colloid-facilitated transport is that colloids present in the subsurface form stable colloid suspensions. Colloid suspensions are thermodynamically unstable, and the term "stable suspension" therefore refers to a suspension that is sustained over a specific time period of interest. For subsurface processes, this time

period of interest can range from hours to hundreds of years.

Colloid stability is affected by colloid surface properties, surface morphology, and by the chemical properties of the aqueous phase. A formalized description of colloid stability is given by the DLVO theory, which accounts for attractive and repulsive interactions between individual particles [*Hiemenz and Rajagopalan,* 1997]. The critical coagulation concentration (CCC) is the electrolyte concentration at which the repulsive interaction energy diminishes below the kinetic energy of an individual particle, and colloids aggregate. Critical coagulation concentrations for subsurface colloids have been reported for various clay minerals, and the experimental data demonstrate the dependence of CCC on pH and sodium adsorption ratio (SAR) [*Keren et al.,* 1988*; Arora and Coleman,* 1979*; Miller et al.,* 1990*; Neaman and Singer,* 1995*; Permien and Lagaly,* 1994*; Goldberg and Glaubig,* 1987*; Swartzen-Allen and Matejevic,* 1976*; Goldberg et al.,* 1991].

The batch turbidity method is a common technique to study colloid stability. This method consists of clay dispersions in a series of vials containing different concentrations of electrolytes. After a predetermined time, the turbidity is measured and the CCC is taken at the electrolyte concentration where the turbidity of the suspension decreases considerably. The CCC value determined in such a way will depend on initial colloid concentration, the time allowed for coagulation, and the criteria used to determine when coagulation has occurred [*Keren et al.,* 1988]. In most batch turbidity coagulation studies, high initial colloid concentrations were used, in the order of ≈ 100

to 1000 mg/L [*Keren et al.,* 1988*; Arora and Coleman,* 1979*; Miller et al.,* 1990*; Neaman and Singer,* 1995*; Hesterberg and Page,* 1990*; Goldberg and Forster,* 1990*; Kaplan et al.,* 1996]. Different authors have used different settling times which range from 3 hours [*Goldberg and Forster,* 1990*; van Olphen H.,* 1977] to 7 days [*Keren et al.,* 1988] and even 15 months [*Permien and Lagaly,* 1994]. Coagulation criteria used in the literature range from turbidity decreases of 95% [*Miller et al.,* 1990], 80% [*Goldberg and Forster,* 1990], and 50% [*Arora and Coleman,* 1979*; Kretzschmar et al.,* 1993], and to visual inspection of turbidity [*Neaman and Singer,* 1995].

It is expected that the higher the colloid concentration and the longer the settling time, the lower will be the determined CCC [*Hiemenz and Rajagopalan,* 1997*; Hesterberg and Page,* 1990]. As the CCC determination with the batch turbidity method is affected by the experimental parameters, it is useful to test the effects of these parameters on the CCC. *Hesterberg and Page* [1990] proposed a settling time of 17 hours, after which the CCC determination for illite became time-invariant. No standard protocol exists on the optimal initial colloid concentration for the batch turbidity method. To our knowledge, no batch turbidity measurements have been reported with colloid concentrations in the range of ≈10 mg/L, a concentration more typical for many subsurface systems [*McCarthy and Degueldre,* 1993].

A second common method to determine the CCC is based on the dynamics of aggregate formation in suspension [*Virden and Berg,* 1992*; Holthoff et al.,* 1996*; Behrens et al.,* 2000*; Grolimund et al.,* 2001]. Aggregate size is usually measured by light

scattering and, consequently, low initial colloid concentrations are employed for these measurements [*Hiemenz and Rajagopalan,* 1997]. The principle of colloid stability determination based on light scattering, however, rests on the assumption of monodisperse, spherical particles, and should be applied with caution to polydisperse, non-spherical particles [*Kretzschmar et al.,* 1998].

To assess the role of colloids on the migration of radionuclides at nuclear waste sites, one needs to determine the site-specific stability of subsurface colloids. In this study, we focus on the subsurface chemical conditions affecting colloidal stability at the US DOE's Hanford Reservation, one of the most contaminated sites in the United States. This site, located in southcentral Washington state, is characterized by an arid climate, and sediments have a pH of 7 or higher [*Serne et al.,* 2002]. Previous observations on colloid stability using the batch turbidity method indicated that natural colloids likely will not form stable suspensions in Hanford groundwaters [*McGraw and Kaplan,* 1997]. However, as CCC determinations with the batch turbidity method depend on the specific experimental protocol, no firm conclusions can be made regarding the colloid stability at the Hanford site from the data currently available.

The objectives of this study are to compare different experimental methods to determine CCCs and to quantify colloid stability in Hanford vadose zone pore water. Specifically, we determined CCCs of colloid suspensions from vadose zone Hanford sediments as affected by ionic strength, electrolyte type, SAR, pH, suspended particle concentration, and time. We also determined CCCs for reference clay minerals (kaoli-

nite and montmorillonite) for comparative purposes. The CCCs were measured by batch turbidity, column mobilization, and light scattering techniques.

Comment: Ionic strength has pronounced but opposite effects on colloid and radionuclide transport. High ionic strength enhances the mobility of radionuclides due to competition for exchange sites between electrolyte cations and the radionuclide. On the other hand, colloids are destabilized in solutions of high electrolyte concentration as their diffusive double layer is compressed and the particles are more prone to aggregation (Figure 2.9). ■

2.3 Materials and Methods

2.3.1 Colloid Material and Fractionation

We used three different types of colloids: colloids from sediments at the Hanford site, aluminosilicate source clays (Clay Minerals Repository, Columbia, MO), and pure silica beads (Bangs Laboratories, Fishers, IN). The source clays were used as standards to compare our results with literature data. Silica was used only in the light scattering studies to represent a monodisperse, spherical colloid system. All experiments were carried out at 22±1°C.

Two types of Hanford sediments were obtained from the submarine pit (218-E-12B) at the Hanford site in spring 2001, a coarse and a fine sand. These sediments are char-

acteristic for the Hanford formation (personal communication, Bruce N. Bjornstad, September 2001, Pacific Northwest National Laboratories, Richland, WA). Extensive characterization of the sediments is given elsewhere [*Serne et al.,* 2002]. Sediments were collected in plastic buckets, air-dried, and sieved through a 2-mm square screen. Three types of clay mineral standards, Ca-montmorillonite (STx-1), Na-montmorillonite (SWy-2) and Na-kaolinite (KGa-1), were used as received from the Clay Minerals Repository.

For the experiments in this study, we saturated the cation exchange sites of sediments and source clay minerals with either Na or Ca. The sediments were wet-packed into 2.5-cm diameter acrylic columns and flushed with at least 40 pore volumes with either 1 M NaCl or $CaCl_2$ buffered at pH 10 with 1.67 mM $Na_2CO_3/NaHCO_3$. The sediments were then dialyzed against deionized water using a 12,000 to 14,000 molecular weight cutoff dialysis membrane (VWR Spectrapor) until the electrical conductivity dropped to below 5 dS/m.

The clay mineral standards and silica beads were washed with either 1 M NaCl or 1 M $CaCl_2$ by shaking clay dispersions in 250 mL plastic centrifuge tubes in a reciprocal shaker for 30 minutes. Samples were then centrifuged at 3100×g for 5 minutes, and the supernatant was decanted. This procedure was repeated three times. Finally, samples were washed, centrifuged, and dialyzed against deionized water to remove excess Na and Ca until the electrical conductivity dropped to below 5 dS/m.

Washed sediments and clay mineral standards were transferred as dilute suspen-

sions to 1-L volumetric cylinders, which were filled with either 1.67 mM $Na_2CO_3/NaHCO_3$ buffer for the Na-saturated systems or deionized water for the Ca-saturated systems. Suspensions were stirred, sonicated for 10 minutes, and briefly shaken end-over-end by hand. Colloids, operationally defined as material with equivalent diameter of < 2 μm, were fractionated by gravity sedimentation based on Stokes' law, assuming a specific gravity of 2.65. Colloids were decanted from the cylinders and used for the colloid stability experiments. Colloids were always kept in suspension and used within at most seven days after fractionation. The total amount of colloids in the sediments was quantified by static light scattering (MasterSizer S, Malvern Instruments Ltd., Malvern, UK).

Scanning electron images of the colloids were taken with a Hitachi S-570 SEM. Hanford colloids were further characterized by X-ray diffraction with Cu-Kα radiation (Philips XRG 3100, Philips Analytical Inc., Mahwah NJ) using standard techniques [*Whittig and Allardice,* 1986].

2.3.2 Colloid Stability Experiments

Electrolyte solutions and Hanford pore water composition

Colloid stability was investigated under different electrolyte compositions (Table 2.2). Pure NaCl and $CaCl_2$ solutions were used to determine colloid stability for 1:1 and 2:1 electrolytes. The effect of the SAR was studied in solutions containing different proportions of Na and Ca. Synthetic Hanford pore water solutions were used to mimic

conditions in the Hanford vadose zone. Synthetic Hanford pore water compositions were based on 1:1 w/w soil/water extracts from the sediments used in this study and data presented in Serne et al. [*Serne et al.,* 2002]. All solutions were buffered at pH 10 with 1.67 mM Na_2CO_3/$NaHCO_3$ for the Na systems and with CaOH for the Ca systems to prevent dissolution of carbonates in the Hanford sediments. Chemical composition and concentrations of the different solutions are summarized in Table 2.2.

To determine the pore water composition of the vadose zone sediments used in this study, we extracted pore water from coarse Hanford sediments. Sediment and water were mixed at a 1:1 (w/w) ratio, shaken for one hour in a reciprocal shaker, and centrifuged to remove the solution phase [*Rhoades,* 1996]. Sodium, Ca, K, and Mg concentrations were measured with ICP-AES (Thermo Jarrell Ash IRIS ICP-AES). Experiments were performed in triplicate. Calculations of ideal pore water concentrations were performed with Visual MINTEQ 2.15 (Jon Peter Gustaffson, KTH, Department of Land and Water Resources Engineering, Stockholm, Sweden, based on MINTEQA2 version 4.0; *Allison et al.,* 1991) for solutions in equilibrium with different carbonaceaous solids at 0.00035 atm CO_2 partial pressure and 25°C.

Batch Turbidity Experiments

Critical coagulation concentrations were determined with the test tube method [*van Olphen H.,* 1977] using 30-mL glass vials and initial colloid concentrations of about 50 mg/L. Electrolyte solutions were either NaCl, $CaCl_2$, or a simulated Hanford pore

water composition with various SARs (with the unit of $\sqrt{\text{mmol}_c/\text{L}}$). Vials were capped, shaken by hand end-over-end for about one minute, and then placed in a rack for 19±1 hours. We then took 3.8 mL suspension with a pipette from a depth of 5 cm from each vial (the total suspension height was 12.5 cm), and measured turbidity by spectrophotometry.

To study the effect of colloid concentration on CCC, we tested suspensions of different initial colloid concentrations ranging from 10 to 400 mg/L using the same procedure as described above. To study the effect of time on CCC, we measured turbidity in the suspensions after 3, 6, 9, 18, and 36 hours following preparation. We used initial colloid concentrations of about 10, 50, and 100 mg/L for these tests. For these experiments (effect of time and colloid concentration) we used NaCl electrolyte and Hanford sediments only.

We studied the effect of Hanford porewater composition on colloid stability using solutions containing different electrolytes (Na^+, K^+, Ca^{2+}, Mg^{2+}) in concentrations typical for vadose zone Hanford sediments. We varied the SAR by changing the Ca^{2+} concentration.

A long-term stability experiment was conducted by using 1-L volumetric cylinders. Colloids were suspended in 1 L of 1.67 mM $Na_2CO_3/NaHCO_3$ buffer solutions (pH 10). Colloids were left to settle for three months, and samples were periodically taken to determine colloid concentration in the supernatant. Each time, a 10-mL sample was taken with a pipette at 15-cm depth.

All batch colloid stability experiments were performed in triplicate, except for the study of the effect of colloid concentration, which was done in duplicate. For the determination of the colloid stability, we define the CCC operationally as the electrolyte concentration at which the turbidity of the suspension fell below 20% of the mass concentration of a non-coagulating suspension [*Goldberg and Forster,* 1990]. Colloid concentrations were determined with turbidity measurements at a wavelength of 300 nm using a spectrophotometer (HP 8452A, Hewlett-Packard). Standard curves were generated by diluting a suspension of known concentration (usually 100 mg/L), which was quantified by gravimetry. Standard curves were constructed with mass concentrations of 1, 5, 10, 20, 40, 60, 80, and 100 mg/L. Turbidity versus mass concentration was linear in this range.

Column Experiments

Colloid mobilization experiments were carried out with coarse and fine Hanford sediments. Hanford sediments were packed into acrylic columns of 2.5-cm ID and 13-cm length. Columns were filled with sediments in about 1-cm increments and saturated from the bottom with the highest ionic strength electrolyte solution used for the CCC determinations. Sediments were packed to a total height of 10 cm. A constant head of 2.7 to 3 cm-H_2O was maintained at the top of the sediment surface. A steady-state, gravity-driven flow through the column in downward direction was established. The elevation of the outflow tube was set such that the flow rates were between 25 and 120

mL/h. The range of the flow rates reflects the differences in the hydraulic conductivity of the fine and coarse sediments. Ionic strength of the inflow solution was then lowered incrementally. At least 40 pore volumes of electrolyte solution was passed through the columns for each ionic strength. Columns were repacked with fresh sediment after each ionic strength change. The ionic strength sequence was 327, 167, 87, 47, 27, 17, and 7 $mmol_c/L$ Na^+ including the pH buffer, with an additional 37 $mmol_c/L$ run for the coarse sediments. Inflow solution pH was maintained between 9.5 and 10.5. Column outflow was collected in 30 mL glass vials with a fraction collector, and flow rate, pH, and colloid concentrations were measured. The saturated hydraulic conductivity was calculated with Darcy's law.

Column experiments were also conducted using 0.5 mol_c/L $CaCl_2$ as equilibrating solution with a subsequent flushing with lower ionic strength solutions, but no colloid mobilization was observed. Column experiments with the reference clay minerals were attempted but were not successful due to the low hydraulic conductivity and clogging of the clay-packed columns.

Comment: A schematic of the column setup is shown in Appendix A (Figure 2.10).

■

Dynamic Light Scattering

We used dynamic light scattering to determine the rate of colloid aggregation. Hydrodynamic Z-averaged diameters were measured with a helium-neon laser of 633 nm wavelength and fixed scattering angle of 90° (ZetaSizer 3000 HSA, Malvern Instruments Ltd., Malvern, UK) at 20°C. The colloid suspension was adjusted to the desired electrolyte concentration and immediately analyzed with light scattering. The cuvette was thoroughly cleaned both inside and outside between individual measurements with Nanopure water and isopropanol. The auto-correlation function was accumulated for 50 s, and was repeated up to a total duration of 70 min.

The stability ratio W is defined as the ratio of fast to slow aggregation rates [*Holthoff et al.,* 1996]

$$W = \frac{k_{a,\text{fast}}}{k_a} \tag{2.1}$$

where $k_{a,\text{fast}}$ and k_a are the fast and slow aggregation rates, respectively. It is convenient to use the inverse of the stability ratio, as W^{-1} is equivalent to the collision efficiency in colloid deposition [*Grolimund et al.,* 2001]. The W^{-1} can be calculated as [*Holthoff et al.,* 1996*; Behrens et al.,* 2000]

$$\frac{1}{W} = \frac{n_{\text{fast}}}{n} \frac{\frac{d \ln R_h}{dt}}{\left(\frac{d \ln R_h}{dt}\right)_{\text{fast}}} \tag{2.2}$$

where n_{fast} and n are the initial particle number concentration in the fast and slow aggregation regimes, respectively, and R_h is the hydrodynamic radius measured by light scattering.

The CCC is obtained when fast and slow aggregation rates are equal, i.e., when the stability ratio $W \approx 1$ [*Hiemenz and Rajagopalan,* 1997]. Grolimund et al. [*Grolimund et al.,* 2001] proposed an empirical equation to determine the CCC from stability ratio data

$$\frac{1}{W} = \frac{1}{1 + \left(\frac{CCC}{C_s}\right)^{\beta}} \tag{2.3}$$

where C_s is the molar electrolyte concentration, and β is the slope $d\ln(1/W)/d\ln(C_s)$ for slow aggregation.

A linear (for slow aggregation) and a third-order polynomial (for fast aggregation) were fitted to the experimental data to obtain the slope $d\ln R_h/dt$ needed in equation 2.2. The slope for fast aggregation was obtained when the aggregation rate $k_{a,\text{fast}}$ was independent of the electrolyte concentration [*Holthoff et al.,* 1996]. The initial particle concentrations n and n_{fast} were calculated from the colloid mass concentration and the initial average hydrodynamic diameter. The inverse stability ratio W^{-1} was then plotted as a function of electrolyte concentration C_s in a double logarithmic fashion, and these data were used to fit equation 2.3 to obtain the CCC and the slope β.

2.4 Results and Discussion

2.4.1 Colloid Characterization and Hanford Pore Water Composition

Scanning electron micrographs of the Hanford colloids show predominantly a platy structure, characteristic of 1:1 and 2:1 layered aluminosilicate clays. According to the XRD analysis, the Hanford colloids consist dominantly of quartz, illite, smectite, chlorite, kaolinite, and albite. The colloids from the coarse sediments were richer in mafic minerals than those from the fine sediments. Coarse Hanford colloids also contained the mafic minerals ilmenite, magnetite, and Ca-plagioclase. The coarse sediments contained 1.5% colloids by weight, and the fine sediments contained 3%. All colloids used in this study had a net negative charge in the pH range of 6.6 to 10, indicated by the negative electrophoretic mobility (Figure 2.1). The electrophoretic mobility did not change much between pH 6.5 and 10.

Comment: The sediments of the Hanford site were deposited by several cataclysmic floods during the late Pleistocene period [*Busacca,* 1991]. The site has an arid, desert climate (Figure 2.11) and is dominated by calcareous sandy–gravelly sediments (Figure 2.12). We performed mineralogical (thin section, and X-ray diffraction (XRD)), and elemental (with X-ray fluorescent mass spectrophotometer (XRF-MS)) composition analysis on both the bulk fine and the coarse Hanford sand. X-ray diffrac-

tion and SEM-EDAX analyses were performed on the colloidal fraction of the sediments. Scanning electron microscope (Hitachi S570 SEM) and transmission electron microscope (JEOL 1200 EX TEM) photographs were also taken of the colloidal fraction of the two sands.

Based on the XRD and thin section analyses the bulk coarse Hanford sand is somewhat richer than the fine sand in mafic minerals including nesosilicates (olivine), inosilicates (pyroxene and amphibole), biotite mica, plagioclase feldspars and iron-oxides such as magnetite, hematite, and ilmenite. On the other hand, the fine Hanford sand has a higher content of felsic minerals such as, muscovite mica, and orthoclase feldspars. The fine Hanford sand also has considerably higher chlorite and calcite content, somewhat higher quartz content, and much less albite than the coarse sand. The XRF-MS results also supported these finding as the fine sand has higher Si an Al, but lower Fe and Mg contents than the coarse Hanford sand. Native colloids mainly consist of chlorite, smectite, vermiculite, kaolinite, illite and quartz (Figure 2.13, 2.14, 2.15).

The scanning electron microscope images revealed the dominantly platy structure of the Hanford colloids (Figure 2.16). The results of the SEM-EDAX elemental analysis indicate considerable fraction of Fe-oxides (hematite, magnetite and ilmenite), and calcite in the coarse Hanford colloids (Figure 2.17).

The transmission electron micrographs indicated the presence of calcite, micas, and halloysite in the colloid fraction of the Hanford sediments (Figure 2.18, 2.19). ■

Cation composition of the pore water in the Hanford sediments determined with different methods are shown in Table 2.3. Our measured cation concentrations generally agree with data from *Serne et al.* [2002], except for the Na concentrations, which were much higher for our samples. Consequently, the SAR values for our samples were larger than those calculated from Serne at al. [*Serne et al.,* 2002]. With respect to the equilibrium concentrations of the bivalent cations, calculated with MINTEQ, the experimentally measured Ca is oversaturated with respect to calcite and the experimentally measured Mg is undersaturated with respect to calcite and magnesite.

2.4.2 Colloid Stability

Batch Turbidity Experiments

The stability of the colloid suspensions differed among the minerals and sediments used. For Na systems (SAR = ∞), the montmorillonite suspension was the least stable and the kaolinite suspension was the most stable system (Figure 2.2a). The colloids from coarse Hanford sediments appear to be somewhat more stable than those from fine Hanford sediments (Figure 2.2) and the CCC values were higher for coarse than for fine Hanford sediments (Table 2.4). The Hanford colloids were more stable than the pure montmorillonite, for both Na (SAR = ∞) and Ca (SAR = 0) systems. We did not determine the stability of kaolinite in pure Ca-systems (SAR = 0), because without the presence of Na, no stable kaolinite suspensions could be obtained. According to the Schulze-Hardy rule for symmetric electrolytes [*Hsu and Kuo,* 1995*; Hsu and Kuo,*

1997] the CCC ratio for NaCl to $CaCl_2$ is 42. The observed deviations of the CCC ratio from the theoretical value (Table 2.4) can be explained by particle polydispersity, surface charge heterogeneity, and surface morphology [*Grolimund et al.,* 2001].

Colloid stability as a function of SAR is depicted in Figure 2.3. As the SAR increased, the colloid concentration versus cation concentration curves became less steep, which makes the CCC determination less accurate. The CCC values show that for SAR = 0 to 60 $mmol_c/L$, coarse and fine Hanford colloids have the same CCCs, but at SAR > 60 $mmol_c/L$, the coarse Hanford colloids were more stable than the fine Hanford colloids.

Initial colloid concentration affected the colloid stability, with the colloid suspensions becoming more stable as the initial colloid concentrations decreased (Figure 2.4). The CCC clearly increased as colloid concentration decreased. A sharp concentration decline is observed for initial concentrations of 100 to 270 mg/L, and the corresponding CCCs are well defined. At colloid concentration less than 50 mg/L, the relative colloid concentrations decrease gradually over a large range of electrolyte concentrations. For 10 and 25 mg/L initial colloid concentrations, the CCC was not reached in our experiments (Figure 2.4).

The results of the batch turbidity experiments highlight that, in case of polydisperse, natural colloids, colloid stability determination depends on initial colloid concentrations and the duration of the experiment. The higher the initial colloid concentrations and the longer the duration of the settling period, the smaller will be

the experimentally determined CCC. Critical coagulation concentrations from batch experiments therefore need to be evaluated based on the specific experimental conditions used, e.g., initial colloid concentration and duration of experiment. Critical coagulation concentrations reported in the literature are difficult to compare with our measurements, because most investigators used much higher colloid concentrations. Corroborating our observation of a lower CCC at higher colloid concentration, reported kaolinite CCCs for Na (at pH 9 to 10 and ?? mg/L colloid concentrations) are between 10 and 40 $mmol_c/L$ [*Swartzen-Allen and Matejevic,* 1976*; Goldberg et al.,* 1991], as compared to >100 $mmol_c/L$ in our experiments.

The stability of the colloids in synthetic Hanford pore water is illustrated in Figure 2.6. We plot colloid stability versus the sum of Ca and Mg concentrations for a given concentration of Na in the system. The Na and Ca concentrations cover the range of concentrations observed in the vadose zone Hanford sediments (Table 2.3). The results illustrate that both SAR and the absolute values of Na and Ca concentrations determine the colloid stability. The higher the Na concentration, the higher will be the SAR where colloids become unstable. In Figure 2.6, we also plot the approximate pore water composition of vadose zone Hanford sediments as determined from boreholes at the Hanford site (Table 2.3, Serne et al. [*Serne et al.,* 2002]). These results suggest that conditions in Hanford sediments are likely such that colloids can form stable suspensions, as most of the measured pore waters lie in the stable regime.

The long-term colloid stability experiment in low ionic strength Na systems (7

$mmol_c$/L Na) indicates that a considerable amount of colloids can remain in suspension for an extensive period of time (Figure 2.5). After 113 days, most of the colloids had settled out from the suspension, but a measurable fraction remained suspended. Although this suspended fraction was less than our experimental quantification limit, we still could detect the presence of these colloids. The long-term experiment suggests that the "shelf-life" of the colloids was in the order of several weeks (at pH 10 and 7 $mmol_c$/L Na, which represents an optimal solution chemistry for colloid stability).

We fitted the data with a 2nd-order aggregation model [*Stumm and Morgan,* 1981]

$$\frac{dn}{dt} = -kn^2 \tag{2.4}$$

where n is the colloid number concentration, and k is the aggregation rate coefficient. The model fit the data closely (Figure 2.5). For spherical, monodisperse particles, the rate constant k is related to the collision efficiency α by [*Stumm and Morgan,* 1981]

$$k = \alpha \frac{4k_B T}{3\eta} \tag{2.5}$$

where k_B is the Boltzmann constant, T is absolute temperature and η is dynamic viscosity. The rate coefficient and collision efficiencies (Table 2.5) indicate that the colloidal suspensions were stable, i.e., in the slow aggregation regime. Nonetheless, after several weeks of aggregation, most of the colloids were aggregated and settled out from the suspension.

Column Experiments

Colloid mobilization experiments using packed columns provide an alternative means to determine colloid stability. In contrast to the batch experiments, colloids are initially flocculated and become dispersed as the solution passes through the column. A series of different electrolyte concentrations will allow the determination of the ionic strength when colloids are mobilized. The coarse and fine Hanford sediments columns differed considerably in saturated hydraulic conductivities: 150 to 400 cm/h for coarse sediments and 4 to 8 cm/h for the fine sediments. Conductivities varied from packing to packing, but were fairly constant during most of the mobilization experiments. The average porosities of the coarse and fine sediment columns were 0.44 and 0.42 cm^3/cm^3, respectively.

Colloid concentrations in the effluent from the two sediment columns are shown in Figure 2.7a,b, and the total eluted colloid mass (zeroth moment) as a function of effluent electrolyte concentration is shown in Figure 2.7c. At low electrolyte concentrations, colloids were mobilized and flushed out from the Hanford sediment columns. The colloid elution curves show a sharp breakthrough front and a pronounced tailing. This behavior is typical for colloid mobilization from undisturbed soils [*Laegdsmand et al.,* 1999*; Schelde et al.,* 2002] and packed sediments [*Roy and Dzombak,* 1996*; Grolimund et al.,* 1996*; Grolimund and Borkovec,* 1999*; Flury et al.,* 2002]. In our experiments, colloid breakthrough curves for low Na electrolyte concentrations occurred at about one pore volume (1 pore volume $\approx$ 21 mL cumulative effluent, the exact pore volume

was not determined and varied between packings). The more variable initiation of colloid breakthrough in the coarse Hanford sediments as compared to the fine Hanford sediments (Figure 2.7a,b) was likely caused by experimental difficulties that occurred in the coarse Hanford sediments during switching of the electrolyte solutions. We sometimes lost some electrolyte solution in the inflow when trying to keep the hydraulic head constant, because the flow rates for the coarse Hanford sediments were high: Q = 40–120 mL/h (corresponding to a flux density of J = 8.2–24.5 cm/h). These difficulties did not occur in the fine Hanford sediments, as the flow rates were lower (Q = 25–35 mL/h, J = 4.1–7.1 cm/h).

For coarse Hanford sediments, colloids were mobilized for Na concentrations from 7 to 87 $mmol_c$/L, but at 167 $mmol_c$/L considerably less colloids were eluted (Figure 2.7). This places the CCC between 87 and 167 $mmol_c$/L. This CCC determination corroborates the results from the batch experiments (Table 2.4). For fine Hanford sediments, the drop in colloid concentrations occurred between Na concentrations of 27 and 47 $mmol_c$/L, indicating that dispersion and mobilization are more likely for fine than for coarse Hanford sediments. Colloid mobilization in fine sediments occurred at lower Na concentrations than would be expected from the batch CCC determinations (Table 2.4).

A greater mass of colloids was mobilized from the fine Hanford sediments as compared to the coarse sediments (Figure 2.7c). In addition, the mass of colloids eluted from the fine Hanford sediments was more sensitive to the electrolyte concentration as

compared to the coarse sediments. Due to the smaller grain size of the fine sediments, there was more colloid-fluid contact and smaller pore water velocity than in the coarse sediments. This will likely cause colloid mobilization be more susceptible to pore water chemistry.

Dynamic Light Scattering

The results of the dynamic light scattering experiments are summarized in Figure 2.8. At small electrolyte concentrations, where the inverse stability ratio increases monotonically, aggregation occurs slowly. At larger electrolyte concentrations, aggregation is fast, and the stability ratio becomes independent of electrolyte concentration. The stability plots indicate that the silica beads were the most stable colloidal system, and the montmorillonite was the least stable in both the Na and Ca electrolytes. Silica beads and kaolinite had the most negative electrophoretic mobility of all colloids used (Figure 2.1). Less negative electrophoretic mobility, heterogeneous charge distribution, and polydispersity are likely reasons for the lower stability of the montmorillonite. The coarse and fine Hanford colloids had similar stability, and their stability was intermediate between the silica and the montmorillonite. This intermediate stability is likely because the Hanford colloids are a mixture of quartz, aluminosilicates, and other minerals.

Equation 2.3 fitted the experimental data well (Figure 2.8), and the fitted CCC and β values are listed in Table 2.5. The ratios of the Na- to Ca-CCC were between 50 and

54, which is somewhat higher than theoretical value of 42 [*Hsu and Kuo,* 1995*; Hsu and Kuo,* 1997]. Grolimund et al. [*Grolimund et al.,* 2001] determined a ratio of 40 for colloids from a non-calcareous forest soil, but large deviations from the theoretical values are not uncommon [*Elimelech et al.,* 1995].

The CCCs of the non-calcareous colloids reported by Grolimund et al. [*Grolimund et al.,* 2001] were similar but slightly higher for both Na and Ca (i.e., 155 and 3.2 mmol/L, respectively) than our values for the calcareous Hanford colloids (Table 2.5). Dynamic light scattering studies with pure minerals have been reported by others [*Novich and Ring,* 1984*; Kretzschmar et al.,* 1998], but different electrolytes than NaCl and $CaCl_2$ were used, so that direct comparisions with our data are difficult. Kretzschmar et al. [*Kretzschmar et al.,* 1998] demonstrated the strong dependence of kaolinite stability on pH and organic coatings.

The slopes β of the stability curves (Table 2.5) were considerably steeper than the slopes reported by Grolimund et al. [*Grolimund et al.*, 2001], who reported slopes of 3.8 for NaCl and 2.3 for $CaCl_2$. In our experiments, the ratio of the NaCl to $CaCl_2$ slopes was about 0.5, which is much less than the ratio of 1.6 reported by Grolimund et al. [*Grolimund et al.,* 2001]. It is theoretically expected that the slopes for Na systems are steeper than for Ca systems [*Grolimund et al.,* 2001*; Elimelech et al.,* 1995], but our measurements showed the opposite result.

The theory of light scattering assumes that colloids and aggregates are spherical and monodisperse. These assumptions are not met in experiments with natural colloids.

Consequently, light scattering data will not yield accurate coagulation rates and have to be interpreted with caution. Aggregation further increases polydispersity and makes light scattering data less reliable. This can be a reason for the difference in slopes observed in our experiments. The observed deviation of the CCC ratio for NaCl and $CaCl_2$ from the theoretical value, however, cannot solely be attributed to polydispersity and non-sphericity. The monodisperse, spherical silica in our experiments did not show a CCC ratio closer to the expected value than the clay mineral colloids (Table 2.5).

2.4.3 Comparison of Methods to Determine Critical Coagulation Concentrations

The comparison of the CCCs determined by batch turbidity and light scattering methods indicates the arbitrariness of the batch turbidity method (Tables 2.4 and 2.5). The CCC determined with the batch turbidity method very much depended on the CCC criteria used. The dynamic light scattering CCCs were considerably greater than the batch turbidity CCCs for the 80% removal criteria. The light scattering measurements yielded more consistent CCC_{NaCl}/CCC_{CaCl_2} ratios than the batch turbidity method, and the ratios were closer to the theoretically expected value of 42 [*Hsu and Kuo,* 1995]. As the light scattering method does not depend on specific experimental conditions, this method is the preferred technique to determine CCCs.

According to both the batch turbidity and the dynamic light scattering results, the CCC of natural Hanford colloids was intermediate between that of the kaolinite and

montmorillonite clay mineral standards. This suggests that the clay mineral standards can be used to bracket the behavior of natural Hanford colloids. In contrast to the batch studies, the light scattering studies did not reveal differences in colloidal stability between coarse and fine Hanford colloids.

Comment: Selected plots, illustrating the changes of the hydrodynamic diameter of the particles and aggregates versus time at different ionic strengths are shown in Appendix A (Figure 2.21). Polydispersity in these tests shows a positive correlation with increasing aggregate size, and suddenly increase around the critical coagulation concentration of the the colloids. However, at pronounced aggregation, it can limit the suitability of light scattering for determination of colloidal stability (Figure 2.22).

■

2.5 Implications

Many of the radioactive contaminants sorb strongly to subsurface minerals and are therefore considered fairly immobile. Colloids can potentially facilitate the movement of such contaminants, provided colloids are present, sorb contaminants strongly, form stable suspensions, and are mobile in the subsurface. All of these conditions must be met if colloid-facilitated transport is a relevant transport mechanism.

The results of our colloid stability experiments and the measured pore water com-

positions in vadose zone Hanford sediments indicate that colloids likely form stable suspensions in vadose zone Hanford sediments. The CCCs, which separate the slow from the fast aggregation regime, were consistently higher than the electrolyte concentrations of vadose zone pore water, so colloid stability is favored at Hanford. However, the colloidal stability as defined by the CCC does not necessarily imply that colloids stay suspended for sufficiently long times to play a relevant role for contaminant transport. Long-term stability experiments indeed indicated that colloids from the Hanford sediments will form stable suspensions for several weeks, but over longer time periods, colloids will settle out from suspension. After about 16 weeks, on average 90% of the colloidal mass settled out from suspension.

Measured recharge rates at Hanford range from near 0 to more than 100 mm/year, depending on variation in precipitation, soil type, and vegetation cover [*Gee et al.,* 1992]. One of the most contaminated locations at Hanford, the waste tank area, has some of the highest recharge rates, because of the coarse-textured sediment used for backfill and the absence of vegetation. In addition, the "umbrella effect", i.e., the runoff and redirection of water due to the presence of the tanks, enhances the local recharge rates. The thickness of the Hanford vadose zone, where the waste tanks are located, varies from 40 to 100 m [*Gee and Heller,* 1985*; McKinley et al.,* 2001]. Assuming the worst-case scenario of a shallow vadose zone (40-m thickness), a high recharge rate (100 mm/year), and an average volumetric water content of 10%, the travel time of the recharge water is 40 years. Over this time period, colloidal suspensions at the

Hanford site will not be stable. Estimations based on measured aggregation rates show that after 40 years only 0.05 to 0.08% of the initially suspended colloids remain in suspension.

Under natural conditions, the potential for colloid mobilization and stable colloid suspensions is greatest during infiltration events, when low ionic strength rainwater increases soil moisture. As the water drains to deeper depths, the changes in moisture dampen and the ionic strength increases due to equilibration with soil mineral phases. Our experiments and conclusions regarding colloidal stability were based on these equilibrium ionic strengths, and are therefore representative for the deeper vadose zone at Hanford. In addition to colloid aggregation and sedimentation in suspension, colloids will also be removed from the solution phase by filtration mechanisms in the sediments. As we have shown in previous experiments [*Cherrey et al.,* 2003], colloids will be retained considerably during transport in water-unsaturated Hanford sediments. Colloid aggregation and filtration seem to be favored.

Nonetheless, aggregated colloids can be remobilized when the ionic strength decreases [*Flury et al.,* 2002] or when flow rates increase. At certain locations at the Hanford site, the natural recharge has been disturbed considerably. For instance, at the tank farms, water leaks and fluids from the tanks themselves, in addition to the "umbrella effect", have increased infiltration rates and provided an enhanced water flux [*Lichtner et al.,* 2003] and possibly preferential flow. Under such conditions, travel times in the vadose zone are considerably reduced, and the potential for colloid

movement is enhanced.

Comment: Based on the specific conditions at the Hanford Site in terms of recharge rates and Cs-137 contamination in the subsurface, we can estimate how much Cs-137 can be potentially transported with colloids. We calculated the colloid-assisted cesium flux to the ground water table, assuming that Cs-137 is irreversibly sorbed to colloids. Based on the Cs-137 flux, we can estimate the radiation dose that would occur to an adult if the ground water was used for drinking water purposes. The parameters and values used in this estimation are shown in Table 2.6. The calculations are made for two cases, using two different factors to convert radioactivity (pCi) to dose (mrem). The Environmental Protection Agency's (EPA) drinking water standard is 4 mrem/year [*SRSHES,*, 2004]. The estimated annual dose in both cases is less than the EPA's drinking water standard, which suggests, that under the assumptions made for our calculations, no health risk is associated with colloid-facilitated transport of Cs-137. ■

2.6 Tables and Figures

Table 2.1: Properties of colloids used in this study.

Colloid type	Fe[a]	Electrophoretic mobility[b] at pH∼10	Hydrodynamic diameter[b]	Organic C[c]
	(g/kg)	(μm/s)(V/cm)	(nm)	(g/kg)
Montmorillonite (STx-1)	0.52±0.01	−3.15±0.02	579±41	0.7±0.2
Montmorillonite (SWy-2)	0.88±0.05	−3.41±0.09	494±26	1.3±0.1
Kaolinite (KGa-1)	0.13±0.01	−4.96±0.05	488±45	0.8±0.3
Coarse Hanford	42.02	−3.35±0.09	566±43	6.8±0.2
Fine Hanford	32.94	−3.60±0.07	592±38	3.8±0.2

[a] "Free" iron oxides determined by citrate-bicarbonate-dithionite method described by Loeppert and Inskeep [*Loeppert and Inskeep,* 1996*, p. 647–648*]

[b] measured by dynamic light scattering in 0.01 M NaCl (Malvern Instruments Ltd., Malvern, UK)

[c] measured by dry combustion with a LECO CHN Analyzer (Leco Corporation, St Joseph, MI)

Table 2.2: Electrolyte type and concentrations and initial colloid concentrations of the batch experiments. All solutions were adjusted to pH 10.

Electrolyte[a]	Concentration range used ($mmol_c/L$)	Initial colloid concentration (mg/L)
NaCl, $NaHCO_3$, Na_2CO_3	7.0–107.0 (Na)	≈50, 10–400
$CaCl_2$, $Ca(OH)_2$	0.2–2.2 (Ca)	≈50
$CaCl_2$, $NaHCO_3$, Na_2CO_3	0.0–5.0 (Ca); 5.1 (Na)	≈50
NaCl, $CaCl_2$, $NaHCO_3$, Na_2CO_3	0.0–5.0 (Ca); 5.1-65.1 (Na)	≈50
Hanford pore water[b]	0.0–4.4 (Ca); 0.5, 1.0, or 5.1 (Na); 0.2 (K); 0.6 (Mg)	≈50

[a] All experiments were performed at standard atmospheric pressure with 0.00035 atm CO_2 partial pressure.

[b] Synthetic Hanford pore water; all counterions are Cl.

Table 2.3: Electrolyte composition of porewater of vadose zone Hanford sediments at 20°C.

Solid Phase	Na	K	Ca	Mg	pH	SAR
	———	($mmol_c/L$)	———		(1:1 w/w H_2O)	$(mmol_c/L)^{0.5}$
1:1 solution extracts						
Coarse Hanford sediment	5.38	0.30	0.63	0.22	7.8–8.2	8.25
Fine Hanford sediment	6.38	0.32	0.89	0.37	8.2–8.3	8.04
RCRA Borehole, 299-W22-48[a]	0.62–1.26	0.07–0.12	0.30–0.54	0.09–0.29	7.2–8.0	1.07–2.63
RCRA Borehole, 299-W22-50[a]	0.48–1.22	0.07–0.26	0.26–0.96	0.00–0.35	7.0–10.3	1.02–1.91
MINTEQ simulations[b]						
Calcite	0	0	0.234	0	9.9	na[c]
Calcite and magnesite	0	0	0.057	0.596	10.2	na
Calcite and kaolinite	0	0	0.270	0	9.7	na
Calcite, magnesite, and kaolinite	0	0	0.063	0.662	10.1	na
Calcite, magnesite, and gypsum	0	0	9.64	101	9.0	na
Calcite, magnesite, kaolinite and gypsum	0	0	9.64	101	8.9	na

[a] Resource Conservation and Recovery Act Borehole, Hanford formation sediments, data are from Serne et al. [*Serne et al.,* 2002].

[b] Pore water concentrations in equilibrium with the solid phase at 0.00035 atm CO_2.

[c] na: not applicable.

Table 2.4: Critical coagulation concentrations (CCC) for the different colloids using the batch turbidity method.

Colloid type	CCC defined at 80% removal			CCC defined at 95% removal	
	CCC_{NaCl} ($mmol_c/L$)	CCC_{CaCl_2} ($mmol_c/L$)	CCC_{NaCl}/CCC_{CaCl_2}	CCC_{NaCl} ($mmol_c/L$)	CCC_{CaCl_2} ($mmol_c/L$)
Silica	na[a]	na	na	na	na
Kaolinite	>100	na	na	>100	na
Montmorillonite	35	1.8	19	44	>2.2
Coarse Hanford	100	1.4	71	>100	>2.2
Fine Hanford	70	1.8	39	>100	>2.2

[a] na: not available.

Table 2.5: Rate coefficients (k) and collision efficiencies (α) of 2nd-order aggregation model (equations 2.4 and 2.5), and critical coagulation concentrations (CCC) and slope (β) of the stability curves for the different colloids using the light scattering method (equation 2.3).

Colloid type	k (m^3/s)	α	CCC_{NaCl} (mmol/L)	CCC_{CaCl_2} (mmol/L)	CCC_{NaCl}/CCC_{CaCl_2}	β_{NaCl}	β_{CaCl_2}	$\beta_{NaCl}/\beta_{CaCl_2}$
Silica	na	na	203	3.8	53	6.1	9.6	0.6
Kaolinite	1.63×10^{-17}	8.26×10^{-4}	188	na[a]	na	4.0	na	na
Montmorillonite	0.99×10^{-17}	5.02×10^{-4}	92	1.7	54	3.5	6.6	0.5
Coarse Hanford	2.81×10^{-17}	1.42×10^{-3}	139	2.8	50	4.4	8.2	0.5
Fine Hanford	2.79×10^{-17}	1.41×10^{-3}	148	2.8	53	4.7	9.2	0.5

[a] na: not available.

Table 2.6: Annual radioactivity exposure doses for adults due to water consumption and conditions assumed to calculate the dose. Cases 1 and 2 are based on different radioactivity-to-dose conversion factors.

Condition	Case 1	Case 2
Travel time in vadose zone (years):	40	40
Initial cesium loading on colloids (pCi/g):	$1 \times 10^{7,a}$	$1 \times 10^{7,a}$
Initial colloid conc. in pore water (mg/L):	50	50
Colloids remaining in pore water after 40 years (%):	0.05	0.05
Recharge rate (m/year):	0.1	0.1
Colloids remaining in pore water after 40 years (g/m^3):	0.025	0.025
Radioactivity in pore water (pCi/m^3):	2.5×10^5	2.5×10^5
Half-life of ^{137}Cs (years):	32	32
Radioactivity in pore water after 40 years of decay (pCi/m^2-year):	10,513	10,513
Conversion factor for ^{137}Cs (mrem/pCi):	$4.81 \times 10^{-5,b}$	$2.17 \times 10^{-7,c}$
Human water consumption (L/day):	3	3
Annual dose (mrem/year):	0.554	0.003

[a] Value reported by McKinley et al. [2001]

[b] Value reported by US-DOE [2004]

[c] Value reported by Harrach and Surrano [2004]

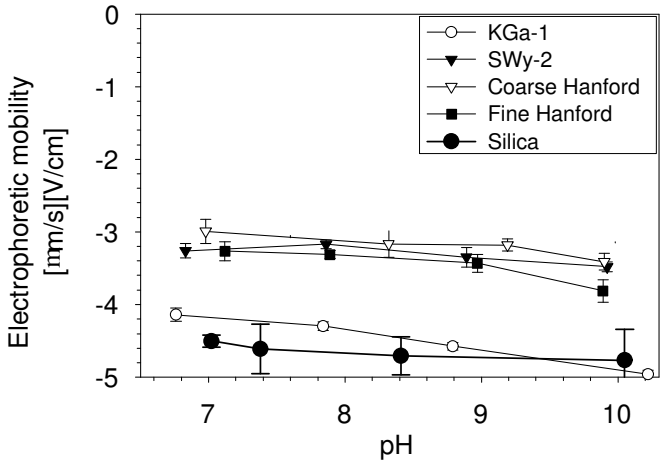

Figure 2.1: Electrophoretic mobility between pH 7 and 10 of the colloids used in this study. Error bars denote ± one standard deviation. Electrophoretic mobilities were determined in 0.01 M NaCl with dynamic light scattering using a Zetasizer 3000HSA with a helium-neon laser of 633 nm wavelength (Malvern Instruments Ltd., Malvern, UK) with particle concentrations adjusted to be between 0.1 and 20 mg/L.

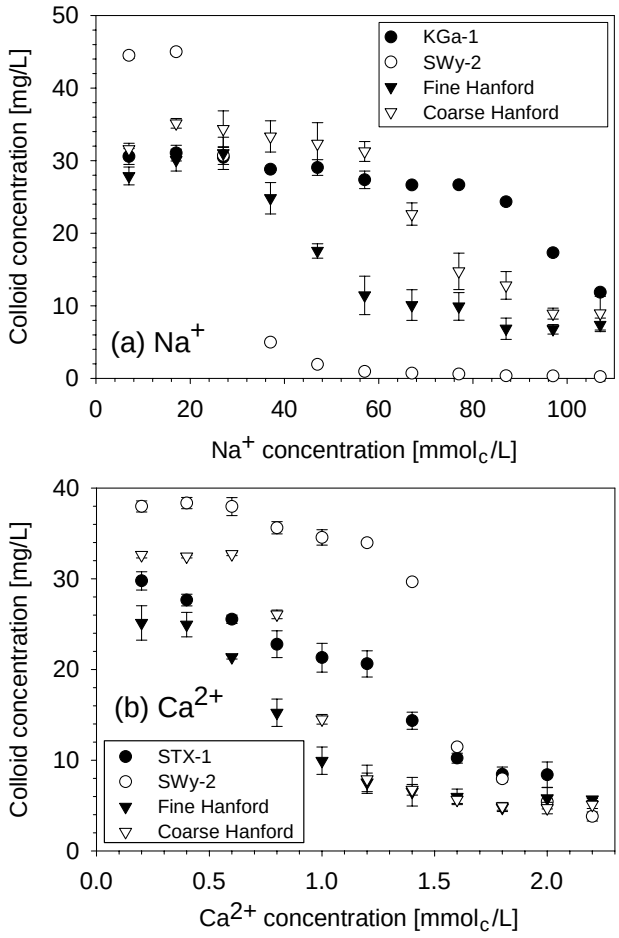

Figure 2.2: Colloid stability at pH 10 as function of (a) Na concentrations (SAR = ∞) and (b) Ca concentrations (SAR = 0). Error bars denote $\pm$ one standard deviation.

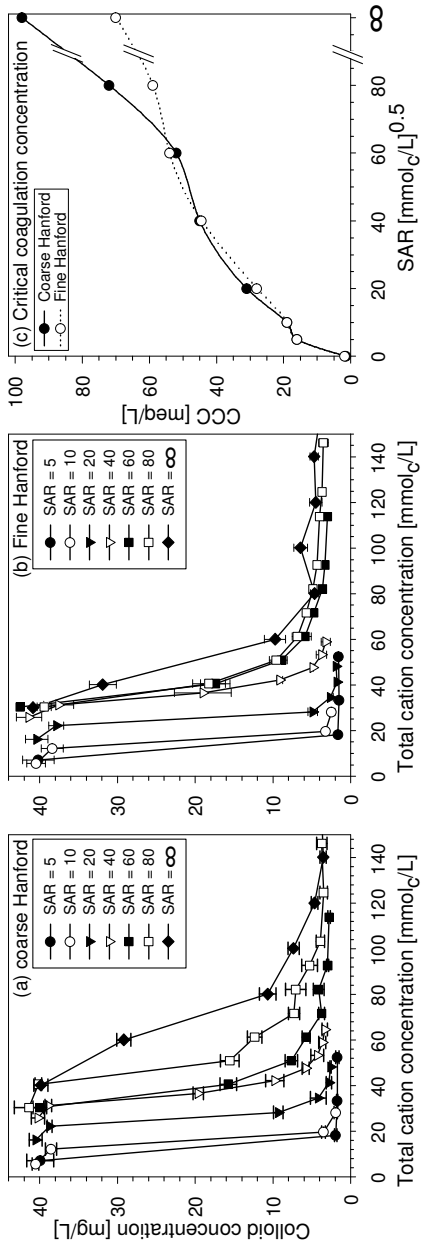

Figure 2.3: Effect of sodium adsorption ratio (SAR) on colloid stability of Hanford colloids at pH 10. (a) Coarse Hanford colloids, (b) fine Hanford colloids, and (c) critical coagulation concentrations (CCC) as function of SAR. Error bars denote ± one standard deviation.

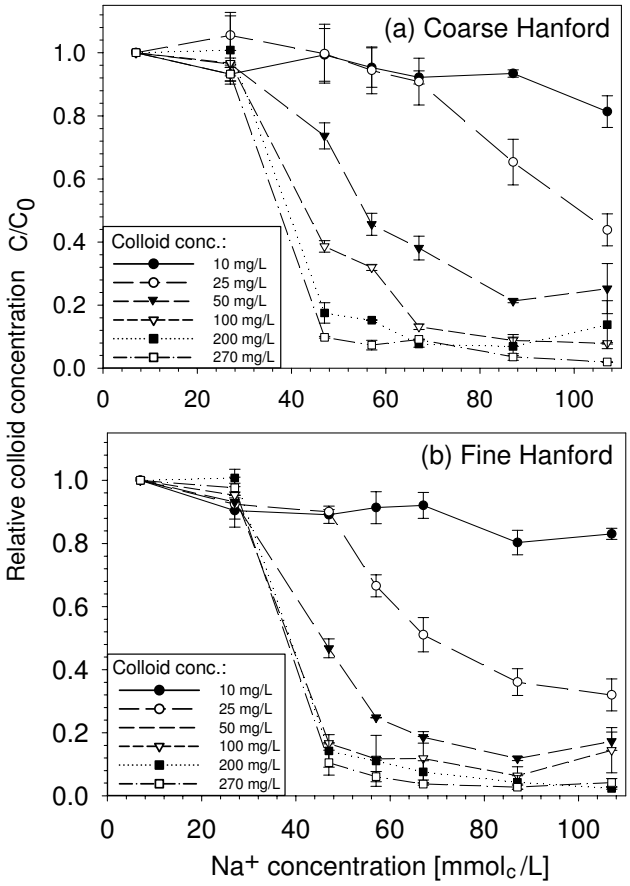

Figure 2.4: Effect of initial colloid concentration on colloid stability in Na electrolyte solutions (SAR = ∞) at pH 10 for (a) coarse and (b) fine Hanford colloids. Colloid concentrations are normalized with the initial colloid concentration in each experiment. Error bars denote ± one standard deviation.

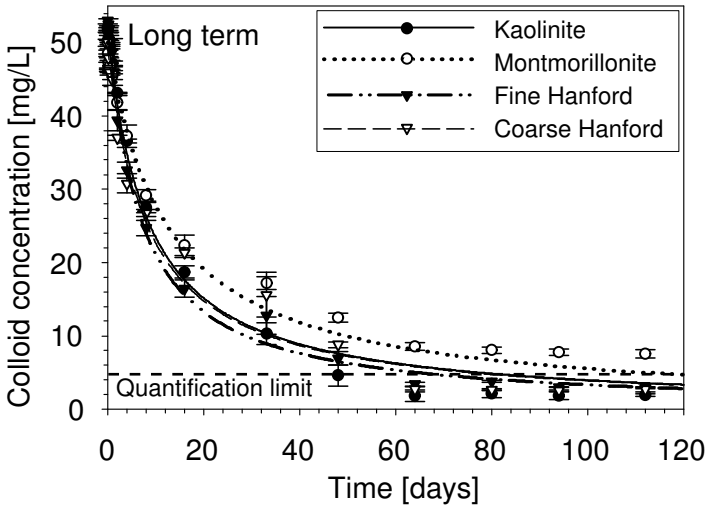

Figure 2.5: Colloid suspension concentration as a function of time in the long-term batch experiments in a pH 10 buffered 1.67 mM $Na_2CO_3/NaHCO_3$ solution. Symbols are experimental data and lines are fitted 2nd-order kinetic model. Error bars denote $\pm$ one standard deviation.

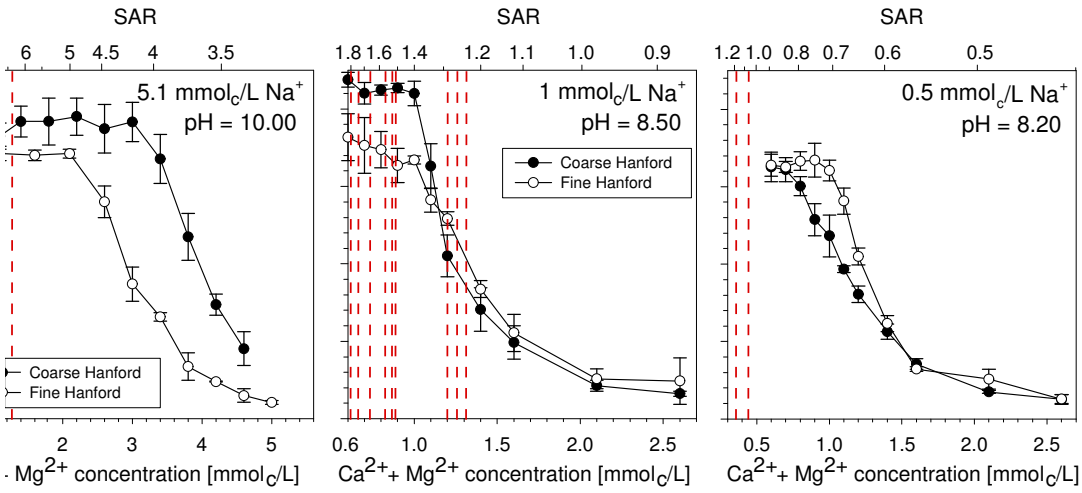

Figure 2.6: Colloid stability in mimicked Hanford pore waters for different Ca concentrations at three constant Na concentrations (a) 5.1 mmol$_c$/L, (b) 1 mmol$_c$/L, and (c) 0.5 mmol$_c$/L. Concentrations of K and Mg were kept constant at 0.2 mmol$_c$/L K and 0.6 mmol$_c$/L Mg. Dashed lines indicate Ca and Mg concentrations in vadose zone Hanford sediments measured by Serne et al. (2002b), and represent *in situ* pore water chemistry from several boreholes (Table 2.3).

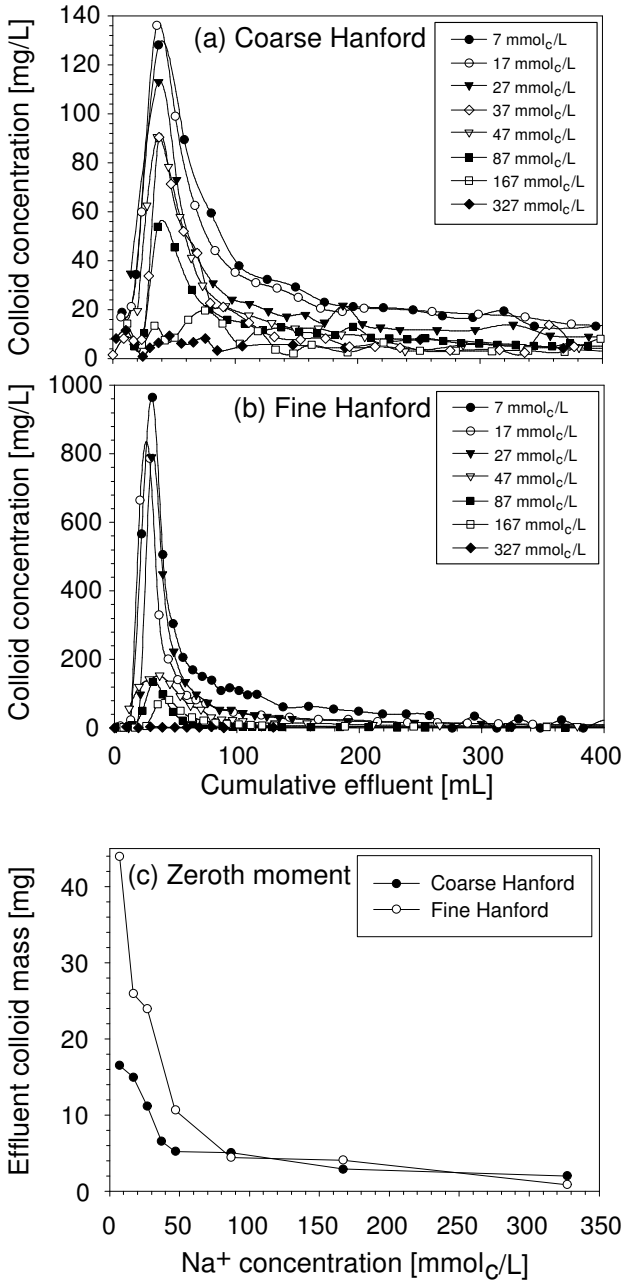

Figure 2.7: Colloid effluent concentrations for different eluent Na concentrations (SAR $= \infty$) for (a) coarse and (b) fine Hanford sediments, and (c) total mass (zeroth moment) of colloids eluted as function of electrolyte concentration. Inflow solutions were buffered at pH 10, 1 pore volume $\approx$ 21 mL cumulative effluent.

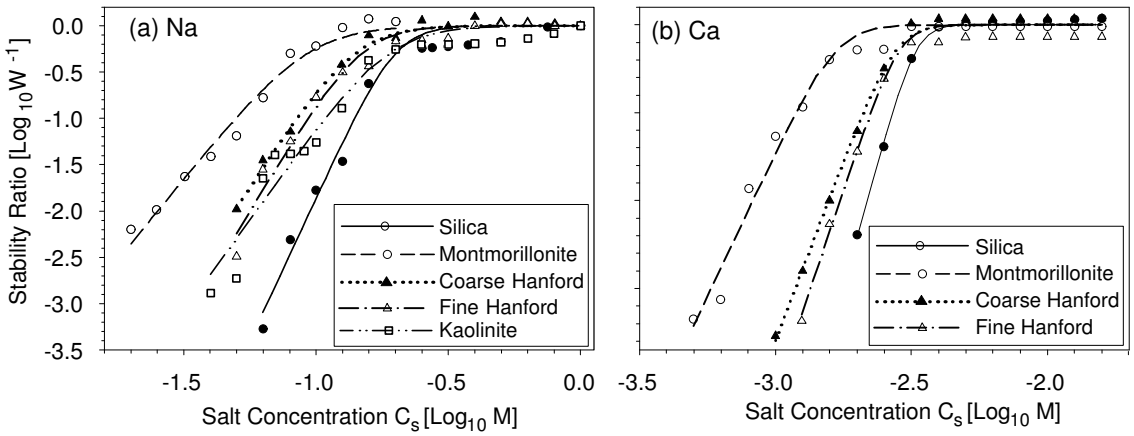

Figure 2.8: Inverse stability ratio W^{-1} at pH 10 as a function of (a) Na and (b) Ca concentration. The symbols indicate the experimentally determined values (equation 2.2), and the lines are best fits of equation (2.3).

2.7 Appendix A

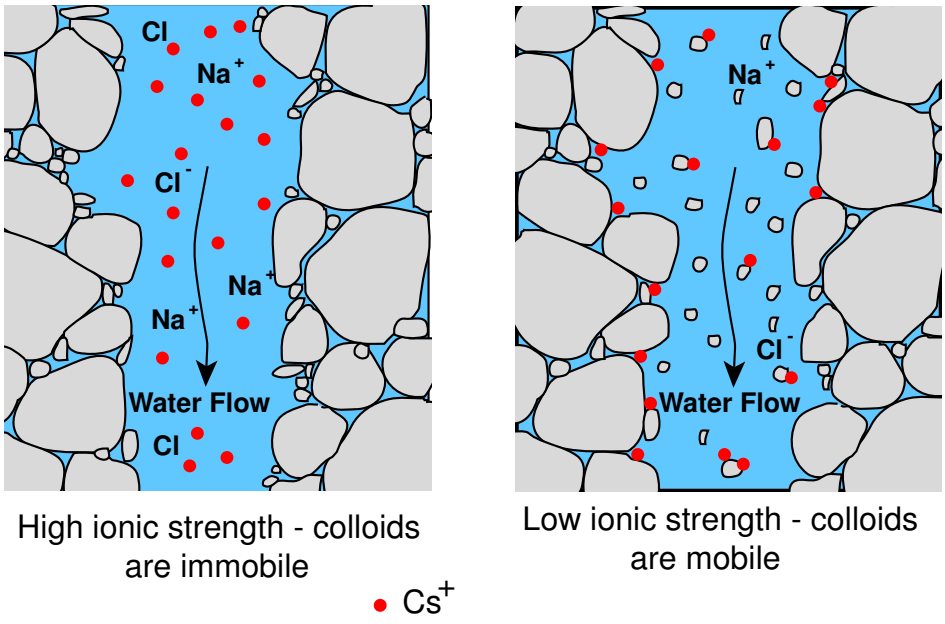

Figure 2.9: Effect of low and high ionic strengths on colloidal mobility and on the transport of radionuclides. At low ionic strength (right) colloids are stable and mobile in the pore water and might facilitate cesium transport.

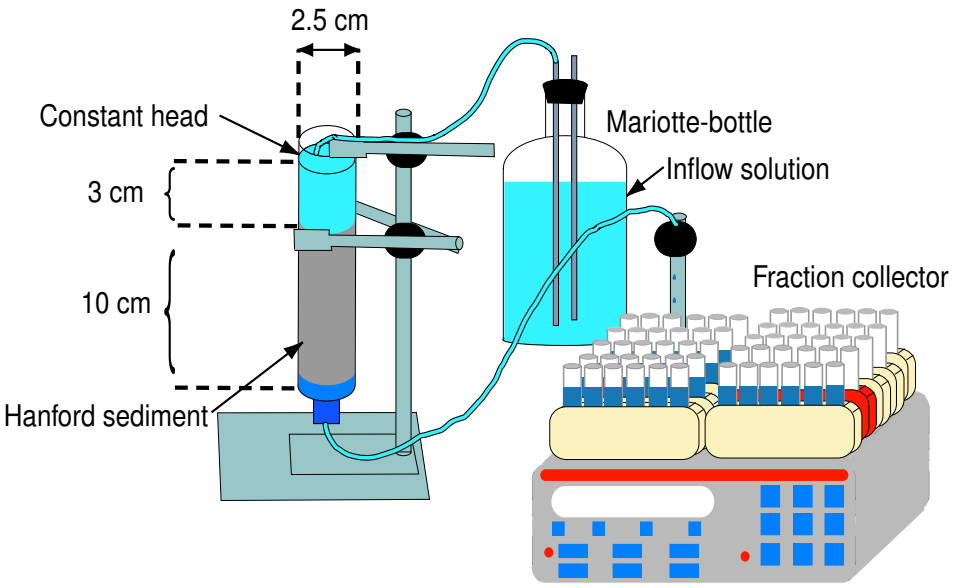

Figure 2.10: Schematic of the experimental setup of the column mobilization experiments.

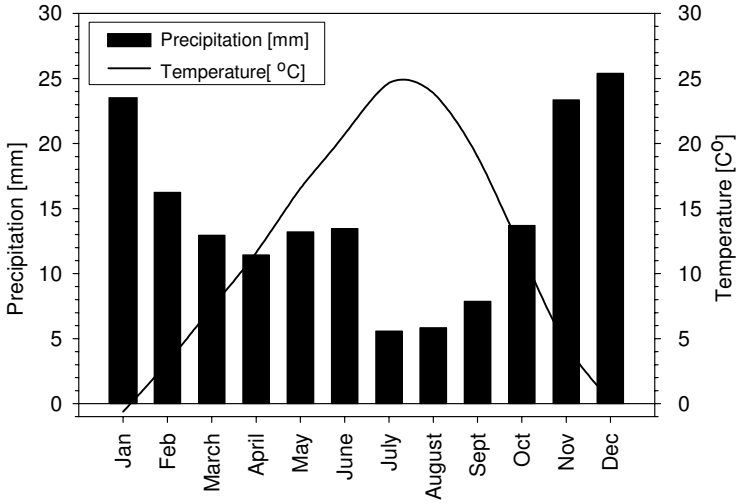

Figure 2.11: Average monthly temperatures and precipitation at Hanford (data collected from 1912 to 1980). Figure drawn based on data from Stone et al. [1983] and Hoitink et al. [2002].

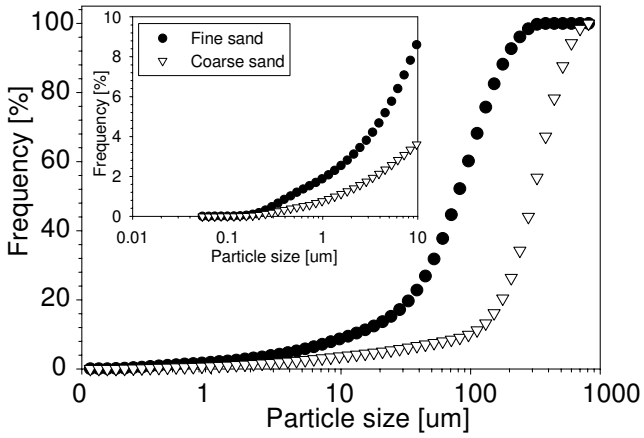

Figure 2.12: Particle size distribution of the fine and coarse Hanford sediment. The inset magnifies the colloid fraction.

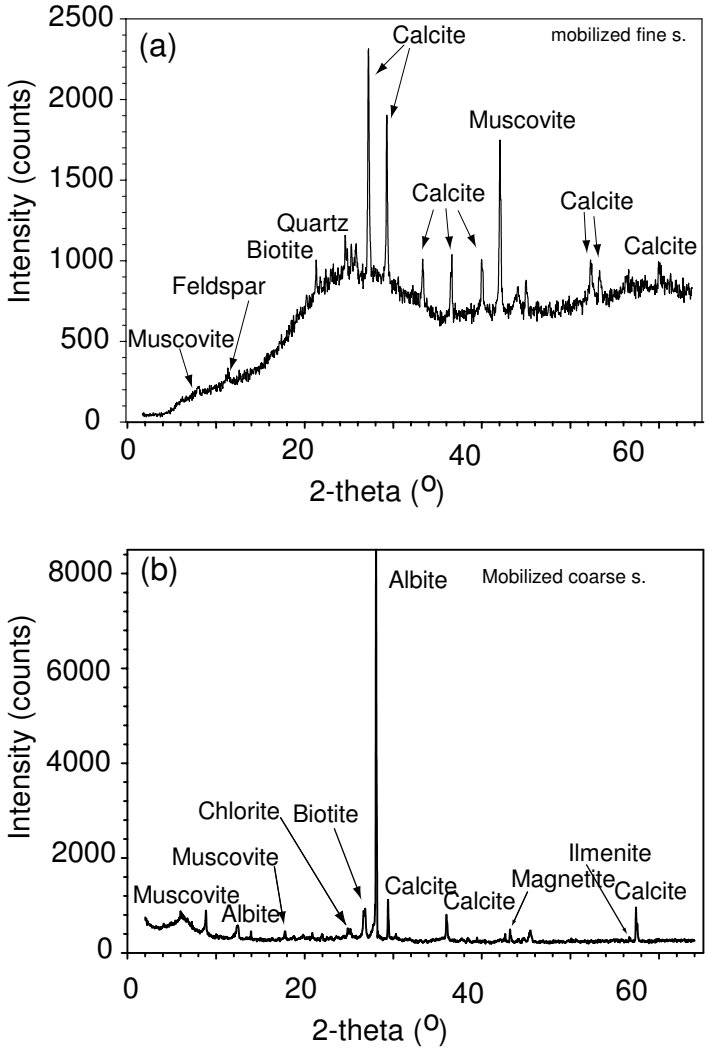

Figure 2.13: XRD diagram of the (a) fine and (b) coarse Hanford sand effluent colloids (7 mmol_c/L).

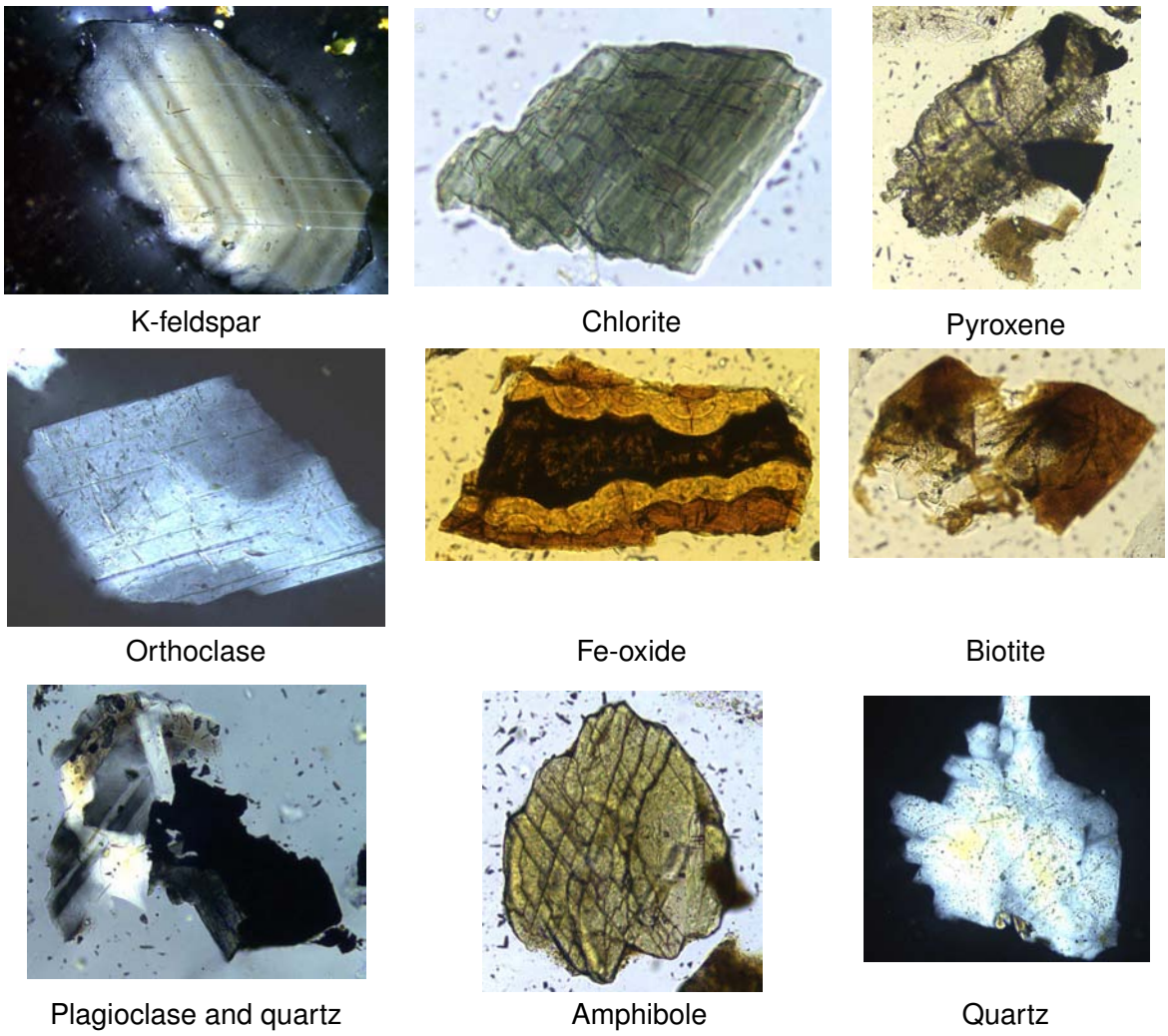

Figure 2.14: Thin section images of mobilized minerals from the bulk coarse Hanford sediment.

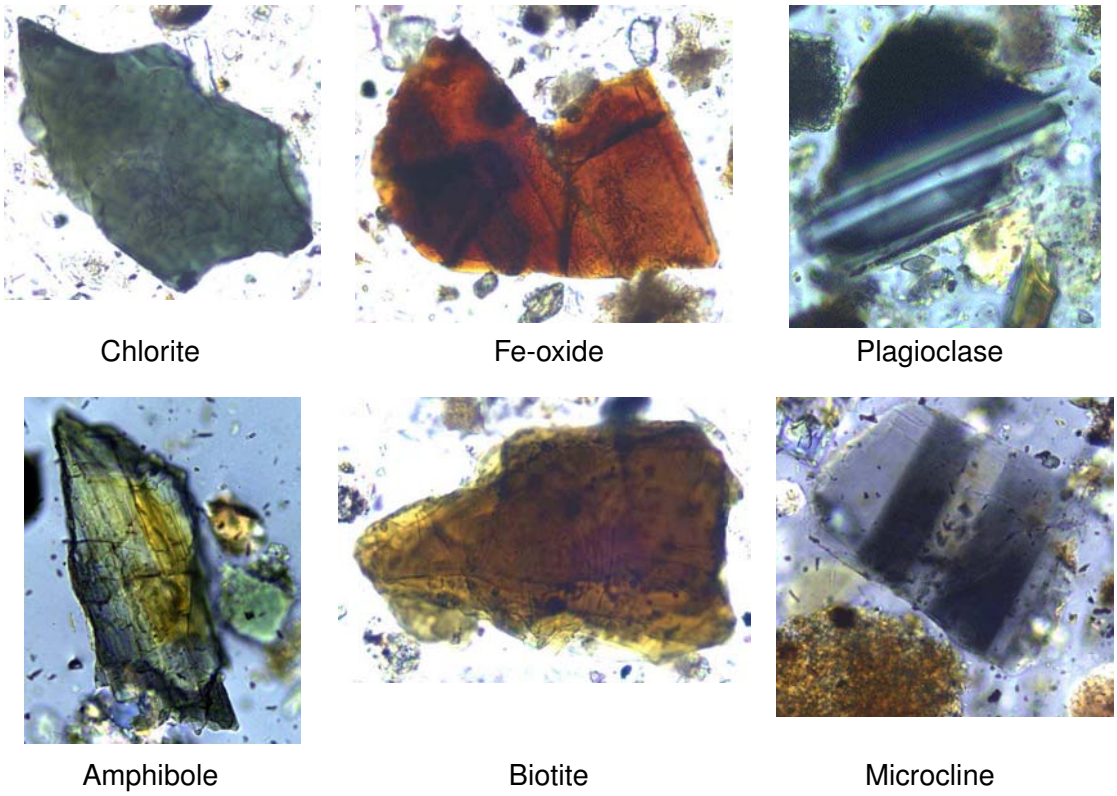

Figure 2.15: Thin section images of mobilized minerals from the bulk fine Hanford sediment

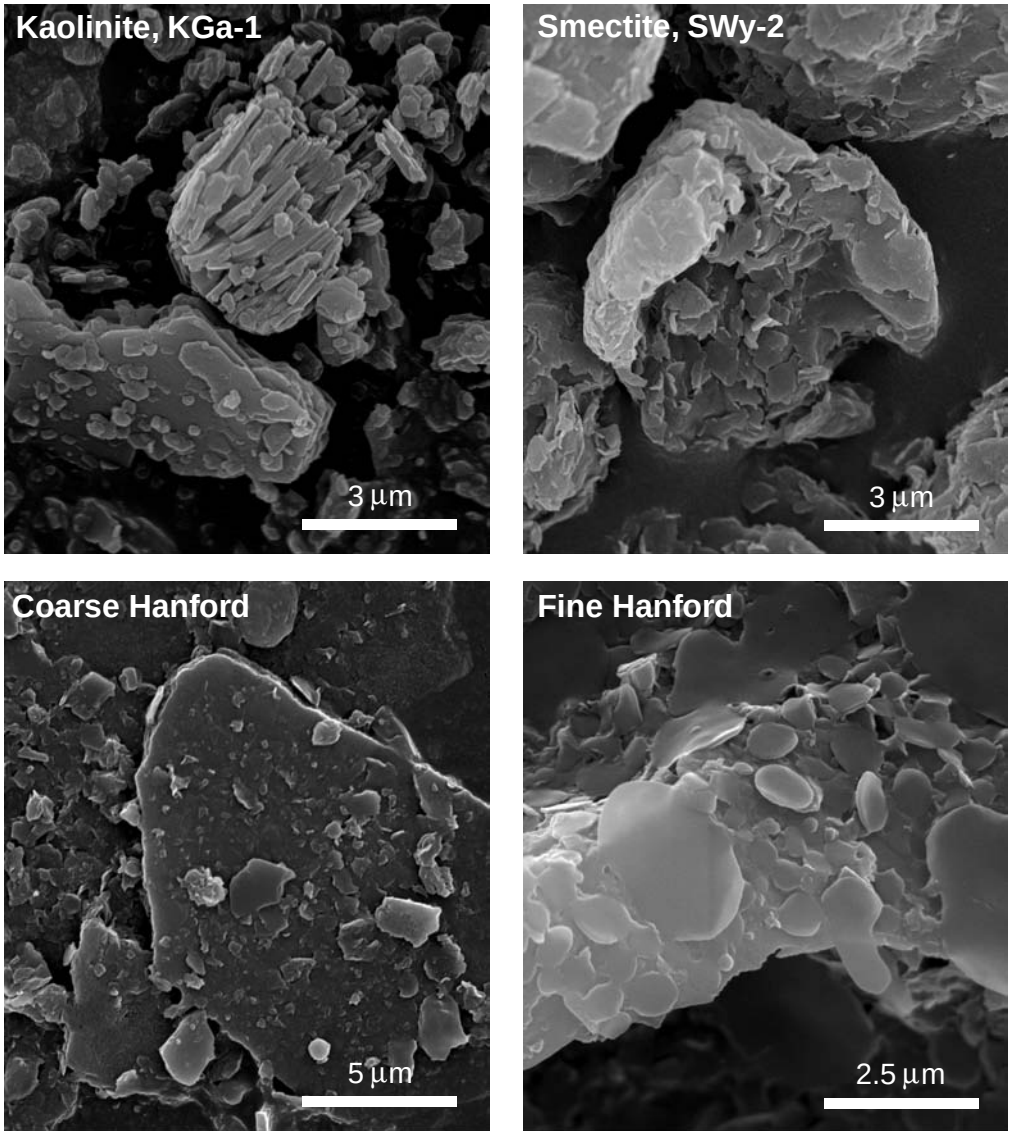

Figure 2.16: SEM micrographs of four of the colloids used in the colloid stability study.

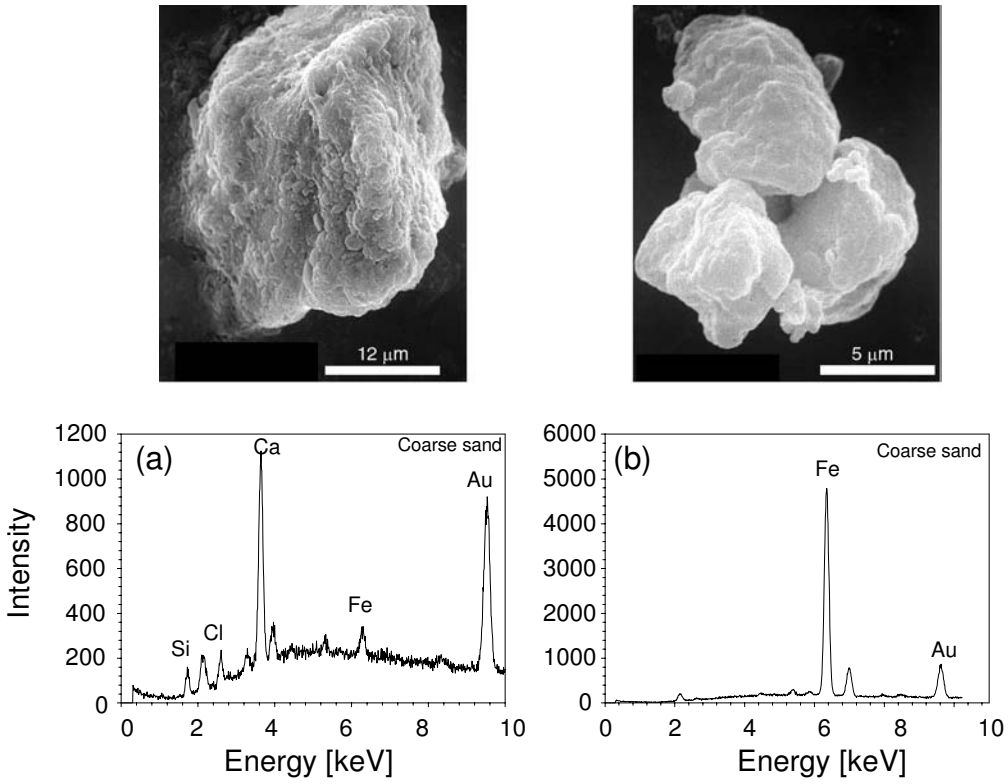

Figure 2.17: SEM-EDAX spectrum of colloidal aggregates mobilized from the coarse Hanford sands. EDAX spectrum (a) depicts a calcite and spectrum (b) illustrates an Fe-oxide particle.

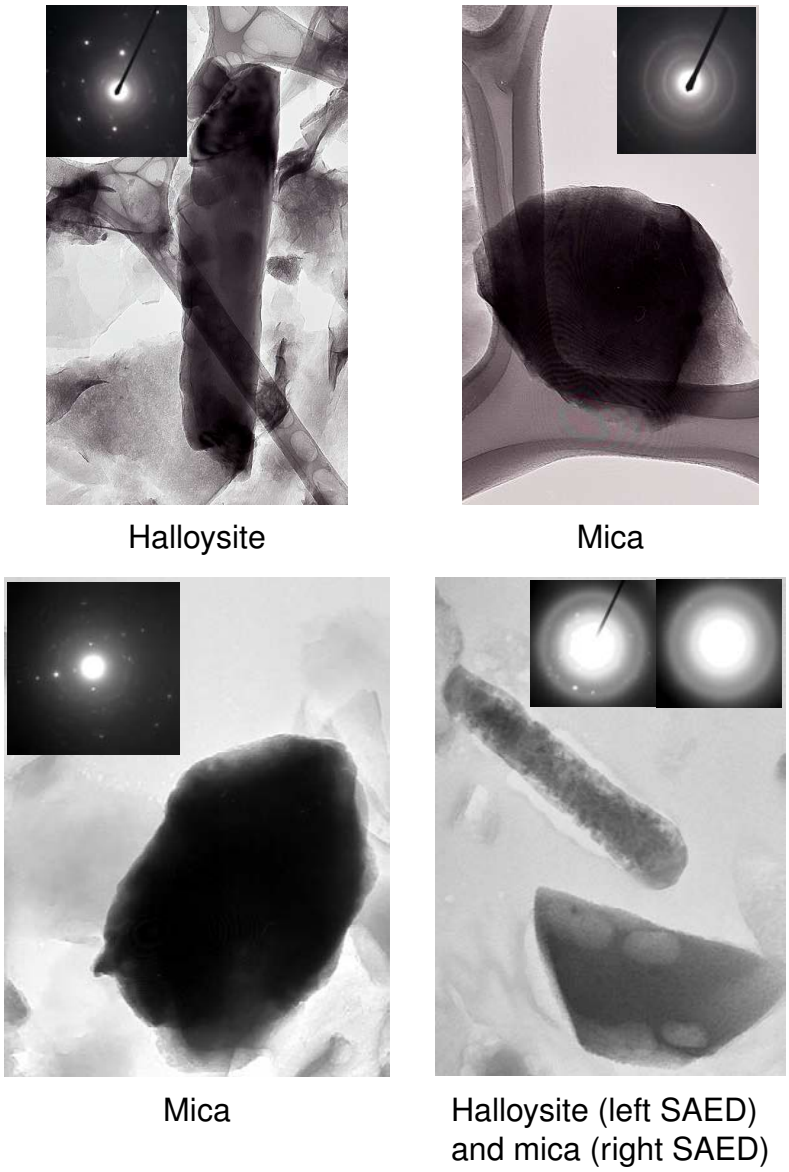

Figure 2.18: TEM micrographs of colloids mobilized from the coarse Hanford sand column.

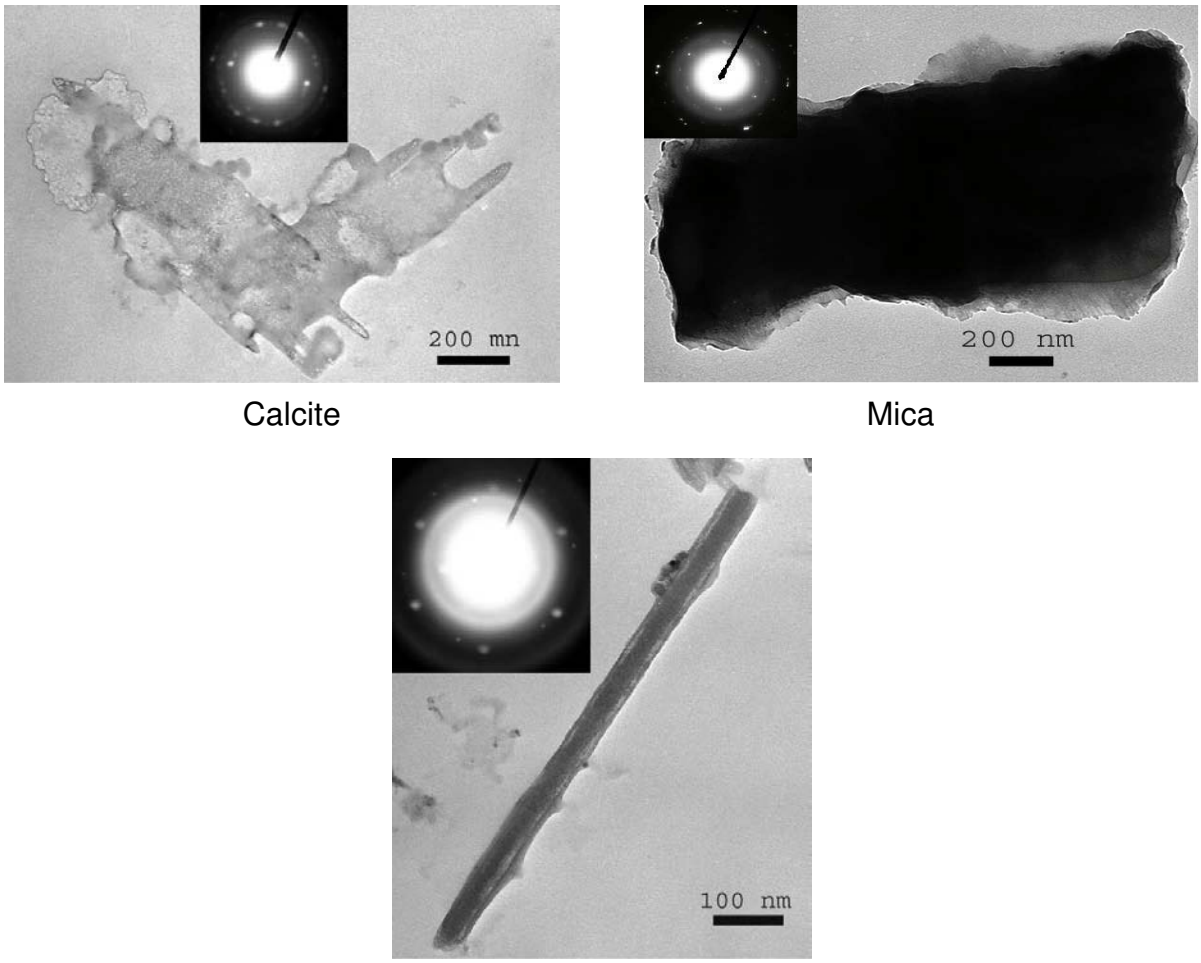

Figure 2.19: TEM micrographs of colloids mobilized from the fine Hanford sand column.

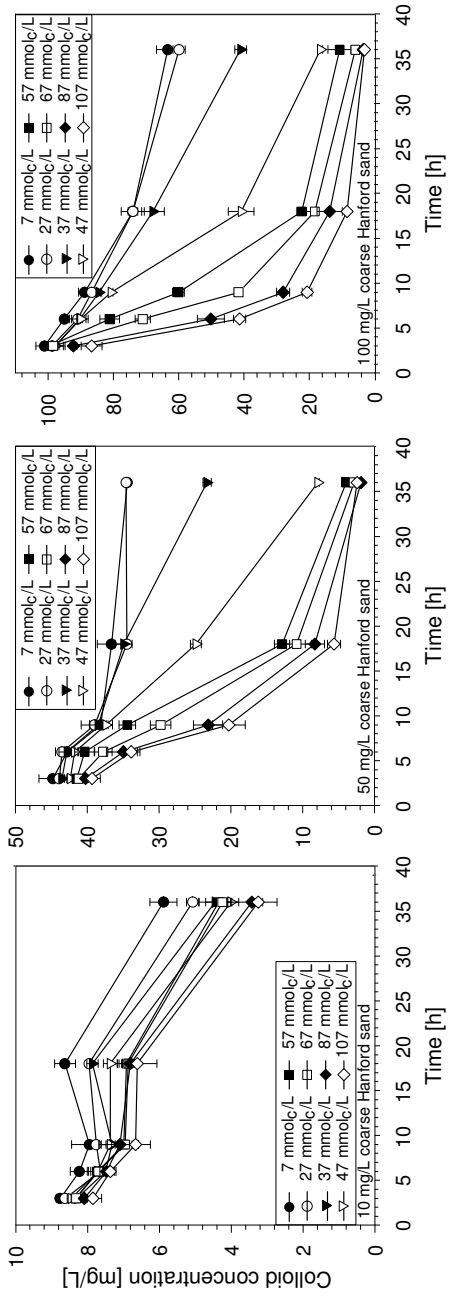

Figure 2.20: Effect of settling time on stability of coarse Hanford colloids in Na electrolyte solutions (SAR = ∞) at pH 10 for different initial colloid concentrations: (a) 10 mg/L, (b) 50 mg/L, and (c) 100 mg/L. Error bars denote $\pm$ one standard deviation.

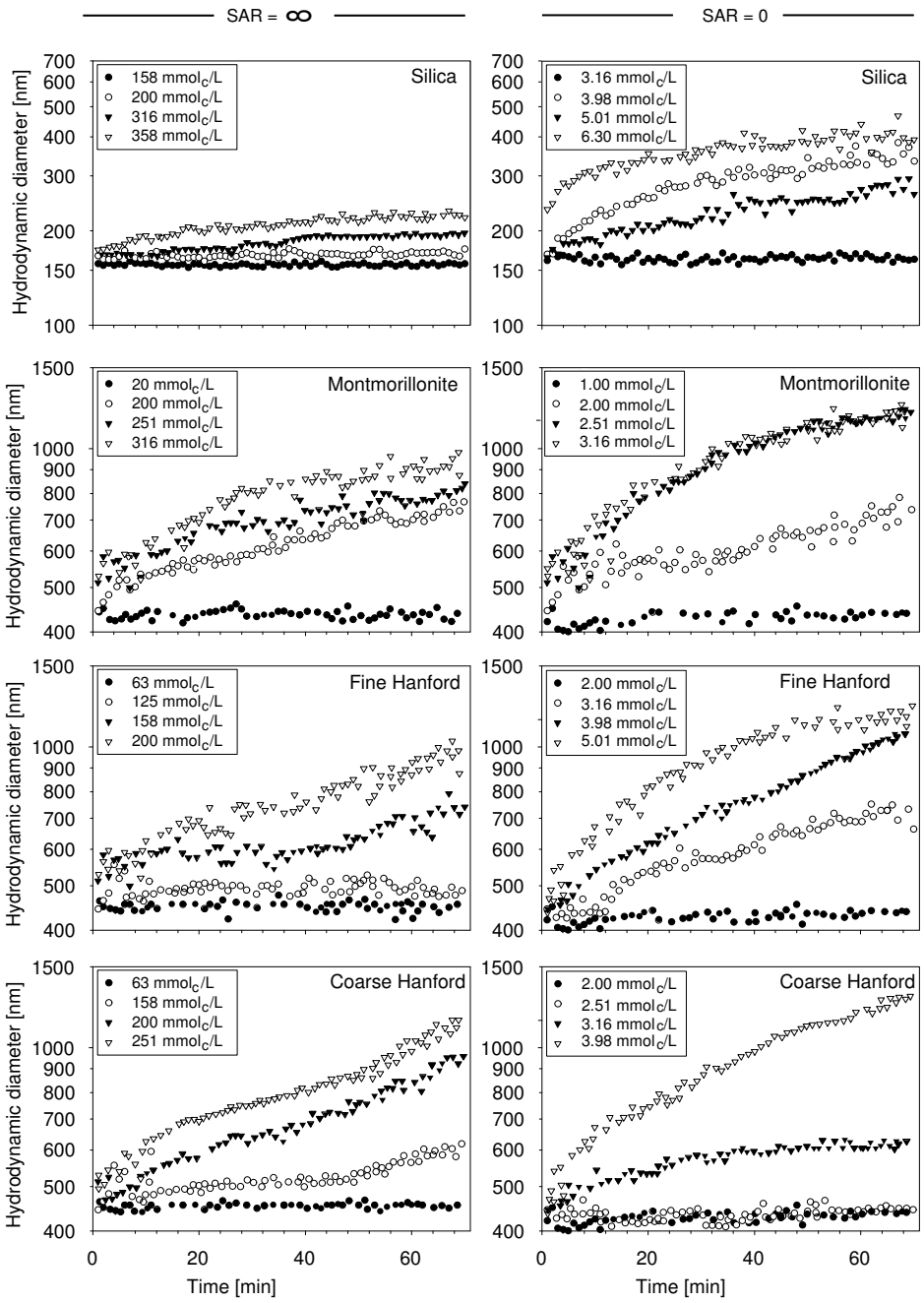

Figure 2.21: Hydrodynamic colloid diameter (Z-averaged) as function of time for selected electrolyte concentrations at pH 10.

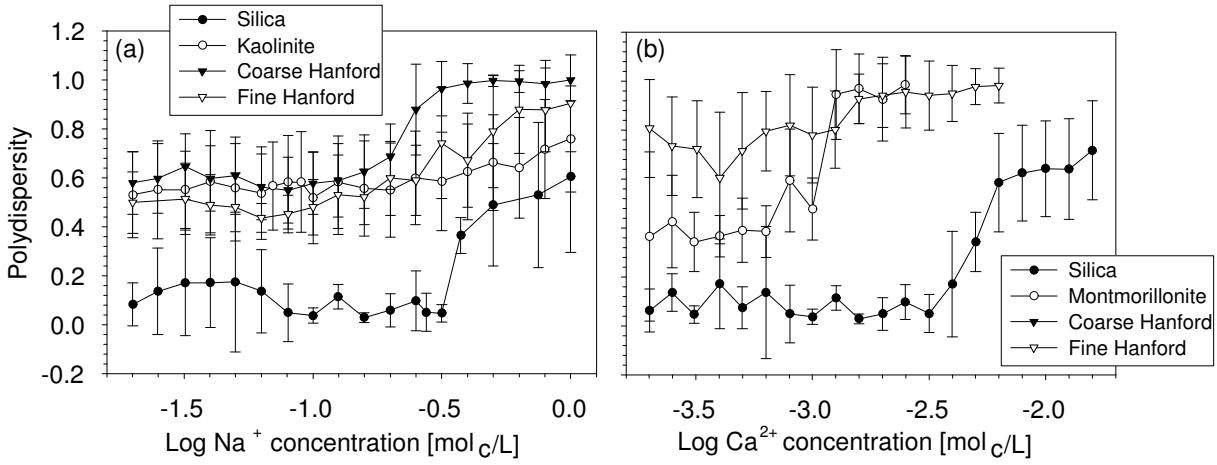

Figure 2.22: Changes in polydispersity as a function of (a) sodium, and (b) calcium concentration for selected colloids.

Chapter 3

Suitability of Fiberglass Wicks to Sample Colloids from Vadose Zone Pore Water

3.1 Abstract

Fiberglass wicks are frequently used to sample pore water and determine water fluxes in soils. In this study we evaluated the performance of fiberglass wicks to sample colloids. Different colloids were used for the wick testing: feldspathoids, ferrihydrite, montmorillonite, kaolinite, and a mixture of mineral colloids extracted from a coarse calcareous sediment. The average diameter of the colloids was about 500 nm, except for the ferrihydrite, which was 3 to 10 nm in diameter. The colloids were dispersed in either a buffered Na_2CO_3/$NaHCO_3$ solution (ionic strength 6.7 mM, pH 10) or

This chapter has been accepted for publication: Czigány, S., M. Flury, J. B. Harsh, B. C. Williams, and J. M. Shira: Suitability of Fiberglass Wicks to Sample Colloids from Vadose Zone Pore Water, Vadose Zone J. (in press).

deionized water. Colloid breakthrough curves through 77-cm long fiberglass wicks were determined for three different flow rates. Flow rate, pH, and colloid type affected colloid breakthrough. Colloid recovery in the effluent was higher at pH 10 than at pH 7, and increased with increasing flow rate. The mixture of mineral colloids extracted from sediment moved almost conservatively through the wicks; the colloid recoveries ranged from 88 to 103%. All other colloids; however, showed lower mass recoveries. At pH 10, colloid recovery ranged from 12% for ferrihydrite to 100% for the mixture of mineral colloids, whereas at pH 7, the recovery ranged from 0% for kaolinite and ferrihydrite to 95% for the mixture of mineral colloids. These results suggest that for certain conditions and colloid types, fiberglass wicks can be an acceptable tool for colloid sampling in the vadose zone. However, under many conditions studied here colloids were significantly retained inside the wicks, and consequently, the use of wicks for colloid sampling in the vadose zone must be considered with caution.

3.2 Introduction

Different techniques are used to sample pore water in the vadose zone, such as free-drainage lysimeters, suction cups or porous plates, and fiberglass wicks or rockwool samplers. Each of these devices has advantages and disadvantages. Free-drainage lysimeters only operate when the soil becomes saturated, and thereby cause hydrodynamic artifacts [*Abdou and Flury*, 2004]. These artifacts are eliminated when using a porous material on which a suction is pulled to remove the pore water from the soil.

Different types of porous materials have been used for that purpose, including ceramic materials, stainless steel, Teflon, or fiberglass.

Fiberglass wicks are attractive because no external vacuum device is needed to extract pore water. They were introduced as pore water samplers by *Brown et al.* [1988] and have been used since in numerous studies [*Gee and Campbell,* 1990*; Boll et al.,* 1992*; Brandi-Dohrn et al.,* 1996*; Louie et al.,* 2000*; Brahy et al.,* 2002*; Cox et al.,* 2002]. The volume of the soil sampled by the wicks can be closely estimated [*Boll et al.,* 1991]. Wick lysimeters are relatively cheap and easy to maintain. The length of the hanging wick determines the suction exerted on the soil above, and it needs to be matched with the soil type and the particular experiment [*Rimmer et al.,* 1995]. Wick lysimeters can collect pore water samples from soils with a wide range of structure [*Holder et al.,* 1991].

Fiberglass wicks need to be cleaned before their use for sampling, as they may contain organic residues [*Knutson et al.,* 1993]. *Knutson et al.* [1993] recommended combustion at 400^{o}C for 3 hours to remove impurities, unless the wicks contain more than 3.5% w/w impurities, for which higher temperature and longer combustion time may be needed. Additional treatments, such as an acid wash in 10 mM HNO_3, may be required if wicks are used to determine pore water composition [*Goyne et al.,* 2000]. *Brahy and Delvaux* [2001] suggest that, besides acid treatment, the wicks should be soaked in deionized water until the electrical conductivity of the water falls below 2 μS/cm.

Wicks have been tested extensively in terms of water and solute collection efficiency [*Boll et al.*, 1991; *Steenhuis et al.*, 1995; *Zhu et al.*, 2002]. Experimental and numerical studies indicate that wicks are useful in determining water fluxes in the vadose zone [*Louie et al.*, 2000; *Gee et al.*, 2002; *Gee et al.*, 2003]. Solute transport characteristics of wicks were assessed with anions and organic dyes, and it is generally reported that dispersion and retardation is much smaller in wicks than in soils [*Boll et al.*, 1992; *Poletika et al.*, 1992; *Knutson and Selker*, 1996]. Only a few studies are available on colloid transport in fiberglass wicks. The results of these studies are inconsistent in terms of the usefulness of wicks for colloid sampling. *Poletika et al.* [1992] reported that only 28.8–52% of an MS-2 virus was recovered in wick outflow. *Biddle et al.* [1995] found that colloids of particle diameter between 0.45 and 2 μm were not retained in the wicks, and colloid mineral composition in the effluent did not differ from that of the bulk soil [*Biddle et al.*, 1995]. It remains to be shown whether fiberglass wicks are useful to sample colloids.

The objective of this study was to systematically test fiberglass wicks for their suitability to sample vadose zone colloids. We conducted transport experiments with five types of colloids: kaolinite, montmorillonite, ferrihydrite, feldspathoids, and colloids extracted from a calcareous sediment. Colloids were directly applied to the top of the wicks and breakthrough curves determined in the outflow. Solution pH was either 7 or 10, and three different flow rates were used.

3.3 Materials and Methods

3.3.1 Colloidal Material and Fractionation

We used different types of colloids in this study: colloids extracted from sediments (mixture of minerals) and mineralogically homogeneous colloids (montmorillonite, kaolinite, and ferrihydrite). The sediments used as colloidal source material were gravelly-sandy, very coarse Hanford sediments obtained from the submarine pit (218-E-12B) at the Hanford site, WA, in January 2000. *Serne et al.* [2002] provide a detailed description of the Hanford formation sediments. The mineralogy of the sediments is dominated by quartz, phyllosilicates (primarily micas, illites, and smectites), and feldspars. Plastic buckets were used to collect and store the sediments. The sediments were air-dried and sieved through a 2-mm square screen. This material served as the source for the "native colloids." An aliquot of the sediments was treated with an alkaline solution, which caused quartz and kaolinite to dissolve, and the feldspathoids, cancrinite and sodalite, to precipitate [*Zhao et al.*, 2004]. These treated sediments served as a source for the "modified colloids". Pure clay mineral standards, Na-montmorillonite (SWy-2) and Na-kaolinite (KGa-1), were obtained from the Clay Minerals Repository (Columbia, MO). Two-line ferrihydrite was synthesized according to *Schwertmann and Cornell* [2000, *p. 105-111*], whereby 10 mmol/L Si was used in the synthesis procedure to stabilize the mineral and prevent mineral transformations. We used X-ray diffraction (Philips XRG 3100, Philips Analytical Inc., Mahwah

NJ) to verify whether the ferrihydrite was stable over the course of the experiments. The shape of ferrihydrite particles was examined by Transmission Electron Microscopy (JEOL 1200EX) and found to be roughly spherical.

To fractionate the colloidal fraction, about 1 kg of Hanford sediments or 200–250 mg of clay mineral standards were dispersed in 1-L glass cylinders. We used two different solutions to disperse the solids: (1) deionized water and (2) a 1.67 mM Na_2CO_3/$NaHCO_3$ solution (pH 10). Dispersions were stirred with a rod, sonicated for 10 minutes, and briefly shaken end-over-end by hand. Colloids, operationally defined as material with equivalent diameter of < 2 μm, were fractionated by decantation based on Stokes' sedimentation law. The mineralogy of the fractionated "native colloids" was dominated by chlorite, smectite, vermiculite, kaolinite, and quartz [*Cherrey et al.,* 2003], and the "modified colloids" were dominated by cancrinite, sodalite, chlorite, smectite, and vermiculite. Ferrihydrite was not fractionated because its particle size was much less than 2 μm. The colloid suspensions were diluted to a particle concentration of about 50 mg/L and used for the wick experiments decribed below. Colloid suspensions were sonicated for 30 minutes before the start of the wick experiments. Colloids were used within at most seven days after fractionation.

Average hydrodynamic diameter and electrophoretic mobility of the colloids were measured by dynamic light scattering (ZetaSizer 3000HSa, Malvern Instruments Ltd., Malvern, UK). Particle size and the electrophoretic mobility were determined in a weak electrolyte solution (1.67 mM $NaHCO_3$/1.67 mM Na_2CO_3).

3.3.2 Wick Treatment and Characterization

Fiberglass wicks of 12.5 mm diameter were obtained from Pepperell Braiding Co. (catalog no. 1381, Pepperell, MA). We treated the wick with a procedure described by *Goyne et al.* [2000]. The wicks were first cut into 77-cm long pieces, weighed, rinsed extensively with deionized water, and combusted in a kiln at 400^{o}C for four hours. The wicks were weighed after combustion to determine the weight loss. Then, they were soaked in deionized water (EC = 3.8 μS/cm) in a 17-L Tupperware plastic container. Six wicks were treated simultaneously. We measured pH and electrical conductivity daily. Water was replaced with clean deionized water each day, until pH and conductivity were constant. It took five to six days to reach constant pH and electrical conductivity. The equilibrated wicks were soaked in a 10 mM HNO_3 solution in the same container. The solution was replaced daily for seven days. After the acid treatment, wicks were soaked again in deionized water for 7 days. It took four to six days to reach a constant pH and EC.

Treated and untreated (as shipped from supplier) wicks were characterized by scanning electron microscopy (SEM) and surface area determination. The SEM images were taken on gold coated samples with a Hitachi S-570 SEM. We also took SEM images of wicks after they were used for colloid transport experiments to check for colloid deposition. For BET surface area determination, about 5 g of wick material was used (ASAP 2010, Micromeritics Inc., Norcross, GA). The specific density of wicks was measured on individual wick braids with a Le Chatelier pycnometer [*ASTM,*

2000]. The bulk density was approximated by weighing oven-dried pieces of wicks and estimating the volume using a circular wick cross section. The porosity was then calculated from these measurements. Quantitative measurements were made with three replicates.

3.3.3 Experimental Setup for Breakthrough Curves

The wick was mounted into an acrylic tube (18.5 mm i.d., length 68.5 cm) topped by a Plexiglas disc 9 cm in diameter (Figure 3.1). The top 4.5 cm of the wick was unwoven and the individual braids were spread and tightened to the disc with a Plexiglas ring and three binder clips. A steady-state flow rate was established by dripping solution onto the center of the wick from a point dripper. The flow rate was controlled with a peristaltic pump (Ismatec IP4, Glattburg, Switzerland). The top of the wick was covered with a plastic beaker and a wrap to minimize evaporation.

Comment: Photographs of the column experimental setup are shown in the Appendix B (Figure 3.9). ■

3.3.4 Nitrate and Colloid Breakthrough Curves

Nitrate and colloid breakthrough curves were carried out at three different flow rates: 5, 10, and 55 mL/h. First, the wick was equilibrated with at least 12 pore volumes

at a flow rate of 55 mL/h, and the flow rate was then adjusted to the desired value. A new wick was used for each experiment to avoid contamination between experiments. Consequently, the wick pore volume slightly differed from run to run. We ran some experiments with the same wick to check for "history" effects in the wick. All experiments were carried out at a room temperature of 22±1°C.

Nitrate was used as a conservative tracer. A pulse of about three pore volumes of 0.2 mM $NaNO_3$ was injected into the wicks. Effluent NO_3^- concentrations were determined with a UV-VIS spectrophotometer (Hewlett Packard HP8452A) at 214 nm wavelength. The pH of the solutions for these experiments was between 6.5 and 7.5.

For the colloid breakthrough experiments, the wicks were first equilibrated with the desired solution, either deionized water (pH ≈ 6.5) or a buffered 1.67 mM $NaHCO_3$/1.67 mM Na_2CO_3 solution (pH 10) for at least 12 pore volumes. The inflow solution was then switched to a ≈50 mg/L colloid suspension for two to four pore volumes. The inflow suspension was continuously stirred at low speed with a magnetic stirrer. Effluent pH was determined with a pH meter and colloid concentrations were determined spectrophotometrically at 300 nm wavelength. Before the measurements, individual vials were vigorously shaken by hand to re-suspend any sedimented particles. The effluent flow rate was determined by weighing every sixth vial. After each breakthrough experiment, wicks were dried at 105°C for 24 hours, and the overall water content was determined gravimetrically. This water content was used to estimate pore

volumes for the breakthrough experiments. Some experiments were repeated to test reproducibility of the results.

To obtain more detailed information about the water content distribution in the wicks, we equilibrated clean wicks with colloid-free buffered solution at the three flow rates used for the colloid transport experiments. The wicks were then cut into 11-cm long pieces, which were oven-dried to determine the water content.

3.4 Results and Discussion

3.4.1 Colloid Properties

The hydrodynamic diameters of the colloids are summarized in Table 3.1. The hydrodynamic diameters of native colloids, modified colloids, montmorillonite, and kaolinite were 475 to 620 nm. The ferrihydrite had the smallest averaged diameter of 3 to 10 nm. The electrophoretic mobilities as a function of pH are shown in Figure 3.2. The values depicted in Figure 3.2 are in the range typical for soil minerals [*Wu*, 2001]. The kaolinite particles had the most negative electrophoretic mobilities at both pH 7 and 10. At pH 7, the ferrihydrite particles had the least negative electrophoretic mobilities of all colloids. The point of zero charge for ferrihydrite was observed at pH≈6.2. Ferrihydrite remained mineralogically stable over the course of the experiments, the X-ray diffraction patterns indicated no mineral transformations.

3.4.2 Wick Treatment and Characterization

The weight loss of the wicks during combustion ranged from 0.5 to 1.5% by weight, which is in the lower range reported by *Knutson et al.* [1993]. When the wicks were soaked in deionized water after combustion, the pH of the water increased from 5.7 to 9.2 within the first 24 hours. After 4 to 6 days the pH remained constant. The pH of the HNO_3 solution remained fairly constant during soaking. The SEM micrographs show some impurities on the surface of the nontreated wicks (Figure 3.3a). The combustion and washing removed these impurities to a large degree, but not completely (Figure 3.3b). Some dark spots, likely caused by combustion, could be observed on the treated wicks. The specific surface areas were 0.48 ± 0.02 m^2/g for the nontreated wicks and 0.46 ± 0.02 m^2/g for the treated wicks. The specific density of the wick material was 2.10 ± 0.08 g/cm^3, and the bulk density was 0.29 ± 0.01 g/cm^3. The corresponding porosity was 0.86 ± 0.01 cm^3/cm^3.

3.4.3 Nitrate Breakthrough Curves

The overall water content of the wicks increased with increasing flowrate. At flow rates of 5, 10 and 55 mL/h, the overall gravimetric water contents of the wick material were 1.54 ± 0.10 g/g, 1.63 ± 0.06 g/g, and 1.78 ± 0.06 g/g, respectively. Exact values vary somewhat between different wick pieces. These water contents were used to estimate approximate pore volumes for the breakthrough experiments. We tested the water balance during the breakthrough experiments gravimetrically. For the 55 mL/h flow

rate, about 3% of the inflow water was lost by evaporation.

The detailed measurements of the water content distribution show that the top of the wick was considerably drier than the bottom (Figure 3.4). No significant differences were observed in the water content distribution among the different flow rates.

The nitrate breakthrough curves indicate that nitrate moved like a conservative tracer through the wicks. Nitrate broke through the wicks after about one pore volume and the breakthrough curves had no tailing (Figure 3.5). The shape of the nitrate breakthroughs was not affected by flow rate. The variability of the breakthrough curves within the same wick at different flow rates was small (Figure 3.5a). The variability among different wick pieces at the same flow rates was small as well (Figure 3.5b,c), indicating that different wick pieces behaved similarly in terms of nitrate transport.

3.4.4 Colloid Breakthrough Curves

The results of the colloid breakthrough curves are shown in Figures 3.6 and 3.7. While there was no effect of flow rate on nitrate transport, the flow rate did affect colloid transport. Generally, as flow rate decreased, fewer colloids were recovered in the effluent. This is consistent with filtration theory, assuming first-order deposition kinetics. The magnitude of the flow rate effect depended on colloid type, as the different colloids have different deposition rate coefficients. For native colloids, the flow rate effect was less pronounced than for modified colloids and pure mineral colloids.

For the deionized water experiments, the pH of the effluent was between 6.5 and

7.5, and we denote the pH of these experiments as pH≈7. For the Na_2CO_3/$NaHCO_3$ solutions, the pH of the effluent was generally 0.5 to 1.0 pH units less than the pH of the influent, with a smaller pH drop when the flow rate was high. We denote the pH of these experiments as pH≈10.

Generally, colloid recovery was less at pH 7 than at pH 10. This can be explained by the increased electrostatic repulsion of colloids in the wicks. The surfaces of the wick silica fibers are negatively charged at the pH values of our experiments (point of zero net proton charge of amorphous silica is pH 3.5 to 3.9; [*Langmuir,* 1997, *p. 351*]. At pH 7 and 10, all colloids used in our experiments had a negative surface charge, as indicated by the negative electrophoretic mobility (Figure 3.2). For native, modified, and montmorillonite colloids the electrophoretic mobility did not change much from pH 7 to 10, suggesting that the transport of these colloids should not be different between these two pH values. Indeed, the breakthrough for these colloids support this hypothesis (Figure 3.6, 3.7a,b).

Compared with all colloids used, native colloids had the greatest recovery in the effluent (Figure 3.6). Except for ferrihydrite at pH 10, the colloid breakthrough curves were fairly consistent among repetitive runs (Figure 3.6a,b). The modified colloids had smaller relative effluent concentration than the native colloids, as a result of the larger particle size of the modified colloids and their less negative electrophoretic mobility (Figure 3.2). The pure mineral colloids had lower recovery than the native colloids.

The observation that native colloids moved with less restriction than the pure

minerals through the wick can be attributed to several factors. Compared with montmorillonite, native colloids had a somewhat more negative electrophoretic mobility at pH 7, making the native colloids more mobile. At pH≈10, the differences between native colloids and montmorillonite were not as pronounced as at pH≈10, but still, the native colloids showed a higher recovery. This is likely due to differences in the mineralogical compositions. Native Hanford colloids are composed of a mixture of aluminosilicates and quartz. Colloidal stability experiments showed that montmorillonite was less stable than "native colloids" at pH 7 and 10 (data not shown), suggesting that the montmorillonite is more susceptible to aggregation and filtration inside the wicks.

No kaolinite and ferrihydrite moved through the wicks at pH 7 (Figure 3.7). The ferrihydrite has little surface charge at pH 7 and is efficiently removed by aggregation and physico-chemical filtration inside the wick. The kaolinite has a pronounced net negative charge at pH 7; however, it also has protonated aluminol groups at this pH [*White and Dixon*, 2002], making the particles susceptible to filtration inside the wicks. Breakthrough curves of ferrihydrite at pH 10 were inconsistent between repetitions. We repeated the 10 mL/h runs three times and the 5 mL/h runs twice (Figure 3.7f). At the flow rates of 5 and 10 mL/h, after reaching the maximum effluent value, the concentration gradually decreased, then suddenly dropped to zero. The magnitude of the initial peak and and the height of the subsequent declining plateau were different in the repeated runs. At the pH of these runs, the ferrihydrite had a negative

charge comparable in magnitude with that of the other colloids, and, consequently, we expected that ferrihydrite would behave similarly as the other colloids. A possible explanation for the erratic ferrihydrite behavior is that the particles aggregated inside the wicks.

Comment: The complete retention of ferrihydrite colloids in a pH 7 solution within, and on the top of the wick is shown in Appendix B (Figure 3.9). ■

In most cases, colloids were deposited on the wick fibers (Figure 3.3c). The mass recovery for the different breakthrough curves ranged from 0% for kaolinite and ferrihydrite at pH 7 to 100% for native colloids at pH 10 (Table 3.2). The varying mass recoveries suggest that the suitability of wicks for colloid sampling depends on flow rates and colloid types.

We tested the differences between repeated colloid breakthrough curves performed in the same wick (in-wick variability) and among different wicks (among-wick variability) (Figure 3.8). We only used the native colloids at pH 10, because the wicks could be cleaned fairly readily by flushing the wicks extensively with the background solution between consecutive breakthrough curves. We did not observe pronounced differences in the subsequent runs.

Colloid removal by the wicks can be explained by two phenomena: (i) physicochemical effects (electrostatic and van der Waals interactions) between the particles and the wick, and (ii) physical straining. Electrostatic interactions dominated removal

when particles with less negative surface charge were transported through the wick. Nonetheless, we observed 100% removal in the case of the kaolinite, which had the most negative charge of all colloids at pH 7. Positive edge charges were likely responsible for strong particle deposition.

Physical straining can play an important role, if the water film on the surface of the wicks is sufficiently thin. Based on the water content distributions along the wick, we can estimate the water film thicknesses by dividing water contents by specific surface areas. The estimated film thicknesses ranged from 1.6–2.0 μm at the top to 5.4–6.8 μm at the bottom, depending on the flow rate. As these film thicknesses are all much larger than the particle diameters, it is unlikely that particles were removed by straining in water films. As the water contents in the wicks were similar for the different flow rates used, we do not attribute the observed dependence of colloid transport on flow rate to physical straining, but rather to physico-chemical interactions.

3.4.5 Alternative Wick Materials

Colloid recovery in our wick experiments depended on the type of colloids used and the pH of the suspensions. It would be useful to test other materials than glass fibers for their suitability for colloid sampling. Wicks are made of fibers with diameters of dozens of micrometers, and these fibers can be composed of different types of materials. Alternative candidates for wick fibers are polymers, graphite, or ceramic. The most suitable materials for colloid sampling in the vadose zone (in temperate climate and pH

conditions where most colloids are negatively charged) should be negatively charged to overcome the attractive van der Waals interactions between colloids and wick surfaces. Non-charged polymers are therefore unlikely to be good candidates for wick materials, as there will be no electrostatic repulsion between colloids and wick fibers. Systematic experimental tests would be required to determine the most suitable material for the use in wicks.

3.5 Conclusions

Flow rate, pH, and colloid type affected colloid breakthrough. Only one of the five colloids (native colloids) used showed complete breakthrough through the wicks, all other colloids were retained to some degree inside the wicks. The mechanism of colloid retention in the wicks was due to physico-chemical deposition rather than straining in water films because the estimated water film thicknesses were much larger than the colloid diameters.

Colloid recovery in the wick was very variable. Greatest recovery was observed for the mineral mixture extracted from sediments, 88 to 103% of the colloid mass was recovered in the wick outflow. In two cases, (kaolinite and ferrihydrite at pH 7) no colloids moved through the wicks. For other cases, colloid recovery varied from 50% to 100%. Feldspathoids and pure montmorillonite showed significant retention inside the wicks. This inconsistency in colloid recovery limits the use of fiberglass wicks for colloid sampling. The results of this study suggest that fiberglass wicks may be

suitable for sampling colloids from vadose zone pore water under certain conditions; however, generally, the wicks seem to retain a significant fraction of colloidal material.

3.6 Tables and Figures

Table 3.1: Z-averaged hydrodynamic diameters of the colloids used in this study.

Colloid type	Z-averaged hydrodynamic diameter (nm)
Native Colloids	497±38
Modified Colloids	621±84
Montmorillonite	493±25
Kaolinite	475±44
Ferrihydrite	185±16

Table 3.2: Experimental mass recovery of colloid breakthrough curves at different flow rates.

	Mass recovery (%)					
	pH 7			pH 10		
Colloid type	5 mL/h	10 mL/h	55 mL/h	5 mL/h	10 mL/h	55 mL/h
Native colloids	88	93	97–99[a]	92	94	98–103[a]
Modified colloids	66	70	80	59	66	97
Montmorillonite	49	53	78	55	61	90
Kaolinite	<5[b]	<5	<5	56	61	89
Ferrihydrite	<5	<5	<5	18–32[a]	20–61[a]	70

[a] Range of mass recovery in repeated breakthrough curves

[b] Measured values were below analytical detection limit

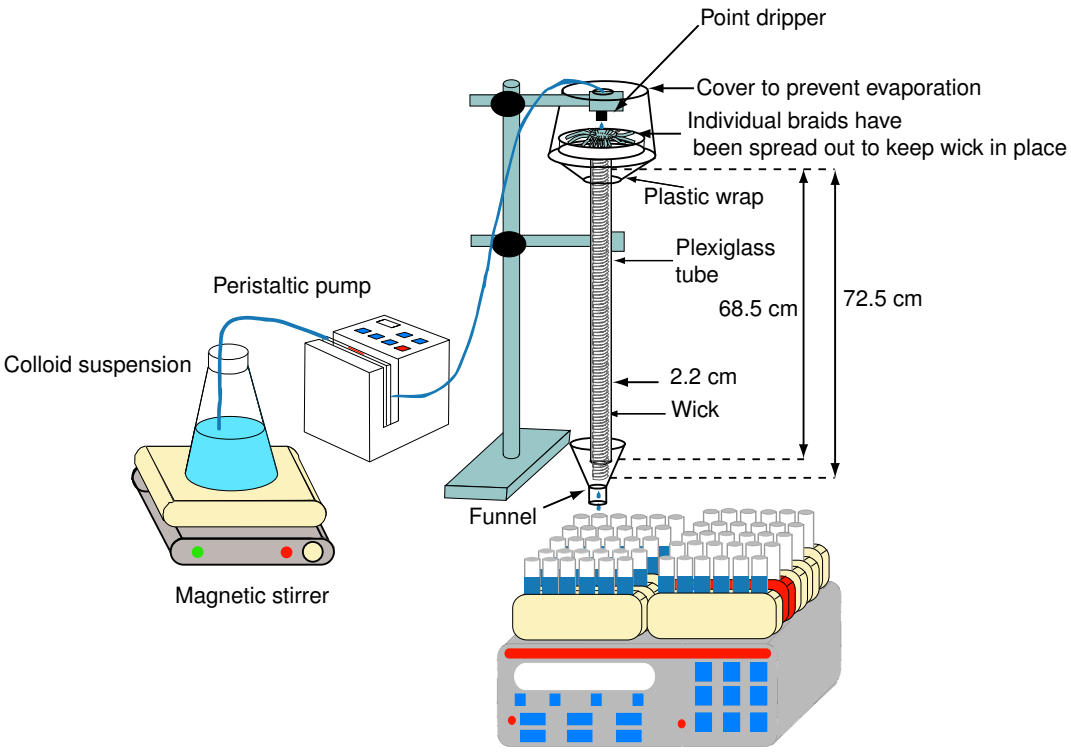

Figure 3.1: Experimental setup for the wick experiments.

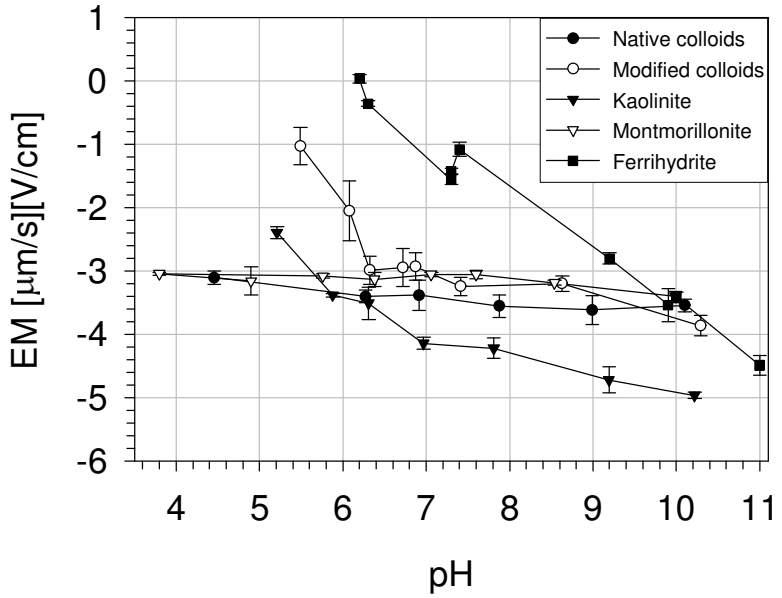

Figure 3.2: Electrophoretic mobility of the colloids as a function of pH. Error bars denote ± one standard deviation.

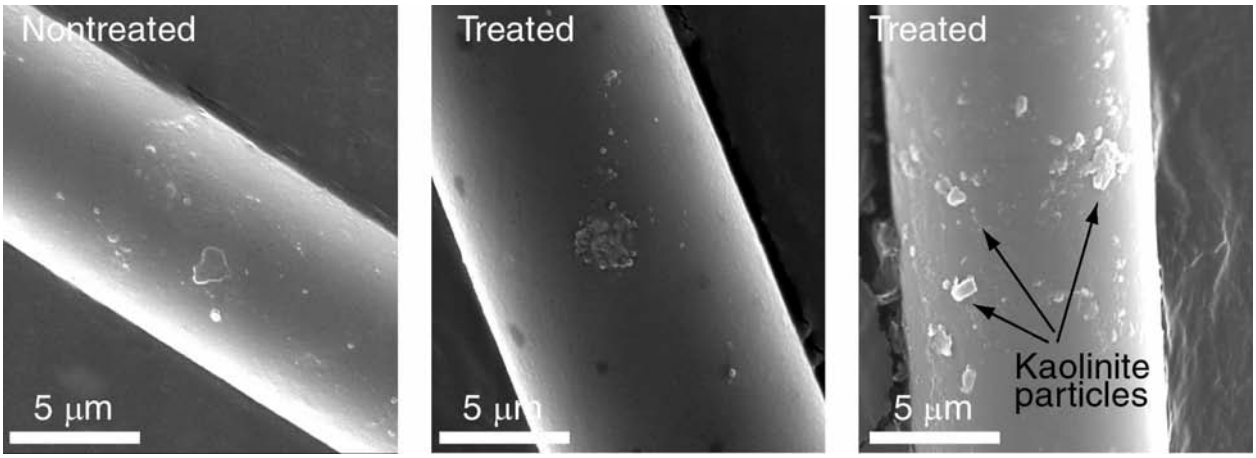

Figure 3.3: SEM micrographs of (a) nontreated wick fiber (as received from supplier), (b) treated wick fiber (combusted and washed), and (c) treated wick fiber covered with kaolinite particles (after kaolinite breakthrough curve).

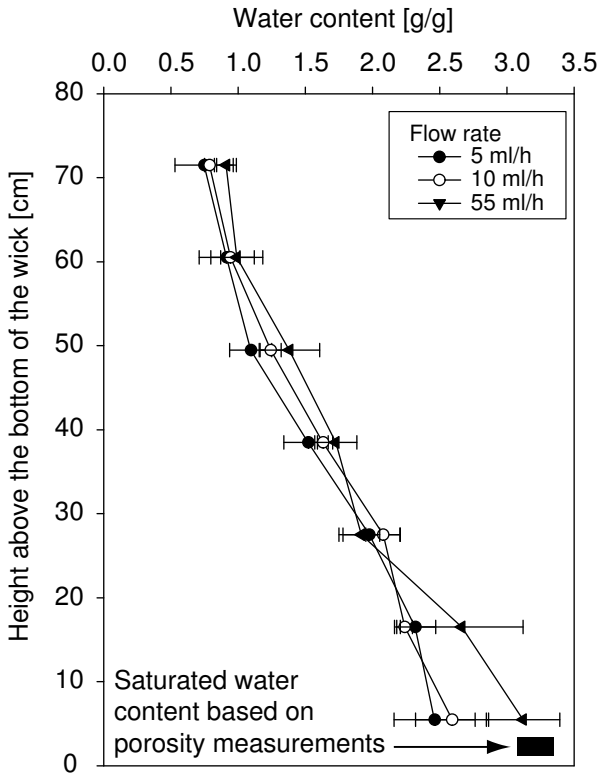

Figure 3.4: Distribution of water content as a function of height above the bottom of the wick for different water flow rates. Error bars denote ± one standard deviation ($n = 3$).

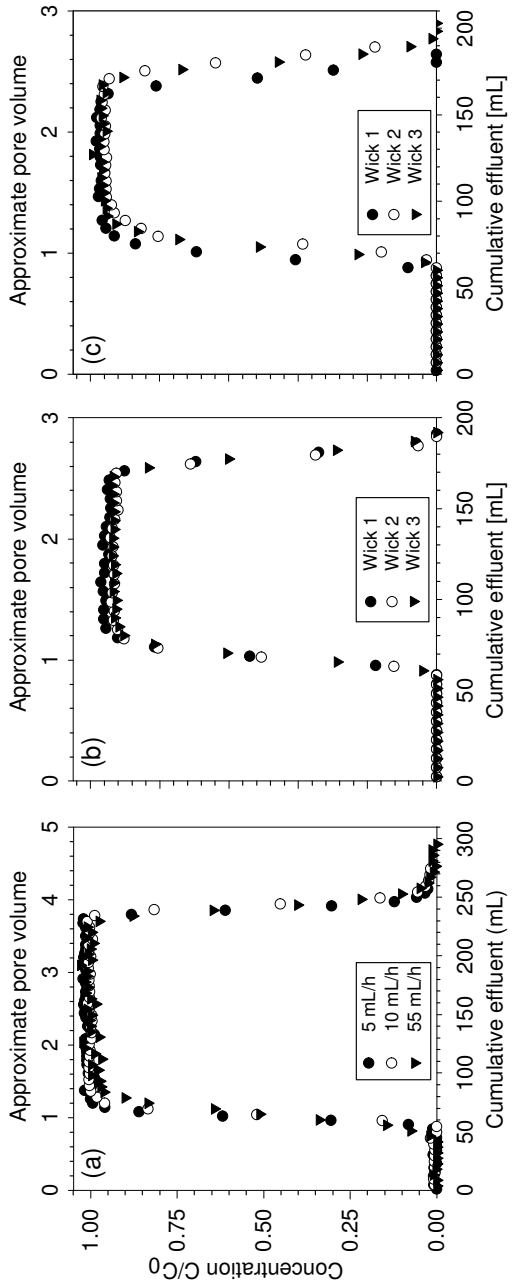

Figure 3.5: Nitrate breakthrough curves at pH $\approx$ 7 (a) for different flow rates in the same wick, (b) for 10 mL/h flow rate in three different wicks, and (c) for 55 mL/h flow rate in three different wicks.

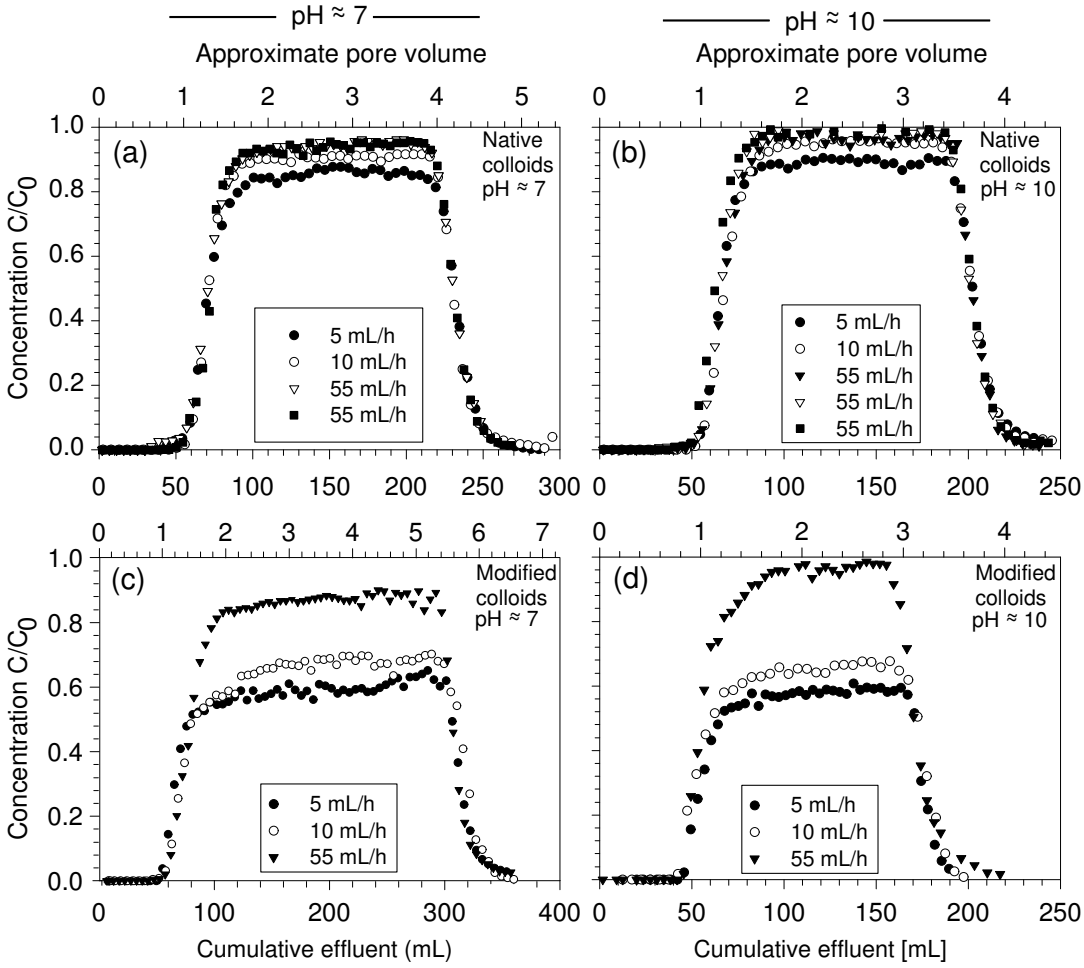

Figure 3.6: Breakthrough curves of native and modified Hanford colloids at different flow rates and pH. Breakthrough curves at the same flow rate within one plot are repetitions with different wicks.

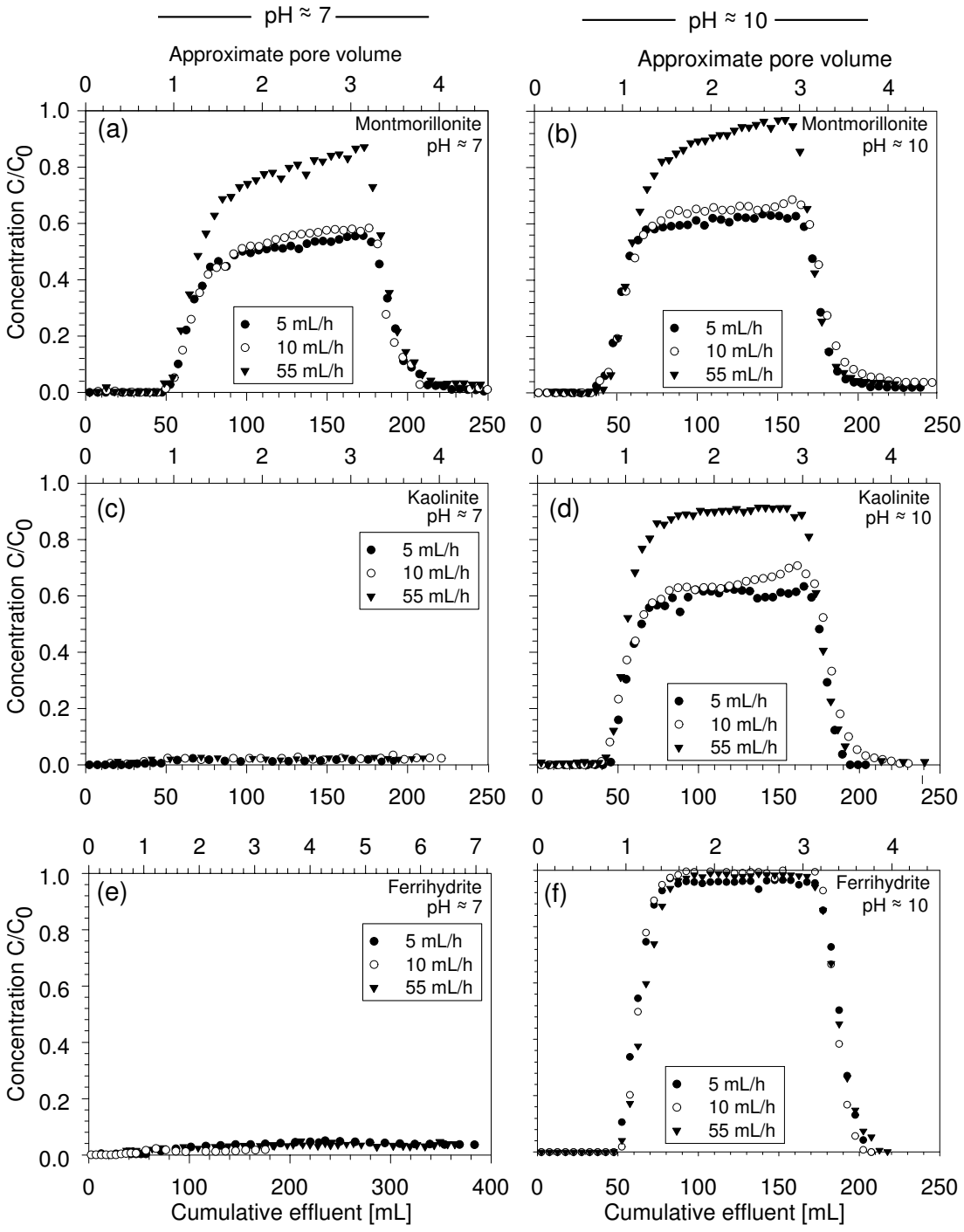

Figure 3.7: Breakthrough curves of pure mineral colloids at different flow rates and pH. Breakthrough curves at the same flow rate within one plot are repetitions with different wicks.

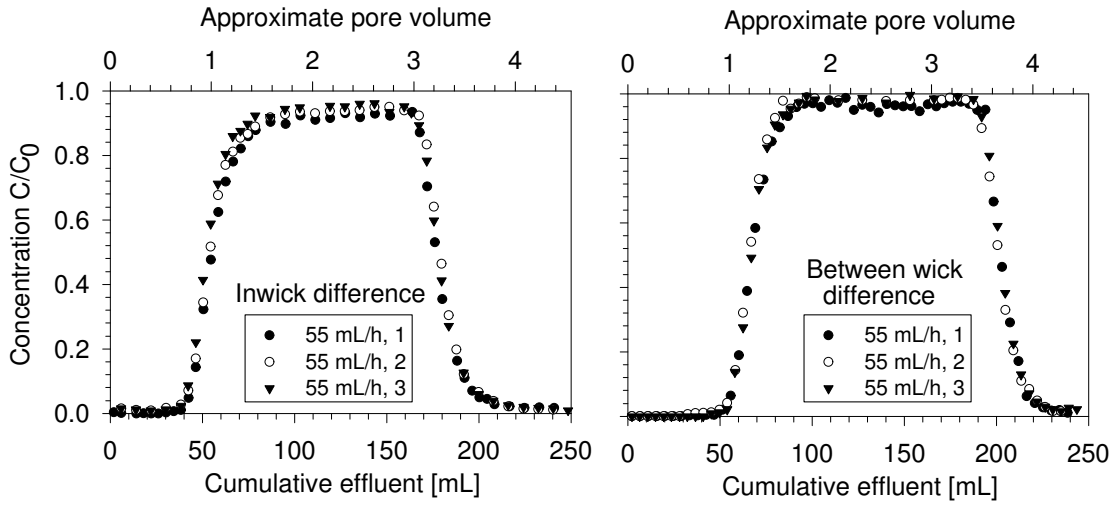

Figure 3.8: In-wick and among-wick variability for three repeated breakthrough curves using native colloids at pH $\approx$ 10.

3.7 Appendix B

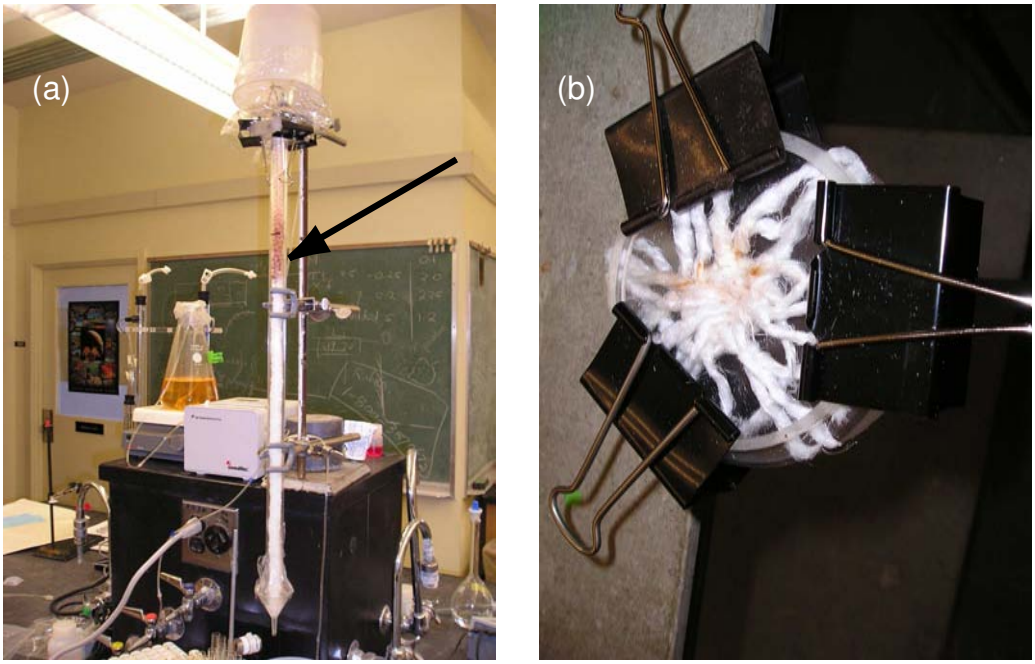

Figure 3.9: Setup of the wick experiments (a), and the unfolded wick in the top of the Plexiglas tube held in place by three binder clips and a Plexiglas ring (b). Note the dark band in the wick on picture (a), indicated by an arrow. The discoloration of the wick was caused by the retention of ferrihydrite colloids at pH 7 and at flow rate of 5 mL/h.

Chapter 4

Colloid Transport in Saturated Porous Media under Centrifugal Acceleration

4.1 Abstract

Flow and transport experiments with unsaturated porous media can take prohibitively long time, because hydraulic conductivities decrease exponentially with decreasing water saturation. Experimental time can be shortened by using centrifuges. However, compelling evidence is needed to assure the applicability of centrifuges for studying colloid transport, as colloid filtration is affected by centrifugation. The objective of this study was to determine the suitability of centrifuges to study colloid transport in porous media. We used filtration theory to predict the effect of particle density and flow rate on transport of colloids as affected by centrifugal accelerations. From filtration theory, a functional relation between centrifugal acceleration and pore water velocity and colloid density was derived, which allows to predict at which acceleration colloid filtration will be dominated by sedimentation. For typical pore water velocities

in the subsurface, it is expected that the filtration behavior of natural subsurface colloids will be impacted at centrifugal accelerations as low as 3 g.

4.2 Introduction

Transport of suspended particles in porous media under variably saturated conditions is affected by chemical and physical factors. Among the physical factors, water flux, matric potential, and hydraulic conductivity play important roles. Hydraulic conductivity exponentially decreases with decreasing degree of saturation, thus, transport experiments under low degree of water saturation can take extremely long time. To shorten the time required to conduct flow and transport experiments under unsaturated conditions, the use of centrifuges has been proposed. Two types of centrifuges are used to study flow and transport phenomena in porous media, the unsaturated flow apparatus (UFA) and the so-called geocentrifuge.

The UFA consists of a standard laboratory centrifuge that has been modified to accommodate porous media samples together with a water supply and drain system [*Nimmo,* 1987]. The UFA has been used to determine hydraulic properties [*Alemi et al.,* 1976*; Nimmo et al.,* 1987*; Conca and Wright,* 1998] and selected transport parameters, such as diffusion and sorption coefficients [*Celorie et al.,* 1989*; Conca and Wright,* 1990*; Conca and Wright,* 1992*; Conca and Wright,* 2000]. The UFA has also been used to study transport of solutes [*Gamerdinger and Kaplan,* 2000*; Gamerdinger et al.,* 2001a*; Gamerdinger et al.,* 2001b] and colloids [*McGraw,* 2000*; Gamerdinger*

and Kaplan, 2001] under unsaturated flow conditions.

Geocentrifuges are large-scale centrifuges (≈1.5 to 9 m radius) which have loading capacities up to 200 g-tons. These centrifuges have mainly been used for geotechnical applications [*Wu et al.*, 1996*; Mitchell,* 1998*; Dewoolkar et al.*, 1999*; Stadler and Ko,* 2002], but are being increasingly used to study flow and transport [*Hensley and Savvidou,* 1992*; Savvidou and Culligan,* 1998]. Geocentrifuges allow the use of much larger samples than possible in the UFA, but the accelerations are smaller in geocentrifuges. Typical accelerations in geocentrifuge studies reach up to 300 g [*Mitchell,* 1998*; ISSMGE-TC2,* 2004], whereas UFAs are capable of reaching up to 10,000 g, although for flow and transport studies in UFA, accelerations seldom exceed 2,000 g [*Nimmo et al.,* 1992].

Comment: The centrifuge method was developed in the first half of the 20th century to determine matric potential and capillary tension of soils at low water contents [*Briggs and McLane,* 1907]. These early centrifuge studies applied centrifugal forces up to 3,000 g to determine the "water equivalent" of soils at a wide range of moisture content [*Briggs and McLane,* 1907*; Briggs and McLane,* 1910]. The "water equivalent" is "the percentage of water retained by the soil, when the moisture content is reduced by centrifugal force and brought into a state of capillary equilibrium with the applied force" [*Briggs and McLane,* 1907]. *Veihmeyer et al.* [1924] modified and further improved the centrifuge method to estimate field capacity of soils. *Joseph and Martin* [1923] investigated the effect of the size of the soil sample on the water retained during

centrifugation and pointed out that the amount of water remaining in sandy and silty soil samples decreases with increasing sample size. Other studies specifically focused on determining the water content at the wilting point (e.g., *Gardner,* 1937*; Russell and Richards,* 1938). ■

The major advantage of using centrifuges for flow and transport experiments is that the driving force can be varied without affecting the moisture gradient, experiments can be conducted with materials of small hydraulic conductivity, and the experimental time can be shortened [*Nimmo et al.,* 1987]. Accelerations larger than $1 \times g$, however, may limit the suitability of centrifuges to study colloid transport, because the centrifugal body force distorts the natural force balance acting on colloidal particles. Several studies on colloid transport in porous media have been conducted with centrifuges [*McGraw,* 1996*; McGraw and Kaplan,* 1997*; McGraw,* 2000*; Gamerdinger and Kaplan,* 2001]; however, the effect of centrifugal force on colloid transport has not been considered explicitly. As colloid filtration, specifically the sedimentation term in filtration theory, is impacted by the body force acting on colloids, it is expected that filtration, and consequently transport, will be different in a centrifuge experiment as compared to an experiment conducted under normal gravity.

Comment: Suspended particles in aqueous systems can be transported to the solid medium (collector) by three processes: (1) gravitational settling, (2) diffusion, and (3) interception [*Rajagopalan and Tien,* 1976*; O'Melia,* 1980]. Particle filtration

inside a porous media is affected, among other properties, by particle diameter, particle hydrophobicity, diameter of the solid medium, flow rate, and particle density [*O'Melia,* 1980*; McGraw,* 1996*; McGraw and Kaplan,* 1997*; McGraw,* 2000]. Particle diameter impacts all the three filtration mechanisms during colloid transport. The magnitude of the effect of particle size strongly depends, among other factors, on pore water velocity, particle density, and residence time [*O'Melia,* 1980*; McDowell-Boyer et al.,* 1986]. O'Melia and coworkers [*Yao et al.,* 1971*; O'Melia,* 1980] related particle diameter to colloid filtration as a function of particle density to determine the fate of colloidal particles in aqueous environments. The effect of particle diameter and flow rate on colloid filtration in porous media was theoretically investigated by *McGraw and Kaplan* [1997] and *McGraw* [2000]. Based on their theoretical calculations, the authors concluded that particles larger than 300 nm in diameter will be removed from suspension by gravitational settling and particles smaller than 300 nm will be removed by diffusion. The authors assumed a specific density of 2.78 g/cm^3, with solid medium diameter of 1 mm and pore water velocity of 3.26×10^{-6} m/s. ■

The objective of this study was to test the suitability of centrifuges for colloid transport in porous media. We used filtration theory to determine the effect of the centrifugal force on retention of colloids during transport, as a function of pore water velocity and particle density. We predict the threshold centrifugal acceleration above which colloid filtration will be altered as compared to normal gravity conditions. The-

oretical calculations were complemented with bench top transport experiments, in which we studied the effects of (1) particle density and (2) flow direction on colloid breakthrough curves.

4.3 Theory

4.3.1 Water Flow

Unsaturated flow in a centrifuge experiment can be described by a modified Darcy's law [*Nimmo et al.,* 1994]:

$$q = -K\left(\frac{d\Psi}{dr} - \rho\omega^2 r\right) \tag{4.1}$$

where q is the water flux density, K is the hydraulic conductivity, Ψ is the matric potential, ρ is the fluid density, ω is the angular velocity, and r is the distance from the center of rotation. As shown in equation 4.1, unsaturated flow in a centrifuge experiment is driven by both the matric potential gradient and the centrifugal force, assuming that gravity can be neglected, i.e., is much smaller than the centrifugal acceleration.

At sufficiently high centrifugal acceleration, the matric potential gradient becomes negligible compared to the centrifugal acceleration ($d\Psi/dr \ll \rho\omega^2 r$) [*Nimmo et al.,* 1992]. When centrifugal force prevails as a driving force, the flux can be easily controlled by changing the acceleration [*Conca and Wright,* 2000], and the modified Darcy's law can be simplified to [*Nimmo et al.,* 1987*; Conca and Wright,* 1990*; Nimmo*

et al., 1994]:

$$q = -K\rho\omega^2 r \tag{4.2}$$

From equation 4.2 we can calculate the hydraulic conductivity as:

$$K = -q/\rho\omega^2 r \tag{4.3}$$

The acceleration, at which the matric potential gradient becomes negligible, depends on the hydraulic properties and the particle and pore size distribution of the medium. Lower centrifugal acceleration are sufficient in sandy media, while higher accelerations are required for a fine-textured media to obtain a uniform matric potential distribution. Uniform matric potential distribution was reported at $220 \times g$ in a sandy soil by *Nimmo and Akstin* [1992].

Several factors can limit the applicability of centrifuges for flow and transport experiments. For saturated transport experiments, due to the larger centrifugal force at the bottom of the column compared to the top of the column, the soil can get desaturated, i.e., the water phase can become discontinuous inside the column [*Nimmo and Mello,* 1991]. Further, the solid phase can be compacted at higher rotational speed [*Nimmo and Akstin,* 1992*; Conca and Wright,* 2000*; Nimmo and Mello,* 1991]. Clayey and silty soils are particularly susceptible to compaction, and compaction of such soils has been observed at about $1,000 \times g$ [*Conca and Wright,* 2000]. For a sandy soil *Nimmo and Akstin* [1992] found negligible compaction for accelerations up to $1,900 \times g$.

4.3.2 Diffusion and Sedimentation

In the absence of particle-particle interactions in a suspension, two opposing processes act simultaneously on any suspended particle. Omnidirectional thermokinetic energy keeps the particles dispersed in the suspension, while sedimentation (due to gravitational or centrifugal forces) removes the particles from the suspension. The diffusion coefficient can be calculated with the Stokes-Einstein equation [*Flury and Gimmi,* 2002]:

$$D = \frac{kT}{f} = \frac{kT}{3\pi\eta d} \tag{4.4}$$

where k is the Boltzmann constant, T is the absolute temperature in K, f is a friction factor, η is the dynamic viscosity, and d is the particle diameter. The right-hand-side of that equation is valid for a spherical particle. Gravity pulls the particle downward and the sedimentation velocity v_s can be calculated by Stokes' law:

$$v_s = \frac{d^2 g(\rho_s - \rho_l)}{18\eta} \tag{4.5}$$

where g is the gravitational acceleration, ρ_s is the specific density of the suspended particles, and ρ_l is the fluid density. From equation 4.5 we can express the sedimentation coefficient s [*Hiemenz and Rajagopalan,* 1997].

$$s = \frac{m\left(1 - \frac{\rho_s}{\rho_l}\right)}{f} \tag{4.6}$$

where m is the particle mass. At equilibrium, when the rate of diffusion and sedimentation is equal, we have [*Hiemenz and Rajagopalan,* 1997]:

$$J_{\text{sed}} = -J_{\text{diff}} \tag{4.7}$$

where J_{sed} is the flux due to sedimentation, given as:

$$J_{\text{sed}} = vc \tag{4.8}$$

and J_{diff} is the flux due to diffusion, which can be described by Fick's first law [*Jury et al.*, 1991]:

$$J_{\text{diff}} = -D\frac{dc}{dr} \tag{4.9}$$

where v is the sedimentation velocity, r is distance, and c is the particle number concentration.

Combining equations 4.5 to 4.9, we obtain [*Hiemenz and Rajagopalan,* 1997]:

$$\frac{m}{f}\left(1 - \frac{\rho_s}{\rho_l}\right) gc = D\frac{dc}{dr} \tag{4.10}$$

In a centrifugal field, g must be replaced by $\omega^2 r$ in equation 4.10 [*Hiemenz and Rajagopalan,* 1997]:

$$\frac{m}{f}\left(1 - \frac{\rho_s}{\rho_l}\right) \omega^2 rc = D\frac{dc}{dr} \tag{4.11}$$

By integrating equations 4.10 and 4.11, we obtain c as a function of r [*Hiemenz and Rajagopalan,* 1997]:

$$\ln\left(\frac{c_2}{c_1}\right) = \frac{m}{fD}\left(1 - \frac{\rho_s}{\rho_l}\right) g(r_2 - r_1) \tag{4.12}$$

and

$$\ln\left(\frac{c_2}{c_1}\right) = \frac{m}{2fD}\left(1 - \frac{\rho_s}{\rho_l}\right) \omega^2(r_2^2 - r_1^2) \tag{4.13}$$

By recalling Stokes-Einstein's law, we can substitute kT for Df and can obtain the equations describing the colloid concentration profiles as a function of particle den-

sity, particle diameter, and gravitational or centrifugal acceleration [*Hiemenz and Rajagopalan,* 1997]:

$$\ln\left(\frac{c_2}{c_1}\right) = \frac{m}{kT}\left(1 - \frac{\rho_s}{\rho_l}\right) g(r_2 - r_1) \tag{4.14}$$

and

$$\ln\left(\frac{c_2}{c_1}\right) = \frac{m}{2kT}\left(1 - \frac{\rho_s}{\rho_l}\right) \omega^2(r_2^2 - r_1^2) \tag{4.15}$$

For gases, where buoyancy can be neglected, equation 4.14 can be simplified to [*Hiemenz and Rajagopalan,* 1997]:

$$\ln\left(\frac{p_2}{p_1}\right) = \frac{Mg(r_2 - r_1)}{RT} \tag{4.16}$$

where p_1 and p_2 are the partial pressure values of the gas at locations r_1 and r_2, respectively, and M is the molecular weight of the gas. This is the "barometric profile".

A recent study indicated that for charged particles the barometric sedimentation profiles expected from equations 4.14 and 4.15 can be altered [*Rasa and Philipse,* 2004]. The barometric sedimentation profile is used to determine colloidal mass in suspension from centrifuge experiments. For charged particles at low ionic strength (0 to 0.35 $mmol_c$/L $LiNO_3$), it was observed that the experimental barometric sedimentation profiles were inflated compared to the ones predicted by equation 4.15 [*Rasa and Philipse,* 2004]. This phenomenon was explained by the uneven distribution of the negatively-charged colloids and their positively-charged counter ions, by which an electrostatic field was produced that counteracted the sedimentation profile [*Rasa and Philipse,* 2004]. This phenomenon is only important a low ionic strength

(< 1 mmol$_c$/L); at high ionic strength, the charges on colloidal particles are effectively shielded by counter ions and a charge separation does not occur. Consequently, this phenomenon is unlikely to be relevant in soils, as soil pore water electrolyte concentration is usually higher than 1 mmol$_c$/L.

4.3.3 Filtration Theory

Colloid removal from the fluid phase during transport in porous media can be described by filtration theory. Filtration theory describes the mechanisms of colloid transport to the solid collector (collector efficiency) and the probability that colloids attach to the collector (collision efficiency). Colloid-collector contact can occur due to interception, diffusion (Brownian motion), and sedimentation. The total collector efficiency, η_{tot}, is the sum of the single collector efficiencies by interception, η_i, sedimentation, η_g, and diffusion, η_d [*Yao et al.,* 1971]:

$$\eta_{tot} = \eta_i + \eta_g + \eta_d \tag{4.17}$$

The single collector efficiencies are given as [*Logan et al.,* 1995]:

$$\eta_i = \frac{3}{2}\left(\frac{d_c}{d_m}\right)^2 \tag{4.18}$$

$$\eta_g = \frac{\Delta\rho g d_c^2}{18 v \eta} \tag{4.19}$$

$$\eta_d = 4\left(v\frac{d_m}{D}\right)^{-2/3} \tag{4.20}$$

where d_c is colloid diameter, d_m is the diameter of the spherical collector, $\Delta\rho$ is the difference between colloid and fluid densities, v is the pore water velocity, η is the

dynamic viscosity, and D is the colloid diffusion coefficient. Depending on pore water velocity, particle size, particle density, and collector diameter, filtration can be dominated either by interception, sedimentation, or diffusion. Under gravitational acceleration, diffusion is the main mechanism for filtration of colloids with diameter $d_c < 400$ nm (assuming a colloid density of 2.65 g/cm^3, collector diameter $> 100d_c$, and a typical subsurface pore water velocity $v_0 = 10^{-5}$ m/s [*Domenico and Schwartz,* 1998]) (Figure 4.1). For small particles (≈ 500 nm) in sandy media, interception can generally be neglected (Table 4.1).

Out of the three single collector efficiency terms, only the sedimentation term, η_g, is affected by acceleration. Increasing acceleration, as is done in a centrifuge experiment, will increase colloid filtration due to sedimentation. We assume that acceleration does not affect colloid filtration as long as:

$$\eta_g \leq \eta_d \tag{4.21}$$

We illustrate the use of equation 4.21 to assess the effect of centrifugal force on colloid filtration by assuming a colloid diameter of 160 nm. We plotted single collector efficiencies due to sedimentation and diffusion as function of dimensionless acceleration a/g, where a is the centrifugal acceleration, for different pore water velocities and colloid densities (Figure 4.2). The collector efficiency due to sedimentation increases linearly with acceleration and intersects the collector efficiency due to diffusion. The acceleration, at which $\eta_g = \eta_d$, increases as the pore water velocity increases and as the colloid density decreases. The relationships between acceleration as a function of pore

water velocity and colloid density can be derived from the equality in equation 4.21 as:

$$a(v_0) = 72\frac{\eta}{\Delta\rho d_c^2}\left(\frac{D}{d_m}\right)^{2/3} v^{1/3} \tag{4.22}$$

Equation 4.22 depicts a cubic-root relationship between acceleration and velocity, and allows to calculate the threshold acceleration at which sedimentation overcomes diffusion as a function of pore water velocity, particle density, and particle size. An example for a 160-nm colloid diameter and 462.5 μm collector diameter is shown in Figure 4.3. The hyperbolic relationship between threshold acceleration and density difference, $\Delta\rho$, is depicted in Figure 4.4, using the same conditions as in the previous example. The higher the pore water velocity, the greater can the acceleration be before sedimentation overcomes diffusion.

Comment: The use of equation 4.22 is further illustrated in Figure 4.5 and Table 4.2. Figure 4.5 shows single collector efficiencies as function of density differences between colloids and fluid phases for different accelerations. The solid horizontal line depicts the collector efficiency due to diffusion. The intersection between η_d and η_g depicts the point above acceleration will alter the filtration behavior. Threshold accelerations for different colloid densities and pore water velocities are listed in Table 4.2. For colloids with low density, e.g., polystyrene with density of 1.05 g/cm^3, threshold accelerations can be as high as 200 to 1,000 g, whereas for colloids with high density, e.g. ferrihydrite with density of 4 g/cm^3, accelerations must not exceed 3.5 to 16 g. ■

4.4 Experimental Case Study

4.4.1 Experimental Methods

General Approach

The theoretical predictions were verified with colloid filtration experiments conducted in flow-through columns. Colloid filtration was assessed by examining colloid breakthrough curves at the column outflow. Colloid and collector diameters, pore water velocity, and solution chemistry were kept constant, whereas colloid density and acceleration were varied.

Types of Colloids

We used three types of colloids: hydrophilic polystyrene particles with COOH surface groups (Bangs Laboratories Inc., Fishers, IN), fluorescent silica particles (Gbr KisKer, Steinfurt, Germany), and 2-line ferrihydrite. The ferrihydrite was synthesized in our laboratory according to *Schwertmann and Cornell* [2000*, p. 105-111*], whereby 10 mmol/L Si was used in the synthesis procedure to stabilize the mineral and prevent mineral transformations. The ferrihydrite stock suspension was kept in a polypropylene bottle at pH 2, and was diluted with 1.67 mM $NaHCO_3$/1.67 mM Na_2CO_3 before the beginning of the experiments. Polystyrene and silica beads were diluted from the commercial stock solutions.

The specific densities of the polystyrene (1.05 g/cm^3) and silica (2.0 g/cm^3) par-

ticles were provided by the suppliers, and the density of the ferrihydrite (4 g/cm^3) was reported by *Schwertmann and Cornell* [2000]. Ferrihydrite may transform to goethite [*Schwertmann and Cornell,* 2000], and we verified ferrihydrite stability during the course of the experiments with XRD (Philips XRG 3100, Philips Analytical Inc., Mahwah NJ). The shape of ferrihydrite particles was examined by transmission electron microscopy (JEOL 1200EX), and the size and the shape of the polystyrene latex and fluorescent silica particles by scanning electron microscopy (Hitachi S-570).

Average hydrodynamic diameter and electrophoretic mobility of the colloids were measured by dynamic light scattering (ZetaSizer 3000HSa, Malvern Instruments Ltd., Malvern, UK) in a weak electrolyte solution (1.67 mM $NaHCO_3$/1.67 mM Na_2CO_3). The pH values for the solutions used for electrophoretic mobility measurements were adjusted with 100 mM HCl and 100 mM NaOH.

Column Filtration Experiments

We conducted a series of bench top filtration experiments using an acrylic column of 2.5-cm ID and 21.4-cm length. The end pieces were made of Teflon with a nylon membrane at both ends. The nylon membrane had a bubbling pressure of 60-cm of H_2O, with a pore opening of 48 μm (square pores). Flow was driven by a peristaltic pump (Ismatec IP4, Glattburg, Switzerland) and a fraction collector was used to collect the effluent suspension (Figure 4.6). A CO_2 trap was employed to prevent pH shifting (Figure 4.7).

The column was packed with silica sand (Mallinckrodt Baker, Inc., Phillipsburg, NJ). The sand was fractionated by dry sieving, and the fraction between 425 and 500 μm in diameter was used in the columns. The sand was treated with 2 M HCl at 80 to 90^0C for eight hours, to remove impurities, such as Fe-oxides, organic matter and carbonates, and was rinsed with deionized water eight times.

A steady-state flow with rate of $Q = 25$ mL/h, corresponding to a flux of $J_w = 5.09$ cm/h and a pore water velocity of 14.1 cm/h $= 3.9\times10^{-5}$ m/s, was established. Colloid suspensions with particle concentrations of 14.4 mg/L (polystyrene), 25 mg/L (fluorescent silica), and 55 mg/L (ferrihydrite) were prepared, which correspond to a constant number concentration of 6.42×10^{12} particles per liter in all three cases. Colloids were suspended in deionized water buffered at pH 10 using 1.67 mM Na_2CO_3/$NaHCO_3$ to adjust the pH. Colloid suspensions were introduced for one pore volume (approximately 40 mL), after which the inflow was switched to colloid-free buffer solution for an additional four pore volumes. The total volume of suspension/solution passed through the column per breakthrough curve was approximately 200 mL, i.e., five pore volumes of through flow for each breakthrough curve.

Acceleration was varied by changing the flow direction. We used upward flow ($-1\,g$), horizontal flow ($0\,g$), and downward flow ($+1\,g$). Flow direction was varied by turning the column. Effluent polystyrene and ferrihydrite concentrations were measured at a wavelength of 300 nm using a spectrophotometer (HP 8452A, Hewlett-Packard), while fluorescent silica concentrations were determined with a fluorescent

spectrometer (Hitachi-F3010, excitation bandpass: 10 nm, emission bandpass: 10 nm, scan speed: 120 nm/min). The excitation and emission peaks of the fluorescent silica particles are at 354 and 450 nm, respectively (Figure 4.8). We performed each column experiment in triplicates to verify reproducibility. Only one breakthrough curve is reported in the results, as the triplicates were almost identical.

Data Analysis

The colloid breakthroughs were analyzed with the deterministic equilibrium CDE model using CXTFIT 2.1 [*Toride et al.,* 1995]. We used the deterministic equilibrium model because there was very limited (no) interaction between the colloids and the silica sand. The pore water velocity v was calculated from the measured water flux, as J_w/θ. The retardation factor, R, the dispersion coefficient, D were obtained by fitting the advection–dispersion equation (ADE) to the experimental data. The Peclet number was calculated from the dispersion coefficient and the pore water velocity.

4.4.2 Experimental Results

Colloid Characterization

The scanning electron micrographs of the polystyrene and the silica beads reveal the spherical shape and the relatively monodispersed character of the colloids (Figure 4.9). The diameters of the polystyrene and the silica colloids in the scanning electron micrographs corresponded well with the values obtained with dynamic light scattering

(Table 4.3).

The size of the individual ferrihydrite particles could not be identified by transmission electron microscopy; the particles formed aggregates (Figure 4.10). Individual particle size was reported to be 2 to 3 nm [*Schwertmann and Cornell,* 2000]. The particle diameters measured by dynamic light scattering indicate that ferrihydrite also formed aggregates in suspension (Table 4.3). The XRD analysis did not indicate mineral transformation of ferrihydrite.

All the colloids had a net negative electrophoretic mobility above pH 7 (Figure 4.11). The ferrihydrite colloids had the least negative electrophoretic mobility and had an isoelectric point at pH 6.2 to 6.4. The silica particles had an isoelectric point at pH≈3.4, which is in a good agreement with the value reported for amorphous silica [*Langmuir,* 1997]. The polystyrene latex particles had the most negative electrophoretic mobility, which was about -4.0 (μm/s)(V/cm) from pH 4 to 11.

Colloid Filtration Experiments

We did not observe any effect of flow direction on the colloid breakthrough curves (Figure 4.12). The model analysis indicated that the colloids behaved conservatively; retardation factors were slightly less than 1 (Table 4.4). Based on the net negative electrophoretic mobility of the three colloids and the sand medium, negative-negative charge repulsion dominated particle-surface interactions. The fitted retardation coefficient can indicate charge-induced exclusion. The calculated dispersion coefficients

were 0.0133 cm^2/min for ferrihydrite, and somewhat higher values were obtained for polystyrene (0.015 to 0.018 cm^2/min) and silica (0.030 to 0.032 cm^2/min).

4.4.3 Comparison of Experiments and Theory

The calculated single collector efficiency due to interception, η_i was in the order of 10^{-7} in the case of all the three colloids and is considered negligible in our experiments (Table 4.3). The collector efficiency values due to diffusion varied with particle diameter, and the collector efficiency due to sedimentation, at the experimental pore water velocity and normal gravity, was much less than that due to diffusion (Table 4.3).

Increasing acceleration causes the single collector efficiency due to sedimentation to increase, and the acceleration at which $\eta_d = \eta_g$ is shown in Figure 4.13. Because of its highest density, ferrihydrite was most affected by acceleration. The threshold acceleration as a function of pore water velocity for the three colloids is depicted in Figure 4.14. Clearly, at the experimental pore water velocity, colloid filtration is not affected by sedimentation under the conditions of our experiment $(-1, 0, +1\ g)$. Centrifugal accelerations up to 8, 20, and 610 g should be possible before sedimentation starts to alter the filtration behavior of ferrihydrite, silica, and polystyrene, respectively (Figure 4.14). Threshold accelerations at different pore water velocities are listed in Table 4.5.

The results from our bench top experiments corroborate the theoretical predictions, i.e., that colloid filtration was not affected by the flow directions. Centrifuge

experiments will now be needed to thoroughly test the theory. The threshold accelerations listed in Table 4.5 provide a useful test matrix that can be evaluated with geocentrifuge experiments. Polystyrene will not be affected by centrifugation under any reasonable fluxes and feasible accelerations (geocentrifuge capacities rarely exceed 200 g), and polystyrene is therefore a useful reference colloid in such experiments.

Comment: The Idaho National Environmental and Engineering Laboratory (INEEL), in Idaho Falls, ID, has a 2-m radius geocentrifuge (Figure 4.15, Model C61-3 Civil Engineering Centrifuge, Actidyn Systémes, France). The bench top column setup described in this work has been designed with the platform specifications of this centrifuge in mind, and the column itself was custom made out of acrylic to ensure mechanical stability during centrifuge experiments. ■

4.5 Conclusions

The theoretical calculations indicate, that colloid filtration will be affected by altered force fields during centrifuge experiments. Increased filtration is expected as acceleration increases. The acceleration, at which $\eta_d = \eta_g$, is affected by (a) density difference between colloid and the fluid, $\Delta\rho$, (b) pore water velocity, and (c) colloid and collector size. The theoretical calculations show that the smaller the density differences and the greater the pore water velocities are, the higher is the "sedimentation tolerance" of the

particle towards acceleration. Filtration theory allows to predict at which acceleration $\eta_d = \eta_g$, for given colloid and collector diameters, density difference, and pore water velocity. It is expected that for natural subsurface colloids, such as silicates and iron oxides, filtration will be different in centrifuge experiments as compared to normal gravity conditions. At typical subsurface flow rates, accelerations as low as 4 g or less can change the filtration behavior.

4.6 Tables and Figures

Table 4.1: Single collector efficiencies for colloids with 160-nm diameter and different densities at 3.9×10^{-5} m/s pore water velocity, $1\times g$ acceleration, and collector diameter of $d_m = 462.5$ μm.

Particle density (g/cm^3)	η_d	η_g	η_i	η_d/η_g	η_d/η_i
1.05	0.0224	5.15×10^{-5}	1.8×10^{-7}	435	1.24×10^{5}
1.5	0.0224	4.95×10^{-4}	1.8×10^{-7}	45	1.24×10^{5}
2	0.0224	9.89×10^{-4}	1.8×10^{-7}	23	1.24×10^{5}
3	0.0224	1.98×10^{-3}	1.8×10^{-7}	11	1.24×10^{5}
4	0.0224	2.96×10^{-3}	1.8×10^{-7}	8	1.24×10^{5}

Table 4.2: Threshold accelerations, where collector efficiency due to sedimentation is equal to that due to diffusion, as function of colloid density and pore water velocity. (Colloid diameter 160 nm diameter, reference pore water velocity v = 5.09 cm/h = 1.4×10^{-5} m/s).

Colloid density	Dimensionless acceleration a/g when $\eta_d = \eta_g$		
(g/cm^3)	$0.1 \times v$	$1 \times v$	$10 \times v$
1.05	210	448	939
1.5	21	45	97
2	6	13	27
3	4.3	9.3	20
4	3.5	7.6	16

Table 4.3: Selected properties of the colloids used in this study and single collector efficiencies (reference pore water velocity $v = 14.1$ cm/h $= 3.9\times10^{-5}$ m/s, $1\times g$ acceleration, and collector diameter of $d_m = 462.5$ μm).

Colloid type	Specific density (g/cm^3)	Particle diameter: light scattering (nm)	Particle diameter: SEM[a] (nm)	Collector efficency: η_d	Collector efficency: η_g	Collector efficency: η_i
Hydrophilic polystyrene (COOH)	1.05	166 ± 2	162 ± 18	0.011	1.9×10^{-6}	1.8×10^{-7}
Fluorescent silica	2.0	199 ± 2	173 ± 28	0.001	5.6×10^{-4}	2.8×10^{-7}
2-line ferrihydrite	4	185 ± 29	na	0.010	1.4×10^{-3}	2.4×10^{-7}

na: not available.

[a] measured on 20 randomly selected particles in each image.

Table 4.4: Parameters of linear equilibrium transport models for the bench top column experiments.

Colloid type	Flow direction	Dispersion coefficient	Retardation factor	Peclet number	$r^{2,a}$	SSQ
		(cm^2/min)	(–)	(–)	(–)	(–)
Polystyrene	up	0.016±0.003	0.93±0.01	132	0.964	0.408
Polystyrene	horizontal	0.017±0.003	0.94±0.01	127	0.973	0.310
Polystyrene	down	0.015±0.004	0.96±0.01	139	0.954	0.478
Silica	up	0.028±0.004	0.96±0.01	76	0.970	0.290
Silica	horizontal	0.030±0.007	0.95±0.01	71	0.939	0.603
Silica	down	0.032±0.005	0.98±0.01	66	0.965	0.335
Ferrihydrite	up	0.013±0.002	0.94±0.01	163	0.988	0.130
Ferrihydrite	horizontal	0.013±0.002	0.93±0.01	163	0.986	0.148
Ferrihydrite	down	0.013±0.002	0.93±0.01	163	0.984	0.130

[a] $r^2 = 1 - \frac{\sum_{i=1}^{N}(C_i - f_i)^2}{\sum_{i=1}^{N}(C_i - \bar{C})^2} = 1 - \frac{\text{SSQ}}{\sum_{i=1}^{N}(C_i - \bar{C})^2}$,where C_i and f_i are observed and fitted data, respectively, and $\bar{C}$ is the mean of all N observed concentrations.

Table 4.5: Threshold accelerations, where collector efficiency due to sedimentation is equal to that due to diffusion, for polystyrene, silica, and ferrihydrite. (reference pore water velocity $v = 14.1$ cm/h $= 3.9\times10^{-5}$ m/s), and pore water velocity, where $\eta_d = \eta_g$ at $1\,g$.

Colloid type	Dimensionless acceleration a/g when $\eta_d = \eta_g$			Pore water velocity v when $\eta_d = \eta_g$ at 1 g acceleration
	$0.1 \times v$	$1 \times v$	$10 \times v$	(m/s)
Polystyrene	283	610	1315	$1.7\times\ 10^{-15}$
Silica	9.4	20	44	$7.3\times\ 10^{-9}$
Ferrihydrite	3.7	7.9	17	$1.05\times\ 10^{-7}$

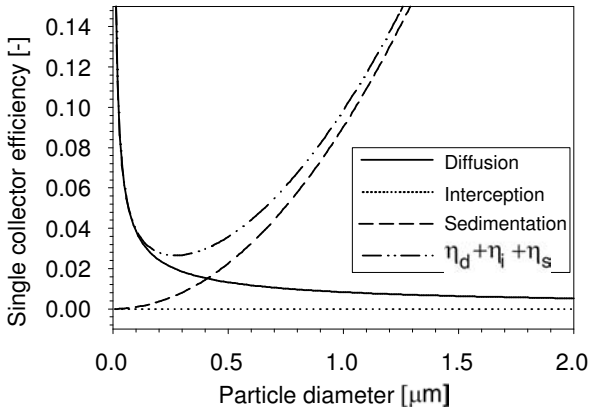

Figure 4.1: Single collector efficiencies as a function of colloid diameter for a colloid density of 2.65 g/cm^3, collector diameter $d_c = 462.5$ μm, and a pore water velocity $v_0 = 10^{-5}$ m/s.

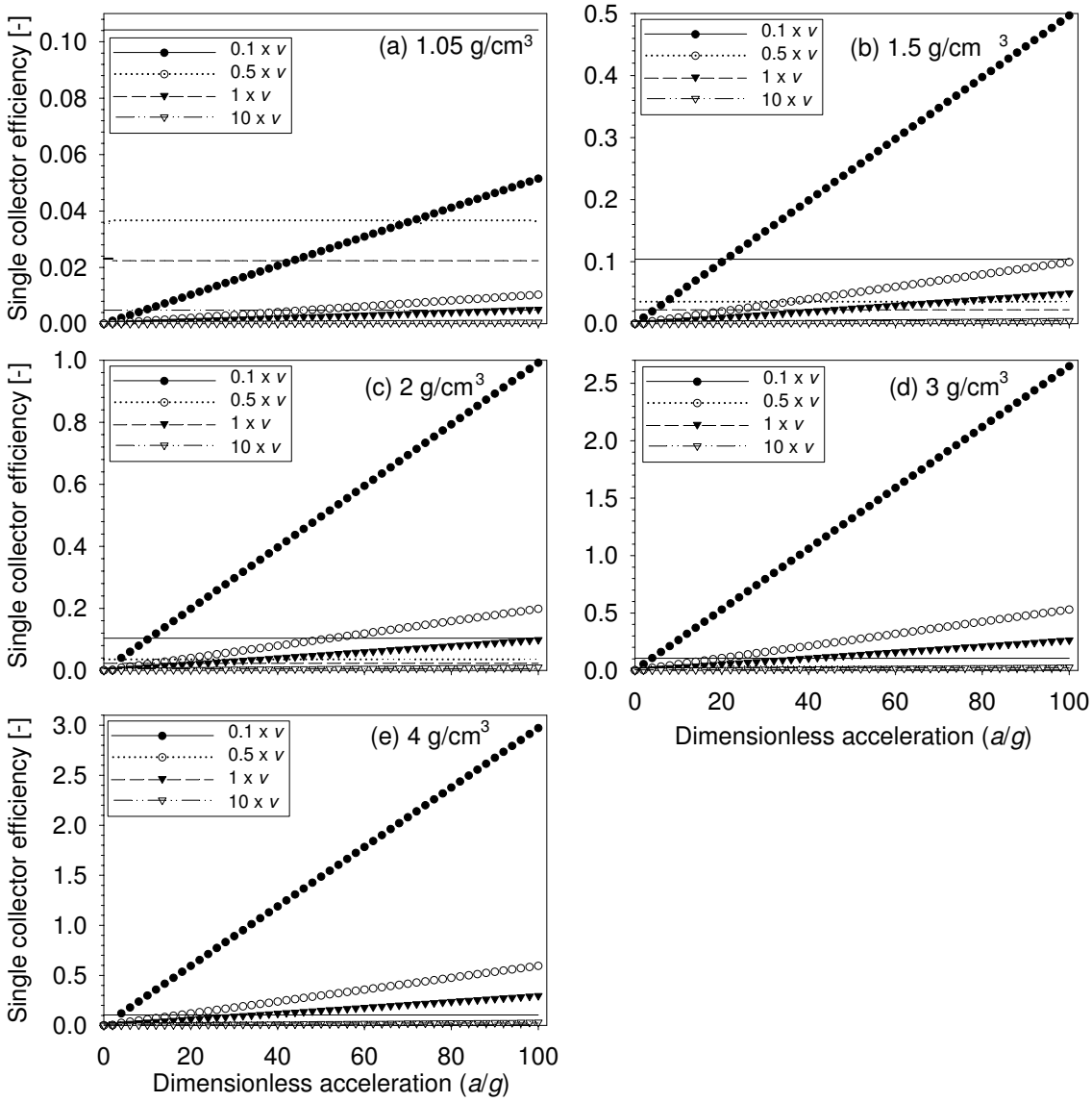

Figure 4.2: Effect of centrifugal acceleration on single collector efficiency due to sedimentation and diffusion for colloids of (a) 1.05 g/cm^3 (b) 1.5 g/cm^3, (c) 2 g/cm^3, (d) 3 g/cm^3, and (e) 4 g/cm^3 and 160 nm in diameter. The reference pore water velocity v is equal to 5.09 cm/h = 1.4×10^{-5} m/s. Symbols indicate single collector efficiency due to sedimentation and lines indicate single collector efficiency due to diffusion.

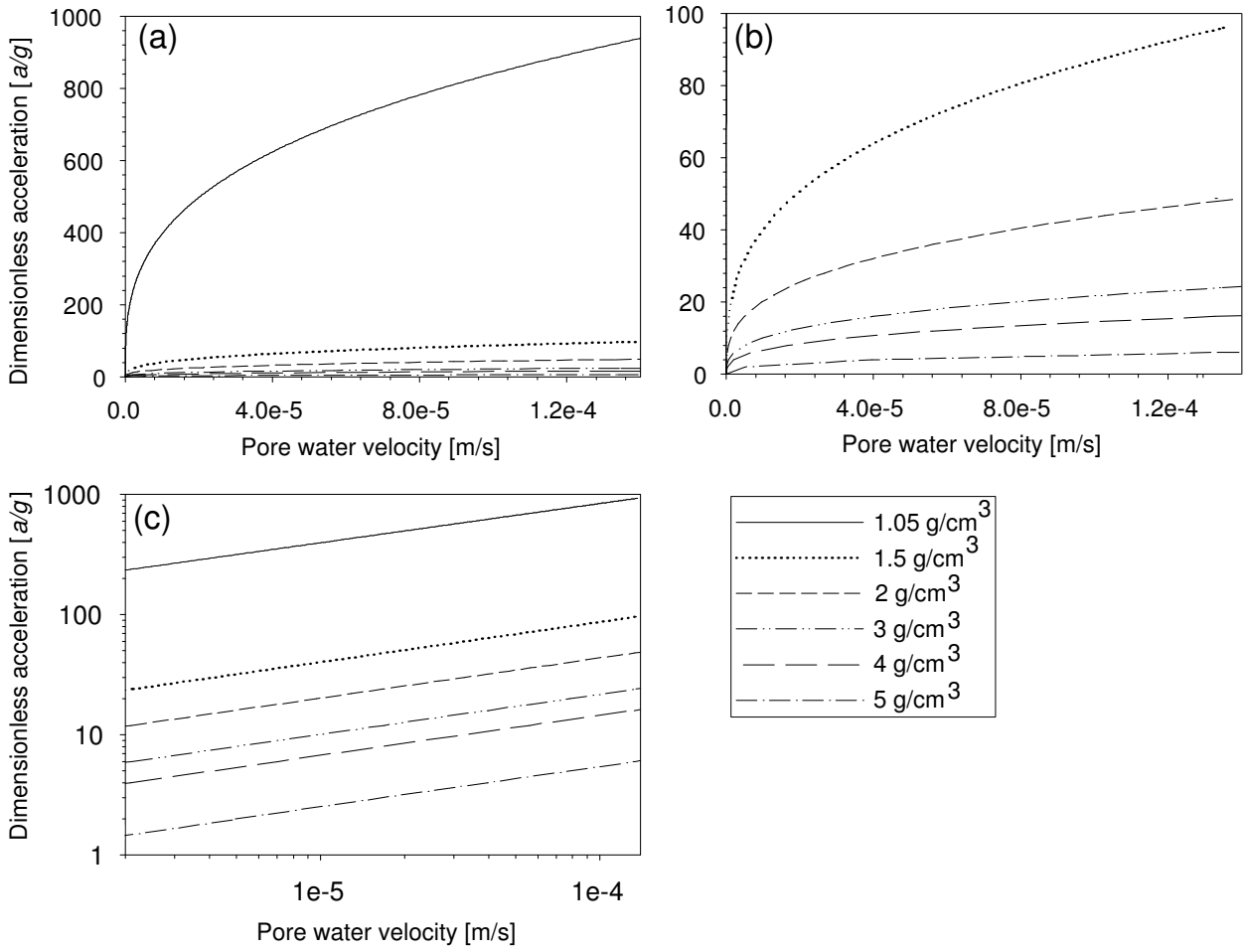

Figure 4.3: Relationship between acceleration and pore water velocity as affected by particle density for colloids of 160-nm diameter (equation 4.22). Figures (a), (b), and (c) show the same data, but with different axis scales.

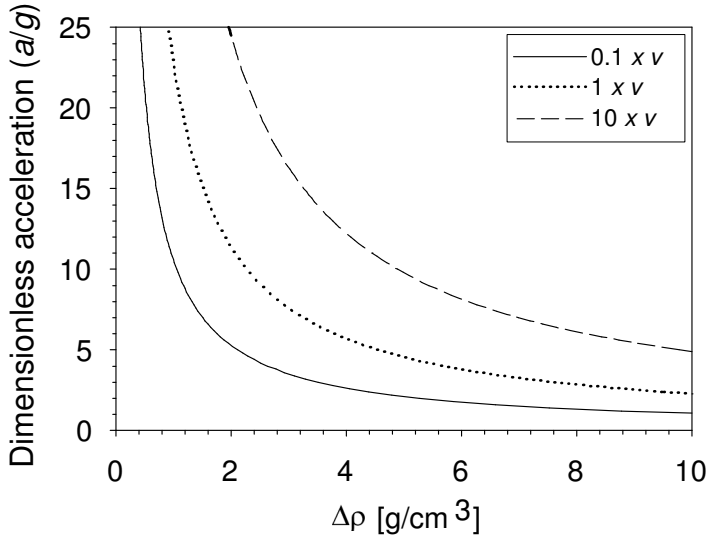

Figure 4.4: Relationship between acceleration and density difference $\Delta\rho$ as affected by pore water velocity (equation 4.22). The reference pore water velocity v is equal to 5.09 cm/h = 1.4×10^{-5} m/s.

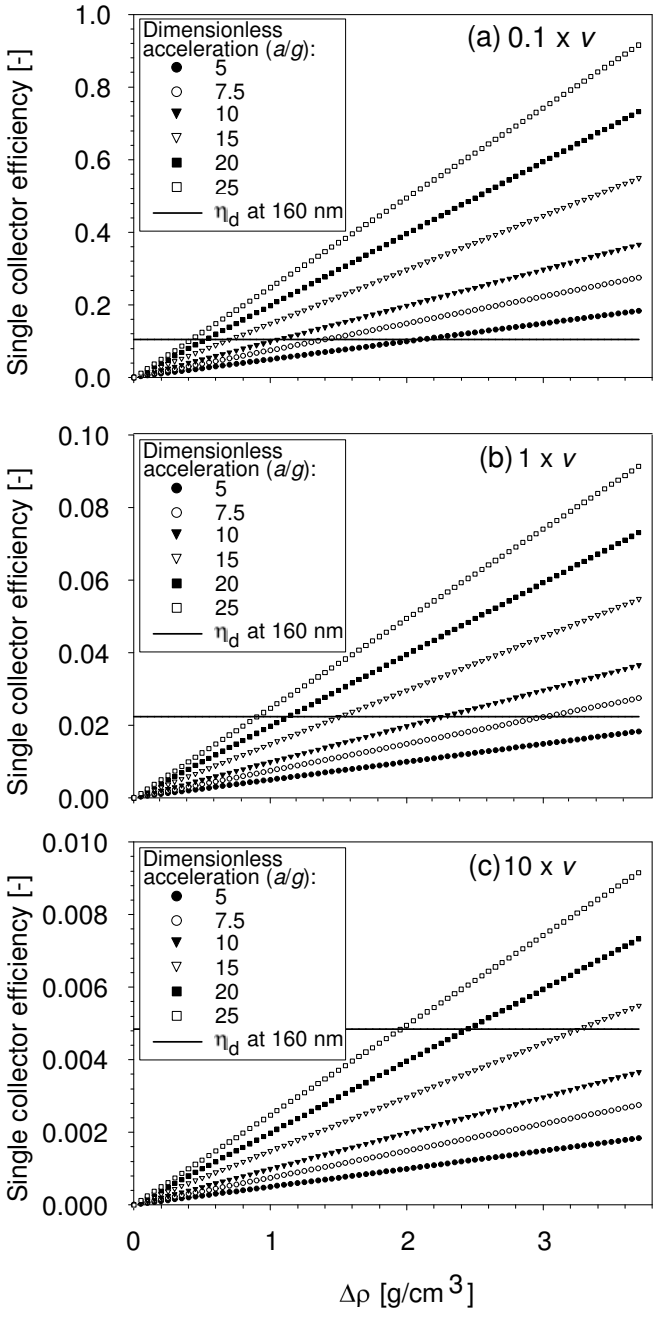

Figure 4.5: Effect of particle density on single collector efficiency due to sedimentation at 0.1 ×, 1 × and 10 × pore water velocity. The reference pore water velocity v is equal to 5.09 cm/h = $1.4{\times}10^{-5}$ m/s.

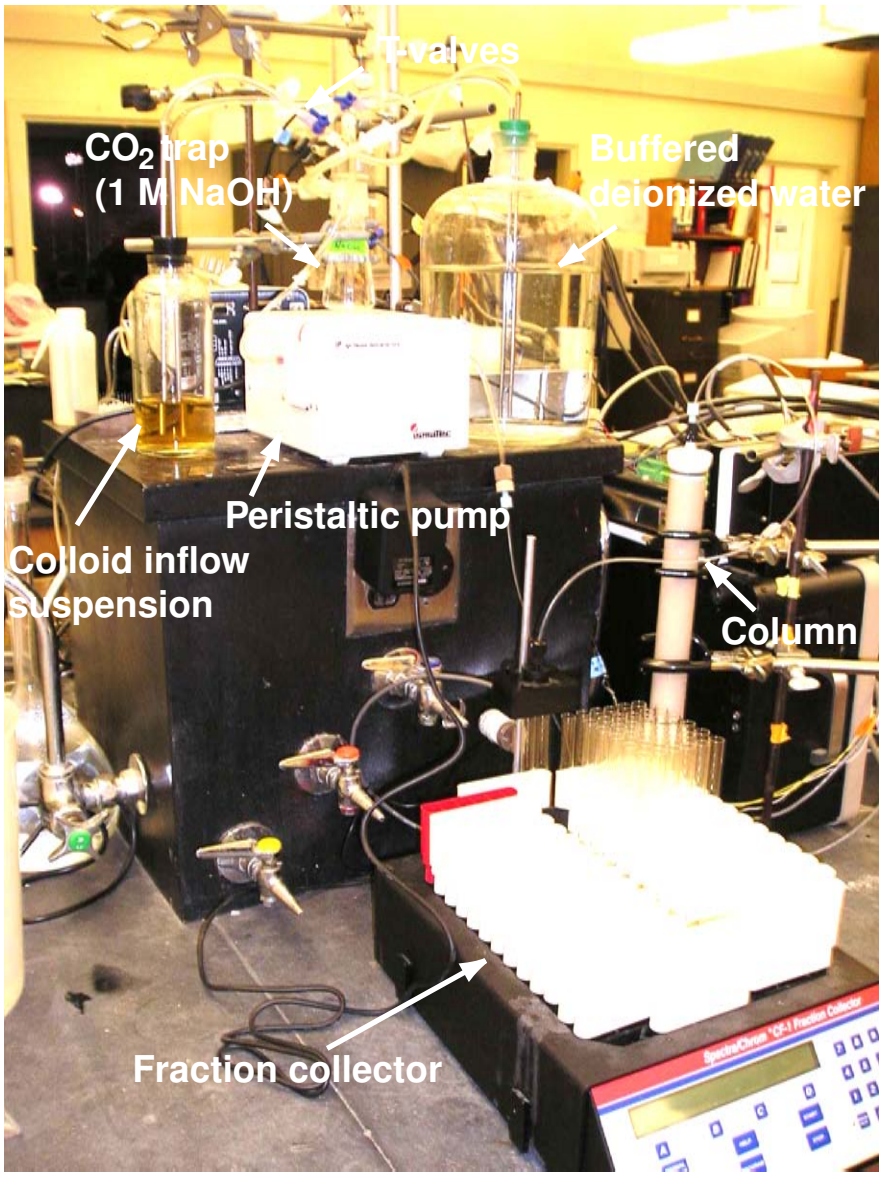

Figure 4.6: Picture of the bench top column filtration setup. The particular setup shown is for upward flow.

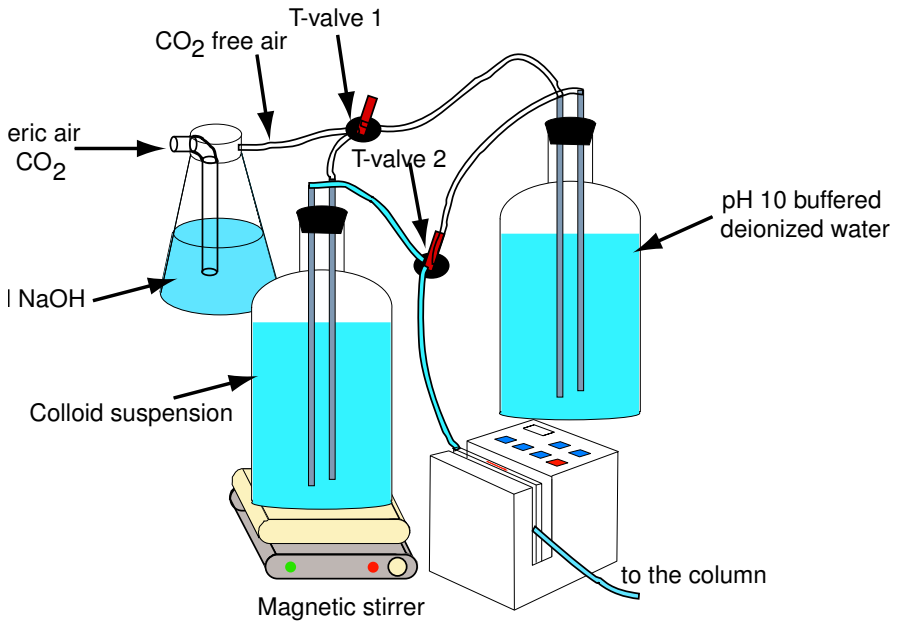

Figure 4.7: Schematic of the CO_2 trap and the column inflow system.

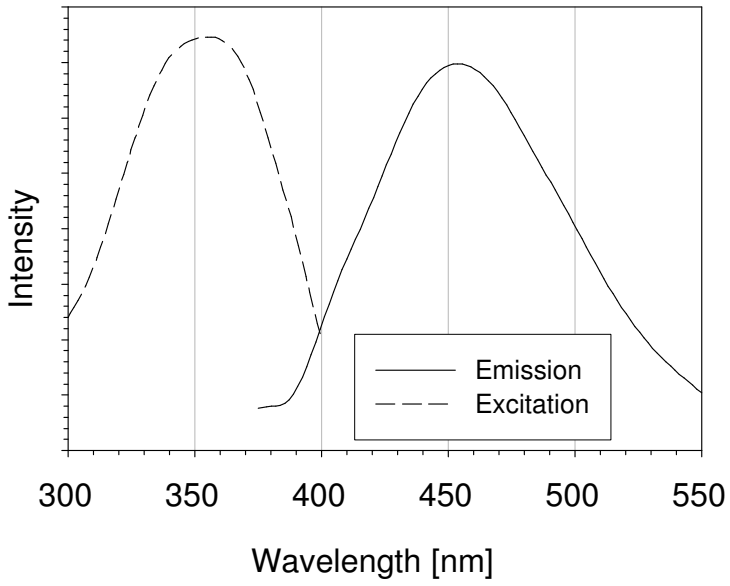

Figure 4.8: Excitation and emission spectra of the fluorescent silica particles.

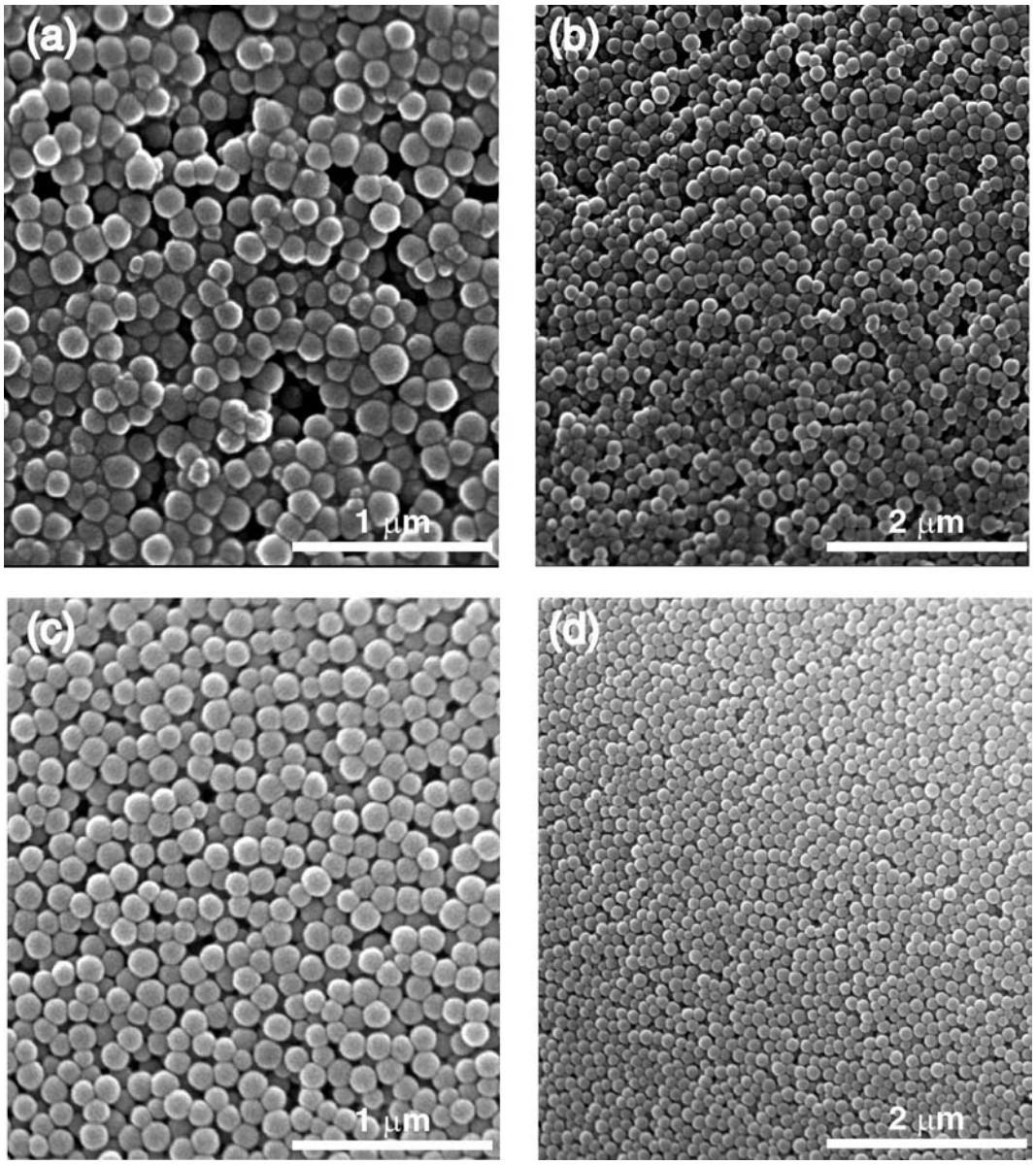

Figure 4.9: Scanning electron micrographs of the fluorescent silica (a, b) and polystyrene colloids (c, d).

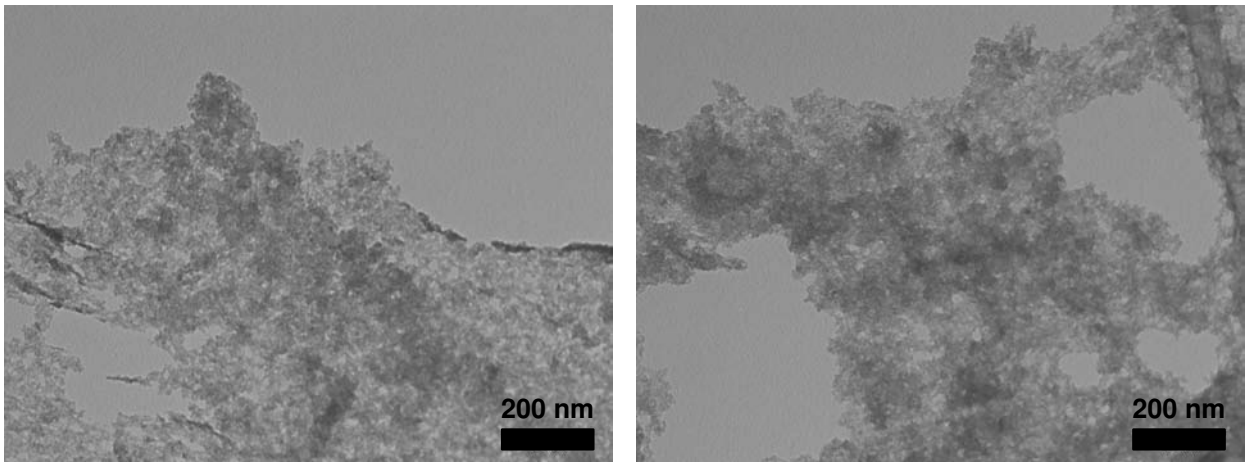

Figure 4.10: Transmission electron micrographs of the 2-line ferrihydrite colloids. Note, that the individual particles are only 2–3 nm in diameter, but they have a high tendency to form aggregates.

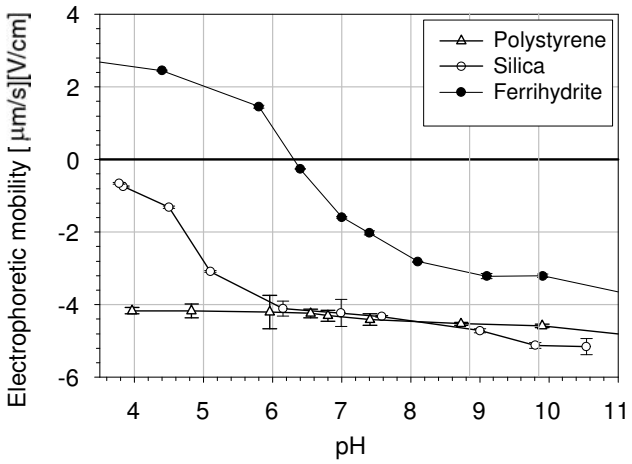

Figure 4.11: Electrophoretic mobility of the colloids as a function of pH. Error bars denote ± one standard deviation.

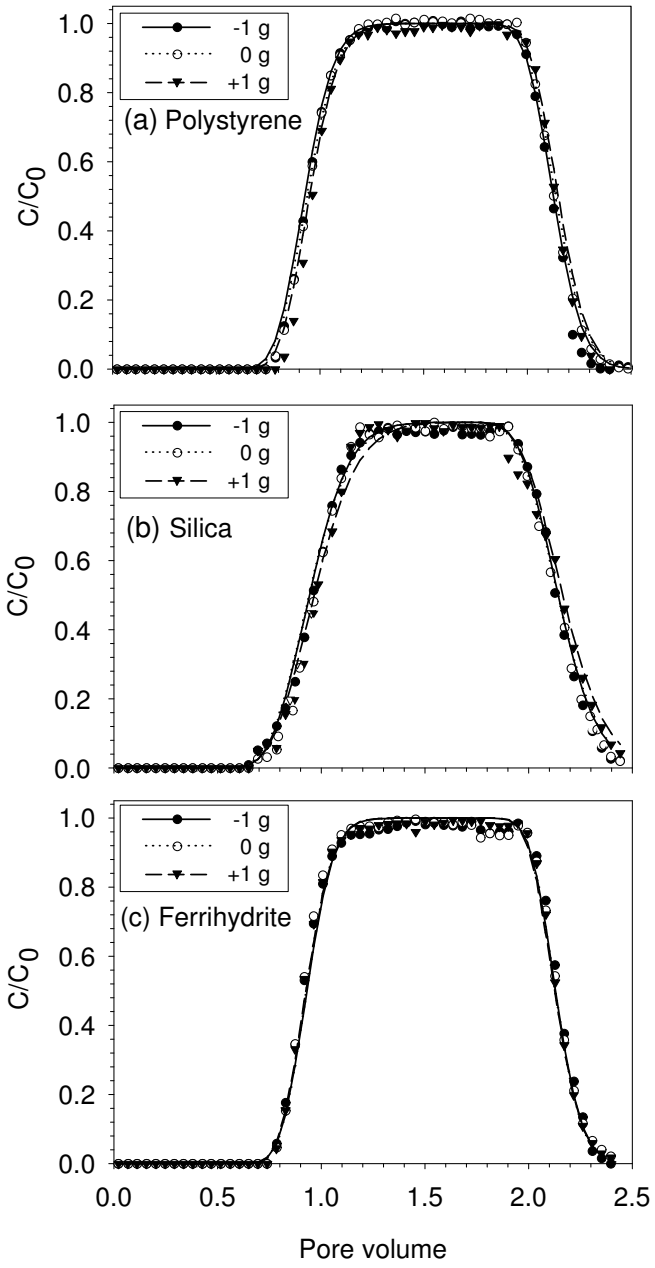

Figure 4.12: Breakthrough curves from bench top experiments using (a) polystyrene latex colloids (1.05 g/cm^3), (b) fluorescent silica beads (2 g/cm^3), and (c) ferrihydrite colloids (4 g/cm^3) in upward ($+1$ g), horizontal (0 g) and downward (-1 g) flow directions. Symbols are the measured data and lines are fitted ADE model.

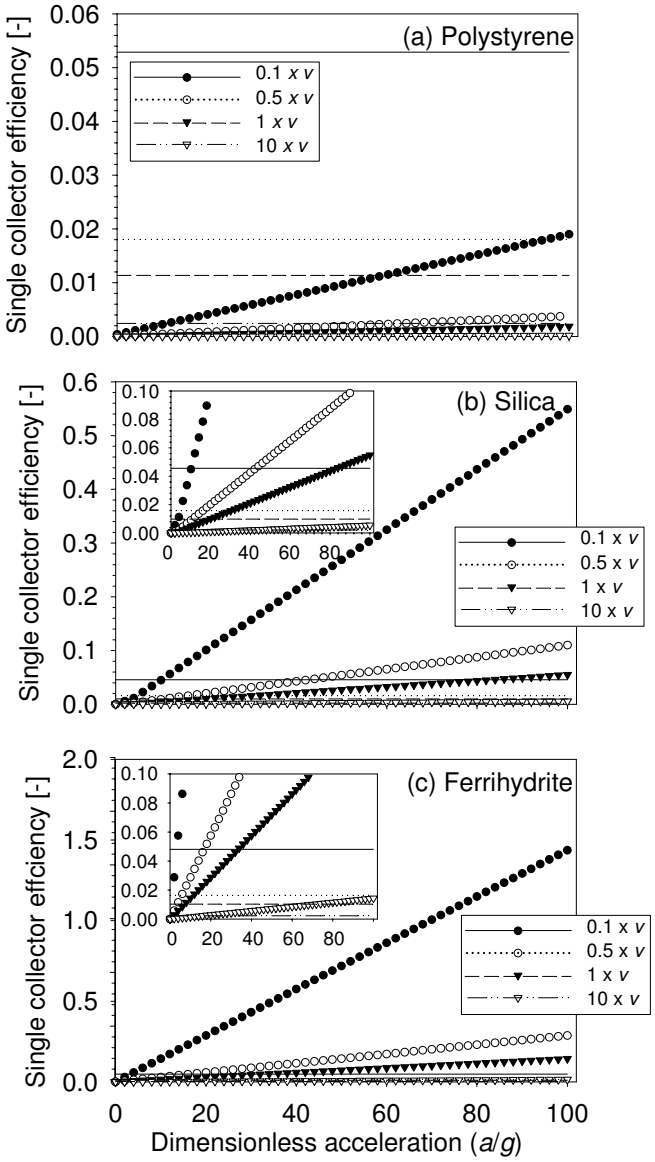

Figure 4.13: Effect of centrifugal acceleration on single collector efficiency due to sedimentation and diffusion for colloids of (a) polystyrene, (b) silica, and (c) ferrihydrite. The reference pore water velocity is $v = 14.1$ cm/h $= 3.9 \times 10^{-5}$ m/s. Symbols indicate single collector efficiency due to sedimentation and lines indicate single collector efficiency due to diffusion.

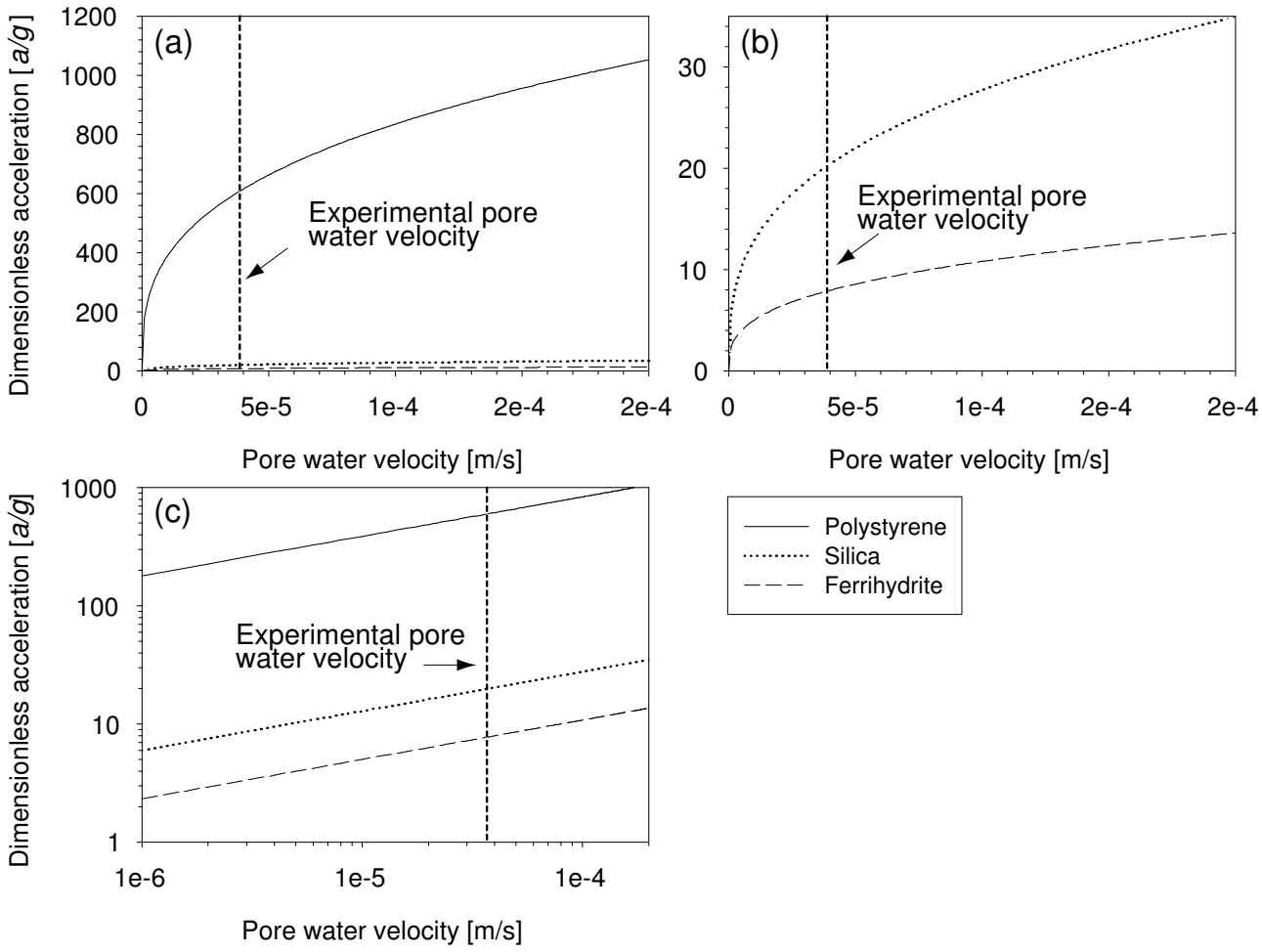

Figure 4.14: Relationship between acceleration and pore water velocity for polystyrene, silica, and ferrihydrite. Figures (a), (b), and (c) show the same data, but with different axis scales.

Figure 4.15: The 50 g-ton, 2-m radius geocentrifuge at the Idaho National Engineering and Environmental Laboratory (INEEL), in Idaho Falls, ID.

Chapter 5

Summary and Conclusions

This study presents results from experiments designed to evaluate the potential role of colloids as carriers for radionuclides and other charged subsurface contaminants. We carried out several batch, miscible displacement, and dynamic light scattering experiments to better understand colloid transport. This dissertation focused on colloid stability in Hanford pore water, applicability of fiber glass wicks for colloid sampling, and a predominantly theoretical treatment of colloid transport under various gravitational and centrifugal accelerations.

Colloid stability is affected by both colloid surface properties and by the composition of the aqueous solution. Colloid stability was investigated with batch turbidity experiments, column mobilization experiments, and dynamic light scattering measurements. Our results show that under pore water chemical conditions in the vadose zone at Hanford reservation, colloids are stable in the time frame of weeks. Dynamic light scattering critical coagulation values were higher than the values obtained from batch turbidity and column mobilization experiments. Similarly, critical coagulation values

values obtained for montmorillonite and kaolinite (*i.e.*, pure mineral systems) by DLS experiments were higher than those reported in the literature. Colloids were mobilized from columns packed with native Hanford sediments, when the inflow solution's Na^+ concentration was decreased from 1,000 $mmol_c/L$ to less than 87 $mmol_c/L$ and 47 $mmol_c/L$ in the case of the fine and coarse Hanford sand, respectively. However, no colloids were mobilized, when we used 1,000 $mmol_c/L$ $CaCl_2$ as equilibrating, and deionized water as flushing solution. To simulate Hanford pore water, we used NaCl, KCl, $CaCl_2$ and $MgCl_2$ as flocculating electrolytes and used sodium adsorption ratio reported by Serne et al.[2002b]. Under such suspension chemical conditions the native colloids were stable for 19 hrs, i.e., the duration of the experiment. CCC_{Na}/CCC_{Ca} ratio obtained by dynamic light scattering ranged between 50 and 55, which is reasonably close to the theoretical value of 42. Many studies indicate, that experimentally obtained ratios can deviate by one or two orders of magnitude from the theoretical value[*Hsu and Kuo,* 1995*; Hsu and Kuo,* 1997*; Grolimund et al.,* 2001]. However, the observed slopes of the stability curves for Ca were steeper than for Na, by a factor of about 2. This discrepancy with the previous literature data can be explained by the surface roughness and the surface charge heterogeneity of the suspended particles and the newly formed aggregates.

The suitability of fiberglass wicks to sample colloids *in situ* seems to be limited, because of the observed inconsistent colloid recovery during the laboratory transport experiments. A considerable portion of the colloids was retained within the wick and

flow rate, pH, and colloid type affected colloid transport. Colloid retention within the wicks can be caused by physico-chemical processes (electrostatic and van der Waals interactions) and by physical straining. We measured the specific surface area of the wicks and calculated the average film thicknesses in 11-cm segments. We found 1.62 to 195 μm water thickness in the top segment. Since water film thicknesses are at least 3 times larger than average the average hydrodynamic diameters; therefore physical straining is unlikely to be responsible for the observed retention of the colloids within the wick. We think, that colloid removal form suspensions was primarily caused by physico-chemical processes. Native colloids showed almost complete recovery at both pH 7 and pH 10. Ferrihydrite was the most sensible colloid for pH change, as it completely broke through at pH 10, but were entirely retained at pH 7. This pronounced effect of pH on ferrihydrite recovery was expected, due to the electrostatic interactions between the particles and the wick material, as the ferrihydrite's isoelectric point is around pH 6.2 to 6.4, and the wick material's (amorphous silica) is between pH 3.6 and 3.9 [*Langmuir,* 1997]. The recovery of the modified colloids ranged between 59 and 97%, and was considerably affected by flow rate. Their poor recovery can be explained by their size and surface charge properties, as modified colloids had the largest particle diameter among the five colloids and had the second highest isoelectric point. Montmorillonite recovery ranged between 49 and 90%, with slightly lower recovery at pH 7. Kaolinite did not break through at pH 7, and relatively poorly recovered at pH 10 (18–70%). The kaolinite behavior can be explained by its surface

charge heterogeneity and positive edge charges were likely responsible for its complete removal at pH 7.

We evaluated the applicability of geocentrifuges for colloid transport under saturated conditions. To determine the applicability of centrifuges for colloid transport studies, we carried out theoretical calculations to study how altered force fields, particle density, and flow velocity affect colloid transport and retention. The theoretical calculations indicated, that sedimentation and diffusion of colloids are strongly affected by flow velocity, particle diameter and specific density when centrifugal force field is applied, and particles have a particle density higher than 2 g/cm^3. We also performed transport experiments with polystyrene, silica, and ferrihydrite colloids for comparative purposes. We did not observe effect of either particle density or flow direction on the shape of the breakthrough curves in the bench top experiments. Modeling the experimental data by employing CXTFIT showed minimal retardation of the colloids. It is expected that for natural subsurface colloids, such as silicates and iron oxides, filtration will be different in centrifuge experiments as compared to normal gravity conditions. At typical subsurface flow rates, accelerations as low as 4 g or less can change the filtration behavior.

Bibliography

Abdou, H. M., and M. Flury, Simulation of water flow and solute transport in free-drainage lysimeters and field soils with heterogeneous structures, *Eur. J. Soil Sci.*, *55*, 229–241, 2004.

Alemi, M. H., D. R. Nielsen, and J. W. Biggar, Determining the hydraulic conductivity of soil cores by centrifugation, *Soil Sci. Soc. Am. J.*, *40*, 212–218, 1976.

Allison, J., D. Brown, and K. Novo-Gradac, *MINTEQA2/PRODEFA2. A Geochemical Assessment Model for Environmental Systems, v. 3.0 User's Manual*, U.S. EPA, Athens, GA, 1991.

Apps, J. A., C. L. Carnahan, P. C. Lichtner, M. C. Michel, D. Perry, R. J. Silva, O. Weres, and A. F. White, *Status of Geochemical Problems Relating to the Burial of High-Level Radioactive Waste*, Lawrence Berkeley Laboratory, Prepared for the U.S. Nuclear Regulatory Commission, NRC FIN B3109, Washington DC, 1982.

Arora, H. S., and N. T. Coleman, The influence of electrolyte concentration on flocculation of clay suspensions, *Soil Sci.*, *127*, 134–139, 1979.

ASTM Standard test method for density of hydraulic cement, c 188-95, *Annual Book of ASTM Standards, Section 4: Construction* pp. 177–178, American Society for Testing and Materials, West Conshohocken, 2000.

Behrens, S. H., D. I. Christl, R. Emmerzael, P. Schurtenberger, and M. Borkovec, Charging and aggregation properties of carboxyl latex particles: Experiments versus DLVO theory, *Langmuir*, *16*, 2566–2575, 2000.

Biddle, D. L., D. J. Chittleborough, and R. W. Fitzpatrick, Field monitoring of solute and colloid mobility in a gneissic sub-catchment, South Australia, *Appl. Clay Sci.*, *9*, 433–442, 1995.

Boll, J., J. S. Selker, B. M. Nijssen, T. S. Steenhuis, J. V. Winkle, and E. Jolles, Water quality sampling under preferential flow conditions, in *Lysimeters for evapotranspiration and environmental measurement*, edited by R. G. Allen, pp. 290–298, ASCE, New York, NY, 1991.

Boll, J., T. S. Steenhuis, and J. S. Selker, Fiberglass wicks for sampling of water and solutes in the vadose zone, *Soil Sci. Soc. Am. J.*, *56*, 701–707, 1992.

Brahy, V., and B. Delvaux, Comments on "Artifacts caused by collection of soil solution with passive capillary samplers", *Soil Sci. Soc. Am. J.*, *65*, 1571–1572, 2001.

Brahy, V., M.-C. Henao-Toro, F. Goor, J.-F. Ledent, and B. Delvaux, Assessing passive capillary-wick samplers for monitoring resident nitrate concentration in real field, *Soil Use Manage.*, *18*, 18–25, 2002.

Brandi-Dohrn, F. M., R. P. Dick, M. Hess, and J. S. Selker, Field evaluation of passive capillary samplers, *Soil Sci. Soc. Am. J.*, *60*, 1705–1713, 1996.

Briggs, L. J., and J. W. McLane, 1907. The moisture equivalents of soils, *Technical Report 45*, U.S. Department of Agriculture, Bureau of Soils, Washington D.C.

Briggs, L. J., and J. W. McLane, Moisture equivalent determinations, and their application, *Proc. Am. Soc. Agron.*, *2*, 138–147, 1910.

Brown, K. W., J. C. Thomas, and M. W. Holder, 1988. Development of a capillary wick unsaturated zone pore water sampler, *Technical report*, U. S. Environmental Protection Agency.

Busacca, A. J., Loess deposits and soils of the Palouse and vicinity, in *Quaternary Non-Glacial Geology of the United States*, vol. K-2, edited by R. B. Morrison, pp. 216–228, Geological Society of America, Boulder, CO, 1991.

Celorie, J. A., S. L. Woods, T. S. Vinson, and J. D. Istok, A comparison of sorption equilibrium distribution coefficients using batch and centrifugation methods, *J. Environ. Qual.*, *18*, 307–313, 1989.

Cherrey, K. D., M. Flury, and J. B. Harsh, Nitrate and colloid transport through coarse hanford sediments under steady state, variably saturated flow, *Water Resour. Res.*, *39*, 1165, doi:10.1029/2002WR001944, 2003, 2003.

Conca, J. L., and J. Wright, Diffusion coefficients in gravel under unsaturated conditions, *Water Resour. Res.*, *26*, 1055–1066, 1990.

Conca, J. L., and J. Wright, Diffusion and flow in gravel, soil, and whole rock, *Appl. Hydrogeol.*, *1*, 5–24, 1992.

Conca, J. L., and J. Wright, The UFA method for rapid, direct measurements of unsaturated soil properties, *Aust. J. Soil Res.*, *36*, 291–315, 1998.

Conca, J. L., and J. Wright, The UFA method for characterization of vadose zone behavior, in *Vadose Zone Science and Technology Solutions*, vol. Additional case studies on CD-Rom, edited by B. B. Looney, and R. W. Falta, pp. 4–24, Battelle Press, Columbus, 2000.

Cox, J. W., D. J. Chittleborough, H. J. Brown, A. Pitman, and J. C. R. Varcoe, Seasonal changes in hydrochemistry along a toposequence of texture-contrast soils, *Aust. J. Soil Res.*, *40*, 581–604, 2002.

Dewoolkar, M. M., H.-Y. Ko, and A. T. Stadler, Substitute pore fluid for seismic centrifuge modeling, *Geotechnical Testing J.*, *22*, 196–210, 1999.

Domenico, P. A., and F. W. Schwartz, *Physical and Chemical Hydrogeology*, 2nd ed., John Wiley & Sons, New York, 1998.

Elimelech, M., J. Gregory, X. Jia, and R. A. Williams, *Particle deposition and aggregation*, 1st ed., Butterworth-Heinemann, Woburn, MA, 1995.

Flury, M., and T. Gimmi, Solute diffusion, in *Methods of Soil Analysis, Part 4, Physical Methods*, edited by D. J. H., and G. C. Topp, pp. 1323–1351, Soil Science Society of America, Madison, WI, 2002.

Flury, M., J. B. Mathison, and J. B. Harsh, *In situ* mobilization of colloids and transport of cesium in Hanford sediments, *Environ. Sci. Technol.*, *36*, 5335–5341, 2002.

Flury, M., S. Czigány, G. Chen, and J. B. Harsh, Cesium migration in staurated silica sand and Hanford sediments as impacted by ionic strength, *J. Contam. Hydrol.*, *71*, 111–126, 2004.

Gamerdinger, A. P., and D. I. Kaplan, Application of a continuous-flow centrifugation method for solute transport in disturbed, unsaturated sediments and illustration of mobile-immobile water, *Water Resour. Res.*, *36*, 1747–1755, 2000.

Gamerdinger, A. P., and D. I. Kaplan, Physical and chemical determinants of colloid transport and deposition in water-unsaturated sand and Yucca Mountain tuff material, *Environ. Sci. Technol.*, *35*, 2497–2504, 2001.

Gamerdinger, A. P., D. I. Kaplan, D. M. Wellman, and R. J. Serne, Two-region flow and rate-limited sorption of uranium (VI) during transport in an unsaturated silt loam, *Water Resour. Res.*, *37*, 3147–3153, 2001a.

Gamerdinger, A. P., D. I. Kaplan, D. M. Wellman, and R. J. Serne, Two-region flow and and decreased sorption of uranium (VI) during transport in Hanford groundwater and unsaturated sands, *Water Resour. Res.*, *37*, 3155–3162, 2001b.

Gardner, R., A method of measuring the capillary tension of soil moisture over a wide moisture range, *Soil Sci.*, *43*, 277–283, 1937.

Gee, G. W., A. L. Ward, T. G. Caldwell, and J. C. Ritter, A vadose zone water fluxmeter with divergence control, *Water Resour. Res.*, *38*, DOI 10.1029/2001WR000816, 2002.

Gee, G. W., and M. D. Campbell, A wick tensiometer to measure low tensions in coarse soils, *Soil Sci. Soc. Am. J.*, *54*, 1498–1500, 1990.

Gee, G. W., and P. R. Heller, 1985. Unsaturated water flow at the Hanford site: A review of literature and annotated bibliography, *Technical report*, Pacific Northwest National Laboratory, Richland, WA.

Gee, G. W., F. Zhang, and A. L. Ward, A modified vadose zone fluxmeter with solution collection capability, *Vadose Zone J.*, *2*, 627–632, 2003.

Gee, G. W., M. J. Fayer, M. L. Rockhold, and M. D. Campbell, Variations in recharge at the Hanford site, *Northwest Sci.*, *66*, 237–250, 1992.

Gephart, R. E., and R. E. Lundgren, 1997. Hanford tank clean up: A guide to understanding the technical issues, *Technical Report PNL-10773*, Pacific Northwest Laboratory, Richland, WA.

Gephart, R. E., and R. E. Lundgren, *Hanford Tank Cleanup: A Guide to understanding the technical issues*, 4th ed., Battelle Press, Columbus, 1998.

Goldberg, S., and H. S. Forster, Flocculation of reference clays and arid-zone soil clays, *Soil Sci. Soc. Am. J.*, *54*, 714–718, 1990.

Goldberg, S., and R. A. Glaubig, Effect of saturating cation, pH, and aluminum and iron-oxide on the flocculation of kaolinite and montmorillonite, *Clays Clay Miner.*, *35*, 220–227, 1987.

Goldberg, S., H. S. Forster, and E. L. Heick, Flocculation of illite/kaolinite and illite/montmorillonite mixtures as affected by sodium adsorption ratio and pH, *Clays Clay Miner.*, *4*, 375–380, 1991.

Goyne, K. W., R. L. Day, and J. Chorover, Artifacts caused by collection of soil solution with passive capillary samplers, *Soil Sci. Soc. Am. J.*, *64*, 1330–1336, 2000.

Grolimund, D., and M. Borkovec, Long-term release kinetics of colloidal particles from natural porous media, *Environ. Sci. Technol.*, *33*, 4054–4060, 1999.

Grolimund, D., M. Elimelech, and M. Borkovec, Aggregation and deposition kinetics of mobile colloidal particles in natural porous media, *Colloids Surf.*, *191*, 179–188, 2001.

Grolimund, D., M. Elimelech, M. Borkovec, K. Barmettler, and H. Sticher, Transport of *in situ* mobilized colloidal particles in packed soil columns, *Environ. Sci. Technol.*, *32*, 3562–3569, 1996.

Harrach, R. J., and K. A. Surano, *LLNL Environmental report for 1994. Appendix B. Methods of dose calculations*, Lawrence Livermore National Laboratory, on-line at http://www.llnl.gov/saer/saer96/96pdfs/v1.apB.pdf, accessed in August 2004, 2004.

Hensley, P. J., and C. Savvidou, Modelling pollutant transport in soils, *Aust. Geomech.*, *22*, 7–16, 1992.

Hesterberg, D., and A. L. Page, Flocculation series test yielding time invariant critical coagulation concentrations of sodium illite, *Soil Sci. Soc. Am. J.*, *54*, 729–735, 1990.

Hiemenz, P. C., and R. Rajagopalan, *Principles of colloid and surface chemistry*, Marcel Dekker Inc., New York, NY, 1997.

Hoitink, D. J., K. W. Burk, J. V. Ramsdell, and W. J. Shaw, 2002. Hanford site climatological data. Summary 2001 with historical data, *Technical report*, Pacific Northwest Laboratory, Richland, WA.

Holder, M., K. W. Brown, J. C. Thomas, D. Zabcik, and H. E. Murray, Capillary-wick unsaturated zone soil pore water sampler, *Soil Sci. Soc. Am. J.*, *55*, 1195–1202, 1991.

Holthoff, H., S. U. Egelhaaf, M. Borkovec, P. Schurtenberger, and H. Sticher, Coagulation rate measurements of colloidal particles by simultaneous static and dynamic light scattering, *Langmuir*, *12*, 5541–5549, 1996.

Hsu, J.-P., and Y.-C. Kuo, An extension of the schulze-hardy rule to asymmetric electrolytes, *J. Colloid Interface Sci.*, *185*, 254–255, 1995.

Hsu, J.-P., and Y.-C. Kuo, The critical coagulation concentration of counterions: Spherical particles in asymmetric electrolyte solutions, *J. Colloid Interface Sci.*, *185*, 530–537, 1997.

ISSMGE-TC2 *Geotechnical Centrifuges Worldwide*, Centrifuge and Physical Model Testing Technical Committee of the International Society of Soil Mechanics and Geotechnical Engineering, on-line at http://geo.citg.tudelft.nlallersma/tc2/cents.htm, accessed in July 2004, 2004.

Joseph, A. F., and F. J. Martin, The moisture equivalent of heavy soils, *Journ. Agr. Sci.*, *13*, 49–57, 1923.

Jury, W. A., W. R. Gardner, and W. H. Gardner, *Soil Physics*, 5th ed., John Wiley and Sons, Inc., New York, 1991.

Kaplan, D. I., M. E. Sumner, P. M. Bertsch, and D. C. Adriano, Chemical conditions conducive to the release of mobile colloids from ultisol profiles, *Soil Sci. Soc. Am. J.*, *60*, 269–274, 1996.

Keren, R., I. Shainberg, and E. Klein, Settling and flocculation value of sodium-montmorillonite particles in aqueous media, *Soil Sci. Soc. Am. J.*, *52*, 76–80, 1988.

Kersting, A. B., D. W. Efurd, D. L. Finnegan, D. J. Rokop, D. K. Smith, and J. L. Thompson, Migration of plutonium in ground water at the Nevada Test Site, *Nature*, *397*, 56–59, 1999.

Knutson, J., and J. S. Selker, Fiberglass wick sampler effects on measurements of solute transport in the vadose zone, *Soil Sci. Soc. Am. J.*, *60*, 420–424, 1996.

Knutson, J. H., S. B. Lee, W. Q. Zhang, and J. S. Selker, Fiberglass wick prepartion for use in passive capillary wick soil pore-water samplers, *Soil Sci. Soc. Am. J.*, *57*, 1474–1476, 1993.

Kretzschmar, R., H. Holthoff, and H. Sticher, Influence of pH and humic acid on coagulation kinetics of kaolinite: A dynamic light scattering study, *J. Colloid Interface Sci.*, *202*, 95–103, 1998.

Kretzschmar, R., W. P. Robarge, and S. B. Weed, Flocculation of kaolinitic soil clays: Effect of humic substances and iron oxides, *Soil Sci. Soc. Am. J.*, *57*, 1277–1283, 1993.

Laegdsmand, M., K. G. Villholth, M. Ullum, and K. H. Jensen, Processes of colloid mobilization and transport in macroporous soil monoliths, *Geoderma*, *93*, 33–59, 1999.

Langmuir, D., *Aqueous Environmental Chemistry*, Prentice Hall, Upper Saddle River, NJ, 1997.

Lichtner, P. C., S. Yabusaki, K. Pruess, and C. I. Steefel, 2003. Role of competitive cation exchange on chromatographic displacement of cesium in the vadose zone beneath the Hanford S/SX tank farm, *Technical Report LA-UR-03-3890*, Los Alamos National Laboratory.

Loeppert, R. H., and W. P. Inskeep, Iron, in *Methods of Soil Analysis. Part 3. Chemical Methods*, edited by D. L. Sparks, pp. 639–664, American Society of Agronomy, Madison, Wisconsin, 1996.

Logan, B. E., D. G. Jewett, R. G. Arnold, E. J. Bouwer, and C. R. O'Melia, Clarification of clean-bed filtration models, *J. Environ. Eng.*, *121*, 869–873, 1995.

Louie, M. J., P. M. Shelby, J. S. Smesrud, L. O. Gatchell, and J. S. Selker, Field evaluation of passive capillary samplers for estimating groundwater recharge, *Water Resour. Res.*, *36*, 2407–2416, 2000.

Marshall, E., Hanford's radioactive tumbleweed, *Science*, *236*, 1616–1620, 1987.

McCarthy, J., and J. Zachara, Subsurface transport of contaminants, *Environ. Sci. Technol.*, *23*, 496–502, 1989.

McCarthy, J. F., and C. Degueldre, Sampling and characterization of groundwater colloids for studying their role in the subsurface transport of contaminants, in *Environmental Particles*, vol. II, edited by J. Buffle, and H. van Leeuwen, pp. 247–315, Lewis Publisher, Boca Raton, FL, 1993.

McDowell-Boyer, L. M., J. R. Hunt, and N. Sitar, Particle transport through porous media, *Water Resour. Res.*, *22*, 1901–1921, 1986.

McGraw, M. A., *The effect of colloid size, colloid hydrophobicity, and volumetric water content on the transport of colloids through porous media*, Ph.D. Diss. No. 77503, University of California, Berkeley, CA, 1996.

McGraw, M. A., The effect of colloid size, colloid hydrophobicity, and volumetric water content on the transport of colloids through unsaturated porous media, in *Vadose Zone Science and Technology Solutions*, vol. 2, edited by B. B. Looney, and R. W. Falta, pp. 928–938, Battelle Press, Columbus, 2000.

McGraw, M. P., and D. I. Kaplan, 1997. Colloid suspension stability and transport through unsaturated porous media, *Technical Report PNNL–11565*, Pacific Northwest National Laboratory, Richland, WA.

McKinley, J. P., C. J. Zeissler, J. M. Zachara, R. J. Serne, R. M. Lindstrom, H. T. Schaef, and R. D. Orr, Distribution and retention of Cs-137 in sediments at the Hanford Site, Washington, *Environ. Sci. Technol.*, *35*, 3433–3441, 2001.

Miller, W. P., H. Frenkel, and K. D. Newman, Flocculation concentration and sodium/calcium exchange of kaoliniotic soil clays, *Soil Sci. Soc. Am. J.*, *54*, 346–351, 1990.

Mitchell, R. J., The eleventh annual R. M. Hardy Keynote Address, 1997: Centrifugation in geoenvironmental practice and education, *Can. Geotech. J.*, *35*, 630–640, 1998.

National Research Council *Science and Technology for Environmentl Cleanup at Hanford*, National Academy Press, Washington D.C., 2001.

Neaman, A., and A. Singer, Flocculation of homoionic sodium palygorskite, palygorskite-montmorillonite mixtures and palygorskite containing soil clays., *Soil Sci.*, *164*, 914–921, 1995.

Nimmo, J. R., Unsaturated flow in a centrifugal field: Measurement of hydraulic conductivity and testing of Darcy's law, *Water Resour. Res.*, *23*, 124–134, 1987.

Nimmo, J. R., and K. A. Mello, Centrifugal techniques for measuring saturated hydraulic conductivity, *Water Resour. Res.*, *27*, 1263–1269, 1991.

Nimmo, J. R., and K. C. Akstin, Hydraulic conductivity of a sandy soil at low water content after compaction by various methods, *Soil Sci. Soc. Am. J.*, *52*, 303–310, 1992.

Nimmo, J. R., D. A. Stonestrom, and K. C. Akstin, The feasibility of recharge rate determinations using the steady-state centrifuge method, *Soil Sci. Soc. Am. J.*, *58*, 49–56, 1994.

Nimmo, J. R., J. Rubin, and D. P. Hammermeister, Unsaturated flow in a centrifugal field: Measurement of hydraulic conductivity and testing of Darcy's law, *Water Resour. Res.*, *23*, 124–134, 1987.

Nimmo, J. R., K. C. Akstin, and K. A. Mello, Improved apparatus for measuring hydraulic conductivity at low water content, *Soil Sci. Soc. Am. J.*, *56*, 1758–1761, 1992.

Novich, B. E., and T. A. Ring, Colloid stability of clays using photon correlation spectroscopy, *Clays Clay Miner.*, *32*, 400–406, 1984.

O'Melia, C. R., Aquasols: the behavior of small particles in aquatic systems, *Environ. Sci. Technol.*, *14*, 1052–1060, 1980.

Permien, T., and G. Lagaly, The rheological and colloidal properties of bentonite dispersions in the presence of organic compounds III. The effect of alcohols on the coagulation of sodium montmorillonite, *Colloid Polym. Sci.*, *272*, 1306–1312, 1994.

Poletika, N. N., K. Roth, and W. A. Jury, Interpretation of solute transport data obtained with fiberglass wick soil solution samplers, *Soil Sci. Soc. Am. J.*, *56*, 1751–1753, 1992.

Pruess, K., S. Yabusaki, C. I. Steefel, and P. C. Lichtner, Fluid flow, heat transfer, and solute transport at nuclear waste storage tanks in the hanford vadose zone., *Vadose Zone J.*, *1*, 68–88, 2002.

Rajagopalan, R., and C. Tien, Trajectory analysis of deep-bed filtration the sphere-in-cell porous media model, *AIChE J.*, *22*, 523–533, 1976.

Rasa, M., and A. P. Philipse, Evidence for a macroscopic electric field in the sedimentation profiles of charged colloids, *Nature*, *429*, 857–860, 2004.

Rhoades, J. D., Salinity: Electrical conductivity and total dissolved solids, in *Methods of soil analysis. Part 3. Chemical methods*, edited by A. Klute, pp. 417–423, American Society of Agronomy, Madison, Wisconsin, 1996.

Rimmer, A., T. S. Steenhuis, and J. S. Selker, One-dimensional model to evaluate the performance of wick samplers in soils, *Soil Sci. Soc. Am. J.*, *59*, 88–92, 1995.

Roy, S. B., and D. A. Dzombak, Colloid release and transport processes in natural and model porous media, *Colloids Surf. Physicochem. Eng. Aspects*, *107*, 245–262, 1996.

Russell, M. B., and L. A. Richards, The determination of soil moisture energy relations by centrifugation, *Soil Sci. Soc. Am. Proc.*, *27*, 65–69, 1938.

Savvidou, C., and P. J. Culligan, The application of centrifuge modelling to geoenvironmental problems, *Proc. Instn. Civ. Engrs. Geotech. Eng.*, *131*, 152–162, 1998.

Schelde, K., P. Moldrup, O. H. Jacobsen, H. de Jonge, L. W. de Jonge, and K. Komatsu, Diffusion-limited mobilization and transport of natural colloids in unsaturated macroporous soil, *Vadose Zone J.*, *1*, 125–136, 2002.

Schwertmann, U., and R. M. Cornell, *Iron oxides in the laboratory*, Wiley VCH, Weinheim, Germany, 2000.

Serne, R. J., B. N. Bjornstad, H. T. Schaef, B. A. Williams, D. C. Lanigan, D. G. Horton, R. E. Clayton, A. V. Mitroshkov, V. L. LeGore, M. J. O'Hara, C. F. Brown, K. E. Parker, I. V. Kutnyakov, J. N. Serne, G. V. Last, S. C. Smith, C. W. Lindenmeier, J. M. Zachara, and D. S. Burke, *Characterization of Vadose Zone Sediment: Uncontaminated RCRA Borehole Core Samples and Composite Samples*, Pacific Northwest National Laboratory, US Department of Energy, PNNL-13757-1, Richland, Washington, 2002.

Serne, R. J., J. M. Zachara, and D. S. Burke, *Chemical Information on Tank Supernatants, Cs Adsorption from Tank Liquids onto Hanford Sediments, and Field Observations of Cs Migration from Past Tank Leaks*, Pacific Northwest National Laboratory, PNNL-11495/UC-510, Richland, WA, 1998.

SRSHES, *Overview of the SRS Environmental Monitoring Program*, Savannah River Site Health Effects Subcommittee of the National Center for Environmental Health, on-line at http://www.llnl.gov/saer/saer96/96pdfs/v1.apB.pdf, accessed in August 2004, 2004.

Stadler, A. T., and Ko, Physical and numerical modeling of cantilever retaining wall behavior, in *Physical modeling in geotechnics: ICPMG'02*, edited by R. Phillips, P. Guo, and R. Popescu, pp. 877–880, A.A. Balkema Publishers, Lisse, The Netherlands, 2002.

Steenhuis, T. S., J. Boll, E. Jolles, and J. S. Selker, Field evaluation of wick and gravity pan samplers, in *Handbook of vadose zone characterization and monitoring*, edited by L. G. E. L. G. Wilson, and S. J. Cullen, pp. 629–638, Lewis Publishers, Boca Raton, 1995.

Stone, W. A., J. M. Thorp, O. P. Gifford, and D. J. Hoitink, 1983. Climatological summary for the Hanford area, *Technical report*, Pacific Northwest Laboratory, Richland, WA.

Stumm, W., and J. J. Morgan, *DAquatic chemistry. An introduction emphasizing chemical equilibria in natural waters*, 2nd ed., John Wiley and sons, New York, 1981.

Swartzen-Allen, S. W., and E. Matejevic, Colloid and surface properties of clay suspensions III. stability of montmorillonite and kaolinite, *J. Colloid Interface Sci.*,

56, 159–167, 1976.

Toride, N., F. J. Leij, and M. T. van Genuchten, *The CXTFIT code for estimating transport parameters from laboratory or field tracer experiments, version 2.1*, Research Report 137, U.S. Salinity Laboratory, USDA-ARS, Riverside, CA, 1995.

Triay, I., A. Simmons, S. Nelson, H. Nuttall, B. Robinson, W. Steinkampf, and B. Viani, *Colloid-Facilitated Radionuclide Transport at Yucca Mountain*, Los Alamos National Laboratory Report LA-12779-MS, Los Alamos, NM, 1995.

USDOE, *Methdology for estimating ingestion dose for emergency response at Savannah River Site*, United States Department of Energy, on-line at http://sti.srs.gov/fulltext/tr2002035/tr2002035.html, accessed in August 2004, 2004.

van Olphen H. *An introduction to clay colloid chemistry*, Wiley, New York, NY, 1977.

Veihmeyer, F. J., O. W. Israelsen, and J. P. Conrad, 1924. The moisture equivalent as influenced by the amount of soil used in its determination, *Technical Report 16*, University of California, College of Agriculture, Agricultural Experiment Station, Berkeley, CA.

Virden, J. W., and J. C. Berg, The use of photon correlation spectroscopy for estimating the rate constant for doublet formation in an aggregating colloidal suspension, *J. Colloid Interface Sci.*, *141*, 528–535, 1992.

White, G. N., and J. B. Dixon, Kaolin-serpentine minerals, in *Soil mineralogy with environmental application*, edited by J. B. Dixon, and D. G. Schulze, pp. 389–414, American Society of Agronomy, Madison, Wisconsin, 2002.

Whittig, L. D., and W. R. Allardice, X-ray diffraction techniques, in *Methods of Soil Analysis. Part 1. Physical and Mineralogical Methods*, edited by A. Klute, pp. 331–362, American Society of Agronomy, Madison, Wisconsin, 1986.

Wu, T. H., A. T. Stadler, and C. Low, Erosion and stability of a mine soil, *ASCE J. Geotech. Eng.*, *122*, 445–453, 1996.

Wu, W., Baseline studies of the Clay Minerals Society source clays: Colloid and surface phenomena, *Clays Clay Miner.*, *49*, 446–452, 2001.

Yao, K.-M., M. T. Habibian, and C. R. O'Melia, Water and waste water filtration: concepts and applications, *Environ. Sci. Technol.*, *5*, 1105–1112, 1971.

Zachara, J. M., S. C. Smith, C. Liu, J. P. McKinley, R. J. Serne, and P. L. Gassman, Sorption of cs^+ to micaceous subsurface sediments from the Hanford Site, USA, *Geochim. Cosmochim. Acta*, *66*, 193–211, 2002.

Zhao, H., Y. Deng, J. B. Harsh, M. Flury, and J. Boyle, Alteration of kaolinite to cancrinite and sodalite by simulated Hanford Tank Wastes and its impact on cesium retention, *Clays Clay Miner.*, *52*, 1–13, 2004.

Zhu, Y., R. H. Fox, and J. D. Toth, Leachate collection efficiency of zero-tension pan and passive capillary fiberglass wick lysimeters, *Soil Sci. Soc. Am. J.*, *66*, 37–43, 2002.